AALBORG UNIVERSITET

Departament of Energy Tehnology-Pontoppidanstræde 101
Aalborg University, Denmark

Open Loop Low Speed Control for PMSM in High Dynamic Applications

PED 4 - 1031

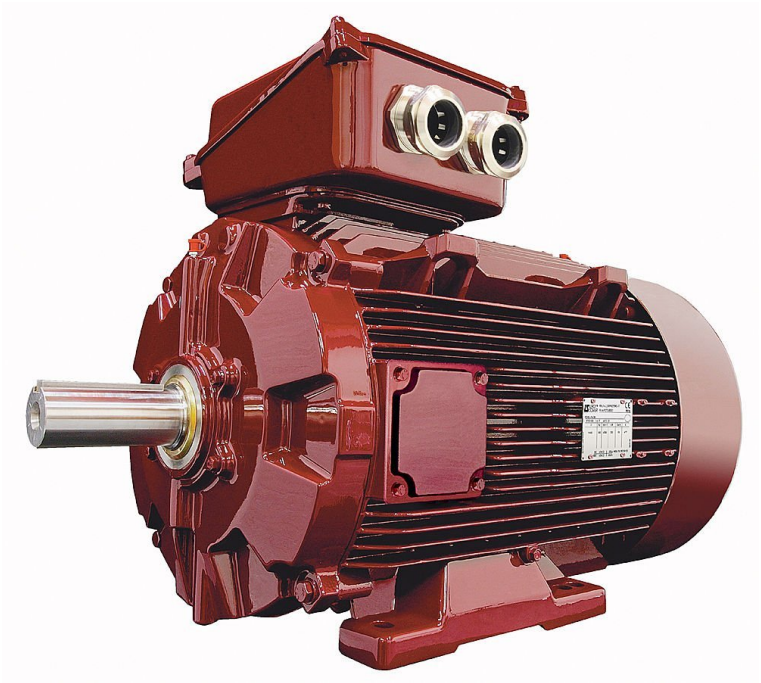

Conducted by group PED 4 - 1031
Spring Semester, 2010

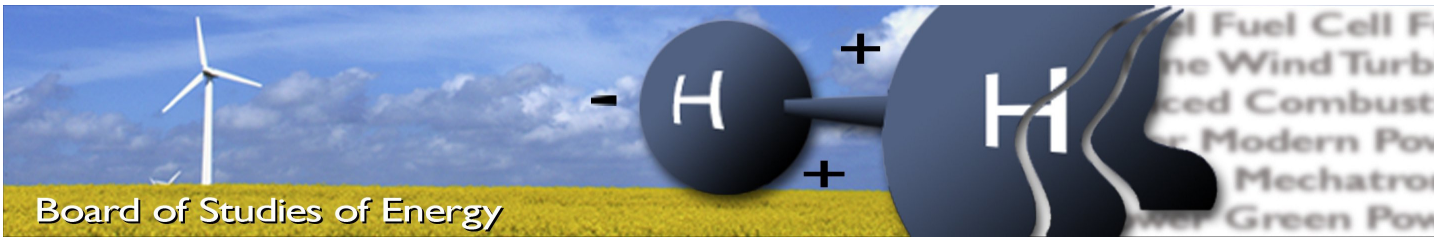

Title:	Open Loop Low Speed Control for PMSM in High Dynamic Applications
Semester:	10^{th}
Semester theme:	Master Thesis
Project period:	01.02.10 to 02.06.10
ECTS:	30
Supervisor:	Remus Teodorescu Johnny Wahl Jensen Ömer Göksu
Project group:	PED 4 - 1031

SYNOPSIS:

Nowadays sensor-less motor control is a hot topic for researchears due to its numerous advantages. The focus of this project is the sensor-less control of a surface mounted PMSM (SMPMSM) for low speed in high dynamic applications. First the literature is searched for a suitable sensor-less control strategy and then the selected strategy is implemented and tested in simulations. The sensor-less control strategy is then validated in the laboratory. For all the simulation *Matlab/Simulink* and *Plecs* is used. For the laboratory work a *dSpace* setup is used. Even if the topic of the project is sensor-less control, simulations and laboratory work is carried out for both sensored and sensor-less control of the SMPMSM in order to compare the results. Moreover the control of the loading machine is realized in order to be able to test the SMPMSM control under loading conditions. The performance of the selected sensor-less control strategy is tested and compared with the sensored control in five different study cases. Promising results are obtained in the laboratory at zero and low speeds. The rotor position estimation error becomes larger as the load torque and speed increases. Good results were obtained at speeds up to 200rpm.

Cristian Busca

Copies:	5
Pages, totel:	111
Appendix:	0
Supplements:	5 CDs

By signing this document, each member of the group confirms that all participated in the project work and thereby all members are collectively liable for the content of the report.

Preface

The present project report, entitled *"Open Loop Low Speed Control for PMSM in High Dynamic Applications"* is written by Cristian Busca, student at Power Electronics and Drives, group PED 4 - 1031. The topic of the project was proposed by Danfoss, the main idea being the control of a surface mounted PMSM at low speeds and startup without using a position sensor. The project was carried out at the Department of Energy Technology, Aalborg University between 1^{th} of February and 2^{nd} of June 2010.

Reading Instructions

The references are shown in form of a number placed into square brackets. Detailed information about literature is presented in Bibliography. The format of equations is (X.Y), where X is number of chapter and Y is number of equation. The figures are numbered Figure X.Y, where X is the number of chapter and Y is number of figure. The tables are numbered Table X.Y, where X is the number of chapter and Y is number of table.

In this project the chapters are consecutive numbered whereas the appendixes are labeled with letters. All appendixes are assigned with capital letters and put in an alphabetical order.

Matlab/Simulink and *Plecs* is used for all the simulations. The laboratory work is carried out using *Matlab/Simulink* and *ControlDesk* on a *dSpace* setup.

The enclosed CD-ROM contains the project report written in LATEX and Adobe PDF format, source codes, *Simulink* Models and documents used during the writing of the report.

The author is especially greatful to Remus Teodorescu, Johnny Wahl Jensen and Ömer Göksu who with their patience and generosity devoted valuable time providing great help to the development of this project. Also I would like to thank to *Danfoss* for the awarded scholarship which helped to support myself during the two year master programme.

Contents

1 Introduction **1**
1.1 Background of electrical drives 1
1.2 Problem Formulation 4
1.3 Objectives 4
1.4 Limitations 4
1.5 Project Outline 5
1.6 Summary 5

2 Overview of Sensor-less Control Strategies for PMSM **7**
2.1 Back-EMF calculation based methods 8
2.2 Stator flux linkage based methods 8
2.3 Stator phase inductance calculation based method 9
2.4 Hypothetical rotor position based method 9
2.5 Observer based methods 9
2.6 High frequency signal injection based methods 10
2.6.1 High frequency voltage signal injection method based on the magnetic saliency of the SMPMSM due to the flux of the permanent magnet . 10
2.7 Summary 17

3 Control algorithm design **19**
3.1 PMSM mathematical model 19
3.2 PMSM control methods 21
3.2.1 Scalar control 21
3.2.2 Vector control 22
3.2.3 FOC control properties 23
3.3 Sensored RFOC 24
3.3.1 Control mode block schemes (torque, speed and position mode) . . . 24
3.3.2 Design of controllers 27
3.4 Sensorless RFOC 37
3.4.1 Control mode block schemes (torque, speed and position mode) . . . 37
3.4.2 Detuning of controllers 40
3.4.3 Choosing the filters 40
3.5 Summary 41

4 Modeling and Simulation **43**
4.1 Sensored RFOC simulation results 43
4.2 Sensorless RFOC simulation results 49
4.3 Summary 60

5 Laboratory results **61**
5.1 PMSM frequency and current sensitivity analysis 61
5.2 PMSM rotor alignment to zero position 64
5.3 PMSM sensored RFOC 65
5.3.1 d, $q-axis$ current and speed controller step responses 65
5.3.2 Speed control mode 67
5.4 PMSM Sensorless RFOC 73
5.4.1 d, $q-axis$ current and speed controller step responses 73
5.4.2 Speed control mode 74
5.4.3 Position control mode 89
5.5 Estimation error dependence on load torque 95
5.6 Energy efficiency considerations 96
5.7 IM IFOC (loading machine) 96
5.7.1 d and $q-axis$ current controller step response 96
5.7.2 Speed control mode 97
5.7.3 Load torque validation 100
5.8 Summary 101

6 Conclusions and Future Work **103**
6.1 Conclusions 103
6.1.1 Contributions 104
6.2 Future work 104

Appendix **105**

A SMPMSM parameters **105**

B Contents of CD-ROM **107**

Bibliography **109**

Chapter 1

Introduction

This chapter contains a short introduction about electric motors and drives. Firstly, a few words are said about energy use and then the electricity use is discussed. Key discoveries related to electric motors are presented and different electric motor types are discussed. Finally the chapter is ended with a short discussion about electric motor drives.

1.1 Background of electrical drives

The level of prosperity of a community is related to its capability to produce goods and services. But producing goods and services is strongly related to the use of electrical energy in a smart way. Energy comes into use in several forms such as electrical, mechanical and thermal. Motion and temperature control require a high amount of energy. Part of the electrical energy is used to produce light, heat and electrolysis in industrial applications.[1]

The larger part of the electrical energy is converted into mechanical energy in electric motors.[1]

Electric motors are widely spread in the modern world, almost anything that uses electrical energy has one or more electrical motors in it. Appliances and devices which contain one or more electrical motors are: washing machines, cars, blenders, scooters, electric bicycles, refrigerators, air conditioners, laptops, desktop computers, elevators, DVD players, medical equipment, military equipment, manufacturing facilities, pumps, vacuum cleaners, fans, cranes, hoisting equipment, electric trams, trains, airplanes, submarines, ships, irrigation installations, etc.[2] All these devices and appliances use some kind of electric motor which is specifically designed for a given task. For instance, an electric motor used in a vacuum cleaner will be much different from that used in a DVD player.

Industry consumes more than 40% of total world electricity. About two thirds of the electricity consumed by industry is used by electric motors. Electric machines had been around for a long time and they had been used extensively especially in industrial applications.[3]

The physical principle of producing mechanical force by the interactions of a magnetic field and electric current carrying conductor was known as early as 1821s, it was demonstrated by physician Michael Faraday. The first commutator type DC motor capable of doing useful work was invented by William Sturgeon in 1832. Figure 1.1 illustrates the working principle of a simple brushed DC motor. The brushes transfer the power to the rotor which creates an electromagnetic field which interacts with the field created by the PM and the result is

useful torque.

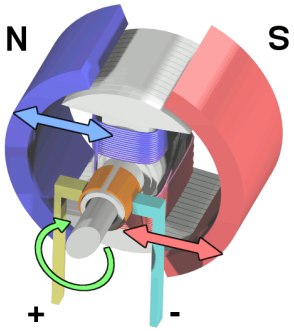

Figure 1.1: *Brushed DC motor working principle illustration*

In 1888 Nikola Tesla invented the first practicable AC motor and at the same time the polyphase transmission network. Electric motors of increasing efficiency were developed during the 19th century. Figure 1.2 shows the inside view of a squirrel cage IM. These kind of motor is widely used both in industry and in residential applications due to the fact that it can be directly connected to the grid without the need for a motor drive.

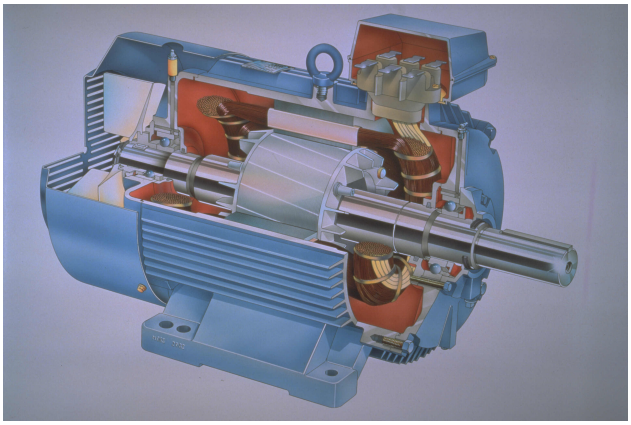

Figure 1.2: *Inside view of a squirrel cage IM*

From the outside is almost impossible to tell what kind of motor you look at. For example figure 1.3 shows an IM but a PMSM can look exactly the same way as the IM from the outside.

Figure 1.3: *Picture of an IM*

Although some motor types can be connected directly to the grid (IM), usually electric motors are connected to the grid through special devices called motor drives. Electric motor drives are specially designed devices to supply and control electric motors. Electric motor drives enable the motors to operate at higher efficiency and performance. A motor drive is supplied by the grid, it converts AC electricity into DC electricity and then by the use of power switches it converts back the DC voltage into variable frequency, phase and amplitude voltage. The power switches are controlled usually by a microprocessor or DSP. The benefits of using a motor drive are high quality motion and energy efficiency.[2] Figure 1.4 shows a Danfoss VLT motor drive.

Figure 1.4: *Danfoss VLT motor drive*

Usually electric motor drives have an input device to enable the used to set various parameters like: motor parameters, control strategy, maximum current and voltage values and so on.

1.2 Problem Formulation

Nowadays, the sensor-less control is a hot topic for researchers due to its numerous advantages like: reduced cost, high reliability and reduced system size.

There are numerous sensor-less control strategies for IPMSM which use the naturally occurring saliency of the IPMSP. However the sensor-less control of a SMPMSM is more problematic since it has almost no saliency. SMPMSM is preferred because of its lower cost due to its simple rotor design (the PM material is mounted on the rotor, not inside the rotor as in the case of IPMSM).

In the medium to high speed region the sensor-less control of a SMPMSM is not an issue as back-EMF based methods may be successfully used. However at zero and low speeds the back-EMF based methods can not be used as the back-EMF becomes very small.

The challenge is to control a SMPMSM at zero and low speeds (with high dynamics) without using a position transducer.

There are promising methods which use high frequency signal injection in order to detect the rotor position. By injecting a high frequency component into the SMPMSM, additional power losses appear. The even greater challenge is to control a SMPMSM at zero and low speeds without the use of a position transducer without considerably increasing the power losses.

1.3 Objectives

The objective of this project is to control a Surface Mounted PMSM without using a position encoder. The selected sensor-less control strategy must be able to provide maximum torque at very low speeds down to standstill. Further, the sensor-less control strategy has to be energy optimized.

The main goals of this project may be summarized as:

- search the literature for suitable sensor-less control strategies;
- implement the selected control strategies in $Matlab/Simulink$;
- validate the simulations in the laboratory using *dSpace* real time interface;
- test the performance of the selected control strategy in different study cases;
- compare the results from the sensored control with the results from sensorless control.

1.4 Limitations

During the project development several limitations had to be imposed. Thus, the most important limitations of this project are presented as follows:

- only the low speed operating region of the SMPMSM is considered;
- due to some issues withe the loading machine drive the SMPMSM control could be tested with load torques up to only 40% of it's nominal load torque.

1.5 Project Outline

This project studies the sensor-less control of a Surface Mounted PMSM and the present report is structured in six chapters.

The first chapter may be seen as a general introduction to the studied subject. Thus, an introduction to the electrical motors and drives is made, followed up by the problem formulation and the objectives of the current project. The project limitations are also presented.

The second chapter represents an overview of the PMSM sensor-less control strategies. Firstly, sensor-less control strategies applicable to PMSM are discussed. After that, the selected sensor-less strategy for the SMPMSM is discussed more in detail. Advantages and disadvantages of each sensor-less strategies are also discussed.

The third chapter deals withe the control algorithm. In this chapter the mathematical model of the PMSM is presented. Different control schemes are discussed and the most common control properties used with FOC are presented. In the last part of the chapter the control schemes for sensored and sensorless control of PMSM in torque, speed and position mode are presented.

The fourth chapter deals with the modeling of SMPMSM and its control. The models of the SMPMSM and its control are developed in $MATLAB/Simulink$ and $Plecs$. The simulation results for the sensored and sensorless control of the SMPMSM are presented and discussed.

The fifth chapter contains the laboratory results. The laboratory experiments are carried out in the *dSpace* laboratory. The experimental results for the sensored and sensorless RFOC are presented and discussed.

In the sixth chapter the conclusions of the project are presented and also ideas for future work are shown.

Moreover, at the end of each chapter a *Summary* containing a brief presentation of the work from that chapter may be found.

1.6 Summary

This chapter was a short introduction to electric motors and drives. Some important discoveries related to electric motors are presented. After introduction the problem formulation is presented where challenges related to sensorless control of SMPMSM are discussed. The main objectives of the project are presented followed by the project limitations. The chapter ends with the project outline where the structure of the project is described.

Chapter 2

Overview of Sensor-less Control Strategies for PMSM

This chapter presents the most common position and speed estimation techniques used for sensor-less PMSM control. Advantages, disadvantages and applicability of each method is discussed. A detailed analysis of the chosen sensor-less control strategy is presented.

PMSM drives are becoming more popular and replace classical brushed DC and IM drives in industrial applications, machine tools and residential applications. In a PMSM the excitation is provided by means of using permanent magnets mounted on the rotor.[4] PMSMs present numerous advantages over brushed DC motors and IMs. [5] These advantages are:

- high efficiency;
- high torque to inertia ratio;
- high power density;
- reliability;
- long life.

Industrial applications require variable speed drive systems. In order to optimally control a PMSM, the position and or the speed of the shaft must be known. The position and speed of the shaft is usually determined using a position transducer or encoder. By knowing the rotor position, the PMSM can be controlled in such a way that it provides full torque at zero speed. This is achieved by maintaining an appropriate angle between the stator and rotor magnetic fields. However the use of a position encoder adds some important disadvantages to the PMSM drive system: [5]

- increased drive system cost;
- increased complexity and maintenance;
- reduced reliability;
- increased size of the drive system.

In order to solve these problems related to the use of position transducers, researchers proposed the sensor-less control of PMSMs. [5] The idea is to get rid of the position transducer and try to determine the actual rotor position by measuring other variables such as voltages and currents in the PMSM. There are a lot of sensor-less control strategies in the literature each of them having its own advantages, disadvantages and limitations.

The term sensor-less control does not mean that the PMSM is controlled without the use of any sensor. Actually it means that there is no position transducer or encoder used but there are sensors which measure the currents or voltages.

2.1 Back-EMF calculation based methods

This method uses the relationship between the back-EMF and rotor position. The idea is to calculate the back-EMF space vector in order to get the rotor angle. Since the rotor permanent magnet flux linkage is aligned with the d-axis (rotating reference frame fixed on the rotor), the back-EMF is always placed on the q-axis. The rotor position can be calculated by projecting the back-EMF vector from the dq-axes on the stationary reference frame ($\alpha\beta$-axes). The $\alpha\beta$-compoments of the back-EMF vector are shown in 2.1 and 2.2. The rotor position is calculated using 2.3. [6]

$$e_\alpha = \omega_e \psi_m \sin(\theta_r) = -u_\alpha + R_s i_\alpha + L\frac{d}{dt} i_\alpha \tag{2.1}$$

$$e_\beta = \omega_e \psi_m \cos(\theta_r) = u_\beta + R_s i_\beta + L\frac{d}{dt} i_\beta \tag{2.2}$$

$$\theta_r = \tan^{-1}\frac{e_\alpha}{e_\beta} \tag{2.3}$$

There are also other back-EMF based methods which require the use of flux observers or Kalman filters. Back-EMF based methods give good results in the medium and high speed operating region. In the zero and low speed region, the back-EMF becomes small as it is proportional to the rotor speed and its measurement becomes problematic. Large errors in back-EMF calculation lead to large position estimation errors. As a consequence, back-EMF based methods can not be used for sensor-less control of a SMPMSM in the zero and low speed region.

2.2 Stator flux linkage based methods

This method estimates the rotor position by using the stator flux linkage vector. The stator flux linkage vector is calculated using the stationary reference frame voltage equations as shown by 3.3 and 3.4. As it may be seen the phase voltages, currents and resistance must be known in order to calculate the stator flux linkage vector.

$$\psi_\alpha = \int (u_\alpha - R_s i_\alpha)\, dt \tag{2.4}$$

$$\psi_\beta = \int (u_\beta - R_s i_\beta)\, dt \tag{2.5}$$

Integration drift is a problem for this estimation method and it should be avoided by using proper integration methods. The initial rotor position is not detectable with this sensor-less technique. [6]

2.3 Stator phase inductance calculation based method

The stator phase inductances of a PMSM are rotor position dependent. There are some sensor-less techniques which obtain the rotor position information from on-line calculation of the stator phase inductances. This technique assumes that the inductances does not change during one switching period due to change in rotor position (this implies high switching frequency). The on-line calculated inductances are compared with a look-up table which contains a given inductance for a given rotor position. [6]

In order to calculate the inductances the stator resistance and PM flux linkage must be known. A switching frequency greater than 10Khz is necessary for accurate calculation of the inductances. [6]

This technique alone is not able to determine the rotor position at zero speed since the voltages are zero at zero speed.

2.4 Hypothetical rotor position based method

In this strategy a rotor position is assumed to be correct and the machine variables (voltages or currents) in the rotor reference frame are calculated. After that the measured variables of the machine (voltages or currents) are transformed to the rotor reference frame using the assumed rotor position. The error between the transformed values and the values obtained from previous model calculation are used to obtain the error in the assumed rotor position. The assumed rotor position is then corrected.

Either the voltage or current error can be used for the position error correction. It was found that the current error based method gives better results than the voltage error based method.[6]

The initial rotor position is not detectable with this sensor-less technique.

2.5 Observer based methods

In this strategy a machine model is used and the model is fed with the same inputs as the real machine (voltages, load torque). The error between the real machine and model output variables such as speed and rotor position is used in the state observer in order to correct any error between the estimated and real speed and position values.

Since the PMSM is nonlinear, the design of a state observer is quite complex. As observers are model based, they are affected by parameter variation of the PMSM. In order to improve the observer based strategy, an on-line parameter estimator may be used. Observer based methods require high processing power and can not detect initial rotor position.[6]

2.6 High frequency signal injection based methods

The principle of these methods is that a high frequency current or voltage is superimposed on the top of the fundamental excitation of the machine. This high frequency injected signal induces voltages or currents which contain information relating to the rotor position. Using suitable signal processing techniques it is possible to estimate the rotor position. This technique can estimate the rotor position at zero speed as the high frequency signal is injected all the time. [7] The high frequency signal injection based methods can be further categorized as: voltage signal injection method, fluctuating voltage signal injection, rotating voltage signal injection depending on where the voltage is injected. There are also different kind of signal processing techniques. Some methods process the resulting high frequency currents while other methods process the resulting zero sequence voltage. [8]

2.6.1 High frequency voltage signal injection method based on the magnetic saliency of the SMPMSM due to the flux of the permanent magnet

High frequency signal injection techniques are especially used for sensor-less control of IPMSM due it's high saliency ratio. However this technique may be used with SMPMSMs exploiting the small amount of saliency produced by the saturation effect of the stator core due to the permanent magnet flux. [5]

Figure 2.1 shows the high frequency current response of the PMSM when the rotor is scanned with high frequency constant magnitude voltage represented by the circle. The magnitude of the injected voltage is v_{inj} while the magnitude of the resultant current is i_{inj}. θ_{inj} is the injection angle and is the angle between the real $d-axis$ and the injection axis. In 2.1 θ_{inj} is negative. Due to the small amount of high frequency saliency present in a PMSM the high frequency current response has an elliptical shape. This means that the reactance on the $d-axis$ is not equal to the reactance of the $q-axis$, there is a small difference. This difference is said to be due to the flux of the permanent magnet which produces some saturation of the magnetic core. [5]

In the case of the PMSM the reactance on the $d-axis$ is lower than the reactance on the $q-axis$ that is why the magnitude of the current is higher on the $d-axis$ than on the $q-axis$ even if the magnitude of the injection voltage is constant. The high frequency inductance on the $d-axis$ is lower than the inductance on the $q-axis$ due to the saturation effect of the magnetic core around the $d-axis$.

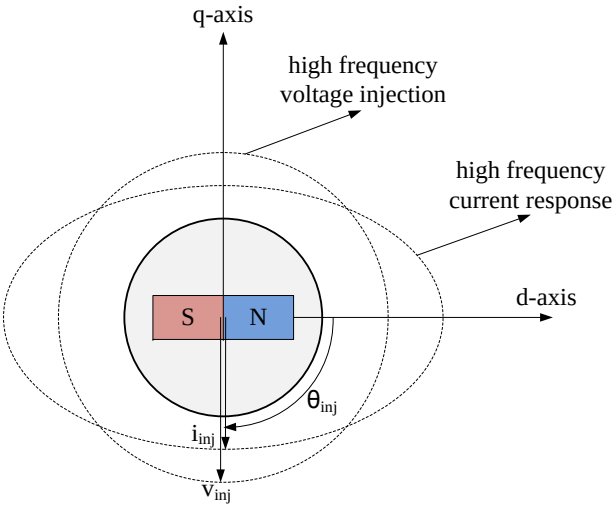

Figure 2.1: *High frequency current response of the PMSM as a function of rotor position when the magnitude of the injected voltage is constant*

Figure 2.2 shows the high frequency impedance curve of the PMSM. As it may be seen for a constant magnitude high frequency injection voltage the high frequency impedance of the PMSM is lower on the $d-axis$ and higher on the $q-axis$. This is also validated by laboratory measurements which are presented in section 5.1.

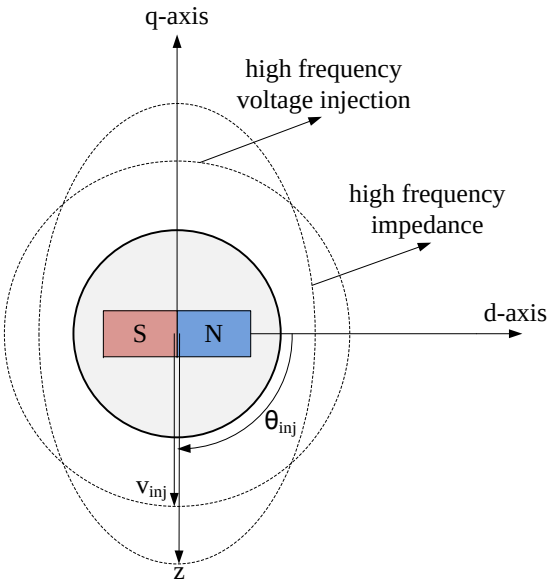

Figure 2.2: *High frequency impedance curve of the PMSM as a function of rotor position when the magnitude of the injected voltage is constant*

Figure 2.3 shows the real and estimated $dq-axes$. The real $dq-axis$ is fixed on the rotor while the estimated $dq-axis$ is not. θ_{error} is defined as the angle between the real and estimated $dq-axis$ and is called the estimation error of the electrical rotor position.

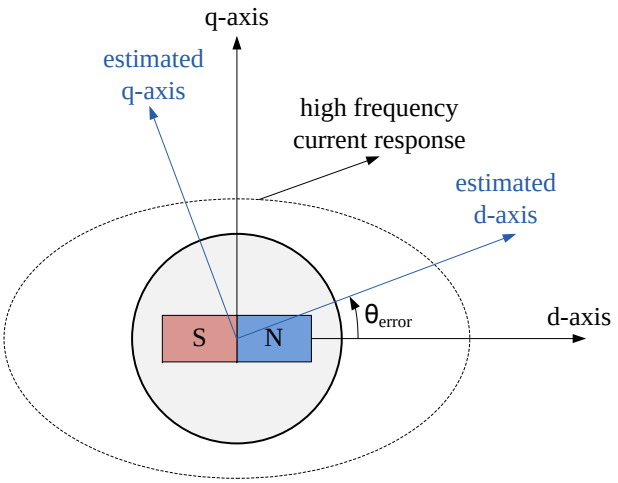

Figure 2.3: *The real and estimated $dq-axes$ (positive estimation error)*

Figure 2.3 shows how the high frequency voltage is injected on the estimated $d-axis$ and projected on the real $dq-axes$.

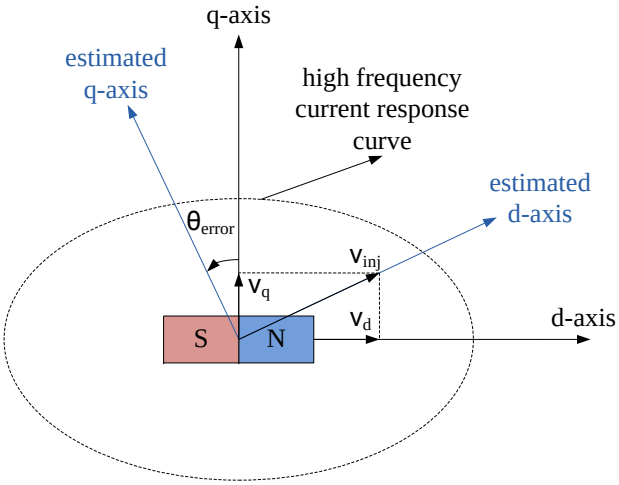

Figure 2.4: *High frequency voltage injection on the estimated $d-axis$ and it's projection on the real $dq-axes$ (positive estimation error)*

Figure 2.5 also shows the resultant $dq-axis$ currents on the real $dq-axis$. The $d-axis$ current is drawn larger than the $d-axis$ voltage just for visual purpose in order to show that the $d-axis$ reactance is lower thus the current is higher. On the other hand the $q-axis$ current is drawn smaller than the $q-axis$ voltage just to point out that the $q-axis$ reactance is higher thus the resulting current is lower. It must be noted that if there were no saliency than the current response would be proportional to the applied $dq-axis$ voltages. As it may be seen the resultant current vector is not in the same direction as the voltage vector. If there were no saliency than the current vector would be in the same direction with the voltage vector no matter what is the estimation error.

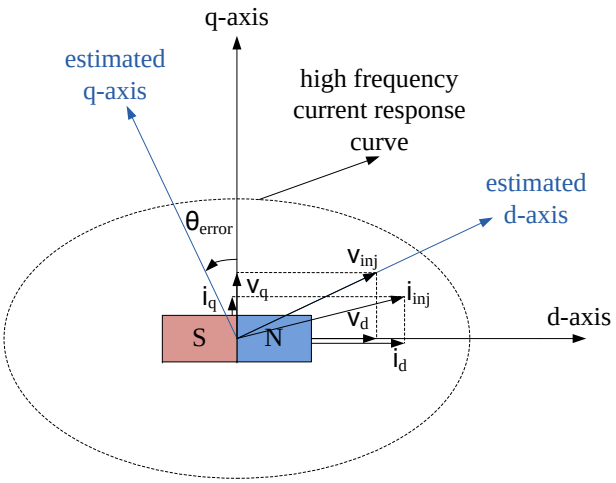

Figure 2.5: *High frequency voltage injection on the estimated $d-axis$ and it's projection on the real $dq-axes$ with the resultant current vector and it's projection on the real $dq-axes$ (positive estimation error)*

Figure 2.6 shows the projection of the current vector back on the estimated $dq-axis$. As it may be observed in this case (positive estimation error) there is a current on the estimated $q-axis$ called iqe. If there were no saliency or the estimation error would be zero than the iqe component would be equal to zero.

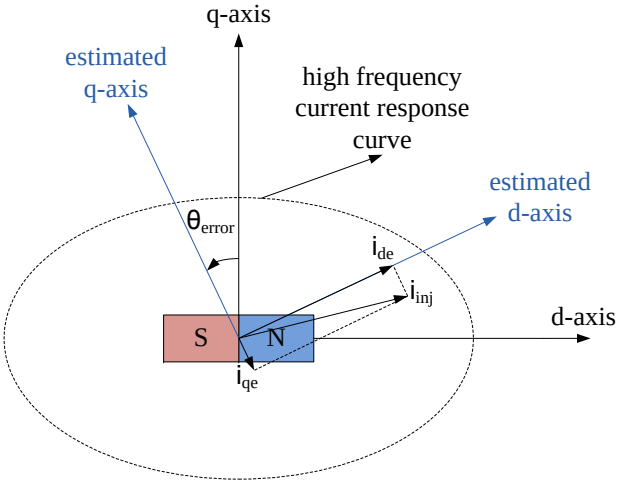

Figure 2.6: *Projection of the current vector on the estimated $dq-axes$ (positive estimation error)*

When there is no estimation error so the position of the real $dq-axis$ is correctly estimated then the current vector has the same direction as the voltage vector as shown in figure 2.7. In this case the iqe component on the estimated axis is zero.

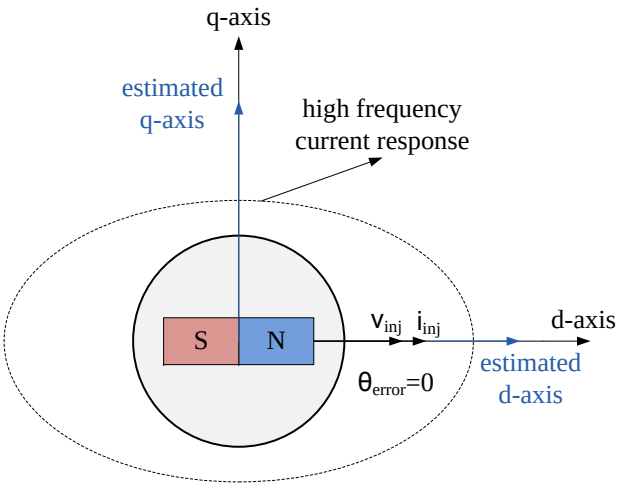

Figure 2.7: *The high frequency voltage vector and the resultant current vector in the case of correct position estimation (zero estimation error)*

Figure 2.8 shows what happens if there is no saliency at all and the current response is represented by a circle instead of an ellipse. In this case the $dq-axis$ currents are proportional to the applied $dq-axis$ voltages and the resultant current vector has the same direction as the injection voltage vector. In this case no matter what is the estimation error, the voltage and current vectors always have the same direction. There is no usable signal for the position estimation.

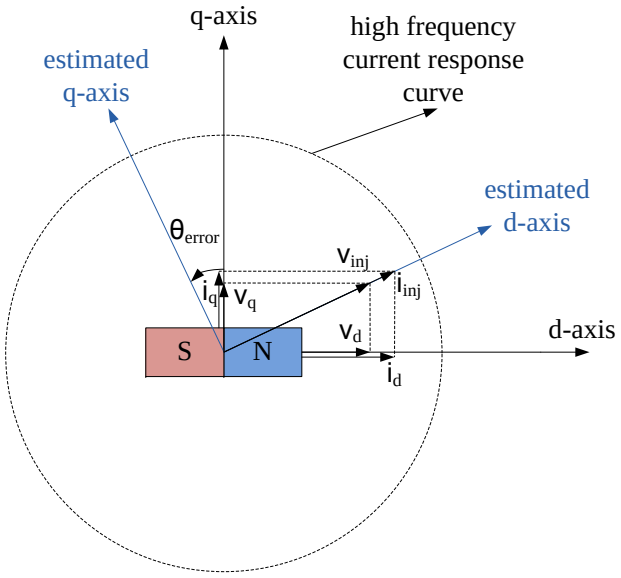

Figure 2.8: *High frequency voltage injection on the estimated $d-axis$ and it's projection on the real $dq-axes$ with the resultant current vector and it's projection on the real $dq-axes$ in the case of no high frequency saliency (positive estimation error)*

In order to use the small signal as a result of the deviation of the current vector from the direction of the injection voltage vector, a measurement rotating reference frame is created as shown in figure 2.9. The measurement $dq-axis$ is -45 apart from the estimated $dq-axis$

(lagging) and it is rotating with the estimated $dq-axis$. This means that the estimated $d-axis$ is between the measurement $dq-axes$.

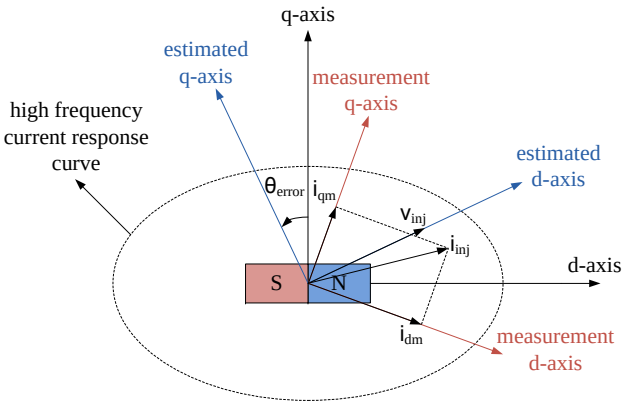

Figure 2.9: *Projection of the high frequency current vector on the measurement axes (positive estimation error)*

The rationale of this measurement axes is that in the case of no estimation error the current vector lies on the estimated $d-axis$ and the projection of this current vector on the measurement reference frame results in two components idm and iqm which are equal in magnitude as it may be seen in 2.10. Whenever there is an estimation error the current vector deviates from the estimated $d-axis$ and as a result the projection of this current on the measurement axes results in two current components which are not equal in magnitude as it may be seen in 2.9. In this case there is a positive estimation error and as a result the magnitude of idm is higher than the magnitude of iqm.

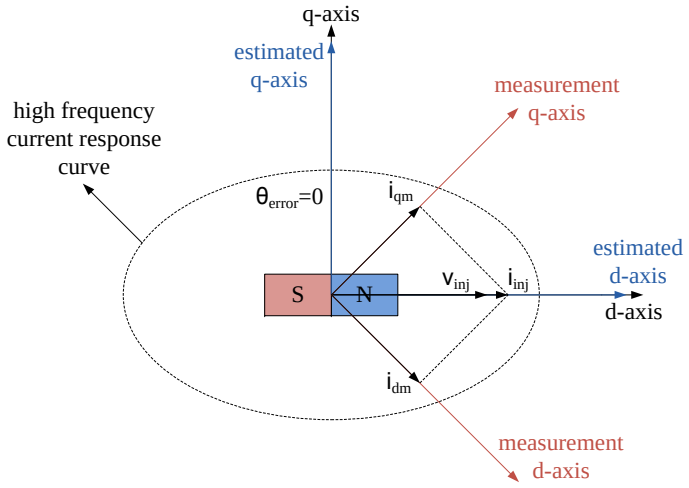

Figure 2.10: *Projection of the high frequency current vector on the measurement axes in the case of correct rotor position estimation (zero estimation error)*

Figure 2.11 shows the deviation of the high frequency impedance curve under loading conditions. When the PMSM is not loaded the minimum impedance point lies on the $d-axis$ which is the permanent magnet flux axis. When the PMSM is loaded the $q-axis$ current iq is non zero and is proportional with the produced electromagnetic torque. This $q-axis$ current produces a magnetic flux with the magnitude equal to $\lambda_q = L_q i_q$. The minimum

impedance point is in the direction of the total flux vector due to the saturation effect that it produces.

Actually when the machine is loaded with $10Nm$ the $q-axis$ current is $i_q = \frac{Te}{\frac{3}{2}n_{pp}\lambda_{pm}} = \frac{10}{\frac{3}{2}\times 4\times 0.123} = 13.55A$ and the flux is $\lambda_q = 0.002 \times 13.55 = 0.0271Wb$. The permanent magnet flux $\lambda_{pm} = 0.123Wb$. The magnitude of the total flux vector is calculated as $\lambda_{total} = \sqrt{\lambda_{pm}^2 + \lambda_q^2}$.

Theoretically the angle of deviation of the minimum impedance point can be calculated as $\theta_{dev} = \arccos\frac{\lambda_{pm}}{\lambda_{total}} = \arccos\frac{0.123}{0.126} = 12.42deg$. During the laboratory experiments a deviation angle of around $10...11deg$ was observed as it is shown in section 5.5.

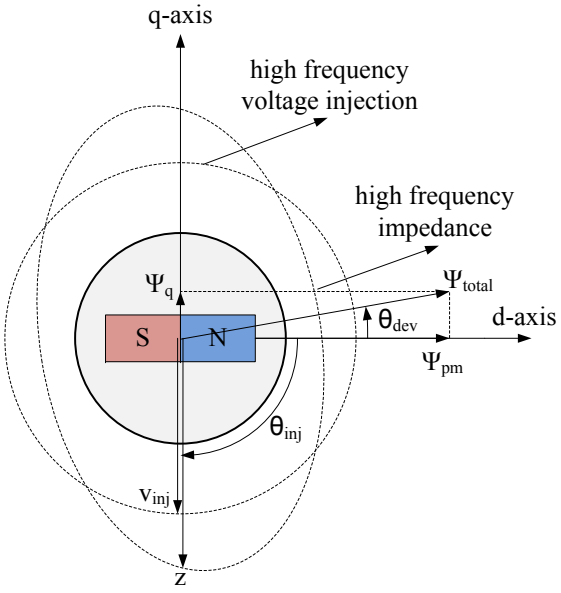

Figure 2.11: *Deviation of the minimum impedance point under heavy loading of the PMSM*

Since in this control algorithm a sinusoidal voltage is injected on the estimated $d-axis$ the signals obtained on the measurement reference frame idm and iqm are also sinusoidal. As a consequence it is necessary to use a special algorithm (heterodyning) to calculate the magnitude of these signals. Figure 2.12 shows the block diagram of the heterodyning algorithm used to obtain the square of the magnitude of the measurement currents idm and iqm which are used for the position estimation. The heterodyning algorithm is used to obtain the magnitude of a specified frequency content of a signal (in this case the $500Hz$ component). [5]

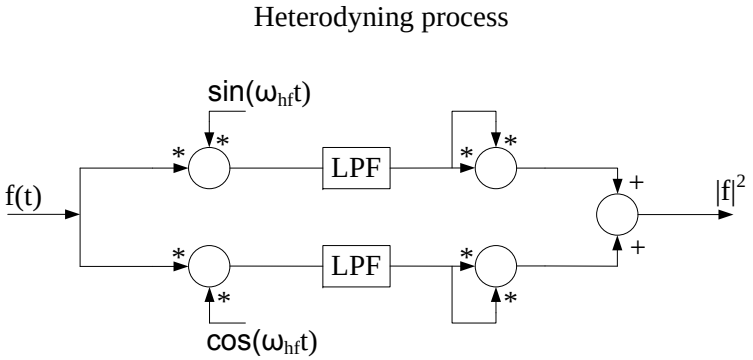

Figure 2.12: *The block diagram of the heterodyning algorithm used to obtain the square of the magnitude of the input signal*

The high frequency signal injection algorithm continues with the presentation and discussion of the control schemes for torque, speed and position control at section 3.4.

2.7 Summary

This chapter presents the most common speed and position estimation techniques used for sensorless control of a PMSM. The working principle of the chosen high frequency signal injection algorithm is presented and discussed. The discussions about the selected control strategy continues with the presentation of the control scheme blocks in the next chapter at section at section 3.4.

Chapter 3

Control algorithm design

This chapter begins with the presentation of the mathematical model of a PMSM in the rotating dq reference frame. The most known control methods used for PMSM control are presented and discussed. Next the most common control properties for FOC are presented. The control block schemes for sensored and sensorless RFOC are presented for torque, speed and position control. The design of the current and speed controllers is also shown.

3.1 PMSM mathematical model

In permanent magnet synchronous machines the rotor flux is generated by permanent magnets thus eliminating the need of an external power source for the rotor flux generation. In classical DC machines the rotor flux is created using rotor windings supplied by an external power source. In contrast to the conventional DC machines PMSM's have far better efficiency, moreover the use of permanent magnets in the rotor structure allows to design these machines less heavy and more compact sized compared to conventional DC machines. The disadvantage of the PMSM's is that the rotor flux can not be easily controlled as in the case of a conventional DC machine by changing the armature current.[6]

In order to simulate the PMSM the mathematical equations are needed. One advantageous way to represent the machine equations is the *dq* rotating reference frame representation. The machine variables like voltages and currents are seen as sinusoidal from the stator side while these variables become DC values during steady state if seen from the rotor side. Since the machine variables are DC values during steady state then PI controllers may be used to control the currents through the PMSM's stator windings. One advantage of the PI controller is that it eliminates steady state error.

The scalar form of the voltage equations in the rotor *dq* reference frame are presented in 3.1 and 3.2.[6]

$$v_{qs}^{r} = r_s i_{qs}^{r} + \frac{d}{dt}\lambda_{qs}^{r} + \omega_r \lambda_{ds}^{r} \tag{3.1}$$

$$v_{ds}^{r} = r_s i_{ds}^{r} + \frac{d}{dt}\lambda_{ds}^{r} - \omega_r \lambda_{qs}^{r} \tag{3.2}$$

where,

- v_{qs}^r is the $q-axis$ voltage in the rotor reference frame $[V]$;
- v_{ds}^r is the $d-axis$ voltage in the rotor reference frame $[V]$;
- r_s is the stator phase resistance $[\Omega]$;
- i_{qs}^r is the $q-axis$ current in the rotor reference frame $[A]$;
- i_{ds}^r is the $d-axis$ current in the rotor reference frame $[A]$;
- λ_{qs}^r is the $q-axis$ flux linkage in the rotor reference frame $[Wb]$;
- λ_{ds}^r is the $d-axis$ flux linkage in the rotor reference frame $[Wb]$;
- ω_r is the electrical rotor speed $[rad/s]$;

The flux equations are shown in 3.3 and 3.4.[6]

$$\lambda_{qs}^r = L_q i_{qs}^r \tag{3.3}$$

$$\lambda_{ds}^r = L_d i_{ds}^r + \lambda_{pm} \tag{3.4}$$

where,

- L_q is the $q-axis$ inductance in the rotor reference frame $[H]$;
- L_d is the $d-axis$ inductance in the rotor reference frame $[H]$;
- λ_{pm} is the permanent magnet flux linkage $[Wb]$;

By substituting the flux equations 3.3 and 3.4 in the voltage equations 3.1 and 3.2 the compact form of the voltage equations is obtained as shown in 3.5 and 3.6.[6]

$$v_{qs}^r = r_s i_{qs}^r + \frac{d}{dt} L_q i_{qs}^r + \omega_r L_d i_{ds}^r + \omega_r \lambda_{pm} \tag{3.5}$$

$$v_{ds}^r = r_s i_{ds}^r + \frac{d}{dt} L_d i_{ds}^r - \omega_r L_q i_{qs}^r \tag{3.6}$$

The expression of the instantaneous electromagnetic torque is shown in 3.20.[6]

$$T_e = \frac{3}{2} npp \left[\lambda_m i_{qs}^r + \left(L_d - L_q \right) i_{ds}^r i_{qs}^r \right] \tag{3.7}$$

where,

- T_e is the electromagnetic torque $[Nm]$;
- npp is the number of pole pairs of the PMSM $[-]$;

In the case of a SMPMSM by neglecting the reluctance torque the expression of the electromagnetic torque becomes 3.8. The reluctance torque component may be neglected in the case of SMPMSM since the synchronous inductances are almost equal ($L_d \approx L_q$).

$$T_e = \frac{3}{2} npp \lambda_m i_{qs}^r \tag{3.8}$$

The expression of the mechanical equation is shown in 3.9.[6]

$$T_e = J\frac{d\omega_m}{dt} + B_m\omega_m + T_l + T_{df} \tag{3.9}$$

where,

- J is the combined moment of inertia of the PMSM and load $[kg * m^2]$;
- B_m is the viscous friction constant $[-]$;
- T_l is the load torque $[Nm]$;
- T_{df} is the dry friction torque $[Nm]$;

Coupling of the voltage equations

The terms $+\omega_r\lambda^r_{ds}$ and $-\omega_r\lambda^r_{qs}$ in 3.1 and 3.2 represent the coupling terms between the two axes. In order to achieve decoupled control of torque and flux the coupling between the two axes must be canceled out. Since 3.1 and 3.2 represent the PMSM's voltage equations in the rotating dq reference frame, the coupling between the two axes can be canceled out by adding the term $-\omega_r\lambda^r_{ds}$ to the $q-axis$ reference voltage and adding the term $+\omega_r\lambda^r_{qs}$ to the $d-axis$ reference voltage in the control scheme.

3.2 PMSM control methods

3.2.1 Scalar control

The principle of the scalar control is to maintain a constant V/Hz ratio almost through the whole speed range operation since only the magnitude and frequency of the supply voltages is controlled. The V/Hz ratio is calculated from the nominal values (voltage and frequency) of the PMSM. By maintaining a constant V/Hz ratio the stator flux of the PMSM can be maintained relatively constant in steady state. If the V/Hz ratio increases then the PMSM becomes overexcited and if it decreases then it becomes under excited.[9] At very low speeds it is necessary to compensate for the stator resistance voltage drop so a V/Hz ratio higher than the nominal one is needed. The scalar control is the most common control strategy used for IM drives.

The PMSM scalar control is a good alternative in applications where good dynamic performance is not required (fans, pumps, blowers). Scalar control is performed without the need of a position encoder and the speed of the rotor can be estimated by looking at the frequency of the supply voltage.[9] When using scalar control there is no need for high capability DSP as in the case of vector control.

Some PMSMs have so called build in damper windings which help to stabilize the PMSM especially when scalar controlled. The damper windings basically are similar to the squirrel cage rotor of an IM. In a PMSM the damper windings produce some amount of asynchronous torque similarly as in an IM when needed thus helping the PMSM to synchronize. When the PMSM is synchronized then there is no current induced in the damper windings since the slip is zero and then there is no asynchronous torque produced.

In a scalar controlled PMSM the stator currents are not controlled directly. A scalar controlled PMSM can become unstable easily especially when the load torque reaches the break down torque value.

Considering its disadvantages the scalar control is not suitable for low speed control of PMSM in high dynamic applications.

3.2.2 Vector control

Vector control offers superior performance when compared to scalar control. Vector control eliminates almost all the disadvantages of scalar control. The main idea of vector control is to control not only the magnitude and frequency of the supply voltages but also the angle. With other words said the magnitude and angles of the space vectors is controlled. There are different kind of vector controls, the two most commonly used being DTC and FOC.

Direct torque control

Direct torque control was introduced on the market by ABB. The DTC has some advantages like simple control scheme, good dynamic response and it does not needs rotor speed or position feedback thus being considered a sensorless control technique.

The control scheme of classical DTC is much simpler than that of FOC as there is no reference frame transformation or position and speed measurement needed. The DTC scheme consists of torque and stator flux estimators, torque and flux hysteresis comparators a switching table and a voltage source inverter. The principle of DTC is to chose a voltage vector to control both stator flux and torque simultaneously. The stator currents and DC-link voltage are sampled and used in the flux and torque estimation. The estimated torque and flux magnitudes are compared with their reference values in the hysteresis comparators and then the outputs of the hysteresis comparators are feed to the switching table in order to select the appropriate voltage vectors in each sampling period.[10]

The drawbacks of classical DTC are high torque and current ripples during steady state operation unless operated at very high switching frequencies ($40Khz$) which increases the overall cost of the drive system.

Field oriented control

The objective of field oriented control is to be able to control the PMSM as a separately excited DC machine meaning that the flux and torque can be controlled separately (in a decoupled way). The instantaneous stator currents are transformed to the dq rotating reference frame by means using mathematical equations and taking into account the rotor position. The flux is controlled through the $d-axis$ current while the torque is controlled through the $q-axis$ current. It is not enough to use only the dq transformation in order to achieve decoupled control of flux and torque since there is coupling between the two axes which may be canceled out by subtracting from the $dq-axis$ reference voltages the appropriate coupling terms. Two types of field oriented control are possible for the PMSM: rotor oriented FOC and stator oriented FOC.

A general block diagram of FOC scheme (torque control) may be seen at section 3.3 in figure 3.1.

Due to it's advantages like low torque and current ripple, constant VSI switching frequency, low audible noise FOC control scheme was chosen for further analysis. The field oriented control scheme is analyzed more in detail in sections 3.3 and 3.4.

3.2.3 FOC control properties

As it may be seen in 3.1 the control property block has as input the reference torque T_{eref} and outputs the $dq-axis$ reference currents. There are several control properties that may be used for a PMSM. The most common control properties are discussed.

Unity power factor strategy

The goal of this control property is to control the $dq-axis$ currents in such a way that the instantaneous stator currents will be in phase withe the instantaneous stator voltages thus obtaining unity power factor. Since the power factor $\cos(\psi) = 1$ the reactive power is zero. That means that the input power to the PMSM is only active power thus the VA rating of the VSI is minimized. [6]

Constant stator flux strategy

In this control property the magnitude of the stator flux is limited thus limiting the stator voltage requirement. When the stator flux is limited then also the torque producing capability of the PMSM is also limited. Usually in the case of the stator flux control for PMSM the magnitude of the stator flux is maintained constant and equal to the permanent magnet flux linkage. This way the stator voltage requirement of the PMSM is kept low and the torque producing capability of the machine is not degraded. [6]

Maximum torque per ampere strategy

By using this control property the torque producing capability of the machine is maximized since the minimum stator current magnitude can be applied to the machine for a required electromagnetic torque. This way the copper losses are minimized. If the core losses are negligible then the maximum efficiency of the PMSM can be also obtained by using this control property. In the case of SMPMSM the maximum torque per ampere control property is the same with the constant torque angle property since there is almost no difference in the $dq-axis$ inductances thus the reluctance torque is almost inexistent. [6]

Constant torque angle strategy

The constant torque angle control property is one of the easiest to implement since the $d-axis$ reference current is set to zero. It is also called $i^r_{ds} = 0$ control property or $\alpha = \frac{\pi}{2}$ control property. The idea of this control property is to maintain a constant angle of $90deg$ electrical between the current space vector and permanent magnet flux axis. This way all the current is projected on the $q-axis$. By using this control strategy for an IPMSM the reluctance component of the torque is lost. This control property is a good choice in the case of a SMPMSM since the reluctance torque is almost inexistent. [6]

In this project the VA rating of the inverter is not an issue since the machine needs to be sensorlessly controlled at low speed. The stator voltage requirement is also not an issue

since the machine is operated at low speed thus the required voltage is not high. Since the machine used in this project is a SMPMSM and it needs to be energy optimally controlled a good choice is the constant torque angle (maximum torque per ampere) control property which is also the maximum efficiency control property if the core losses are negligible.

3.3 Sensored RFOC

3.3.1 Control mode block schemes (torque, speed and position mode)

Figure 3.1 shows the block diagram of the FOC for PMSM using a position encoder for the measurement of rotor position. The use of the control scheme presented in 3.1 allows torque control of the PMSM.

The instantaneous currents through the stator windings of the PMSM are measured by means of using LEM boxes. The measured currents are transformed to the two phase coordinate system fixed on the rotor by means of mathematical calculations using the *abc* to *dq* transformation. The torque command T_{eref} generates the $dq-axis$ reference currents. In this case the $d-axis$ reference current is set to $0A$ since the controlled machine is SMPMSM and the constant torque angle control property is used ($Id = 0A$ control property). The current errors generated by subtracting the values of the measured currents from the reference currents are input of the PI current controllers which outputs the $dq - axis$ reference voltages. The $dq - axis$ reference voltages are transformed to $\alpha\beta - axis$ reference values which are feed into the SVM block. The SVM block calculates the duty cycles which are applied to the VSI by taking into account the actual value of the $DC - link$ voltage.

Decoupling of the $d - axis$ is performed by means of adding the coupling term to the $d-axis$ reference voltage. The decoupling of the $q-axis$ is performed by means of subtracting the coupling term from the $q - axis$ reference voltage. The encoder interface block outputs the electrical rotor position and the mechanical speed of the machine.

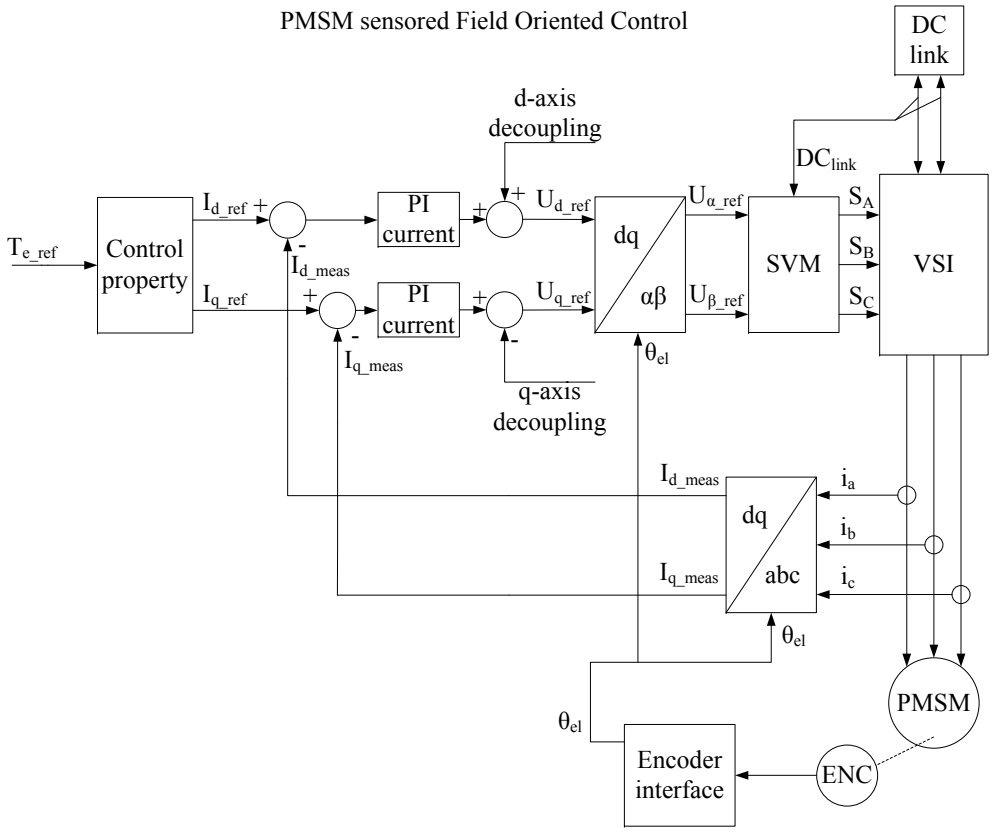

Figure 3.1: *Block diagram of the rotor flux oriented FOC for PMSM (sensored) torque control mode*

The block diagram shown in 3.2 has an added outer speed control loop which allows speed control of the PMSM. The speed reference ω_{mref} is the input set by the user. The speed error is obtained by subtracting the measured mechanical speed from the reference speed. The PI speed controller outputs the torque command T_{eref}. The machine will produce as much electromagnetic torque as it is necessary in order to maintain it's reference speed.

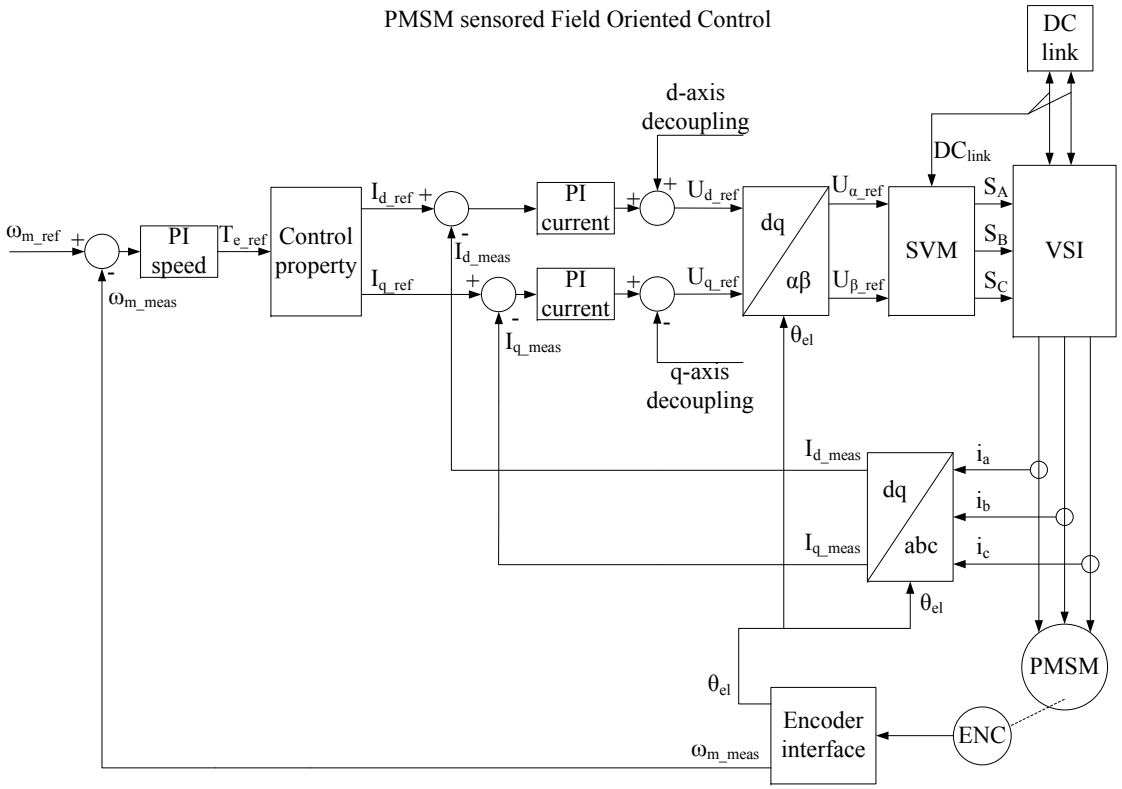

Figure 3.2: *Block diagram of the rotor flux oriented FOC for PMSM (sensored) speed control mode*

The block diagram shown in 3.3 has an added position control loop which allows mechanical position control of the PMSM. The reference position θ_{mref} is set by the user and it's values can be even more than $360deg$ mechanical. The measured mechanical position is subtracted from the reference mechanical position and the obtained error is fed into a proportional type controller which generates the speed reference ω_{mref}. When a position command is given then the mechanical speed will be increased and maintained as long as needed in order to bring the rotor to the commanded position.

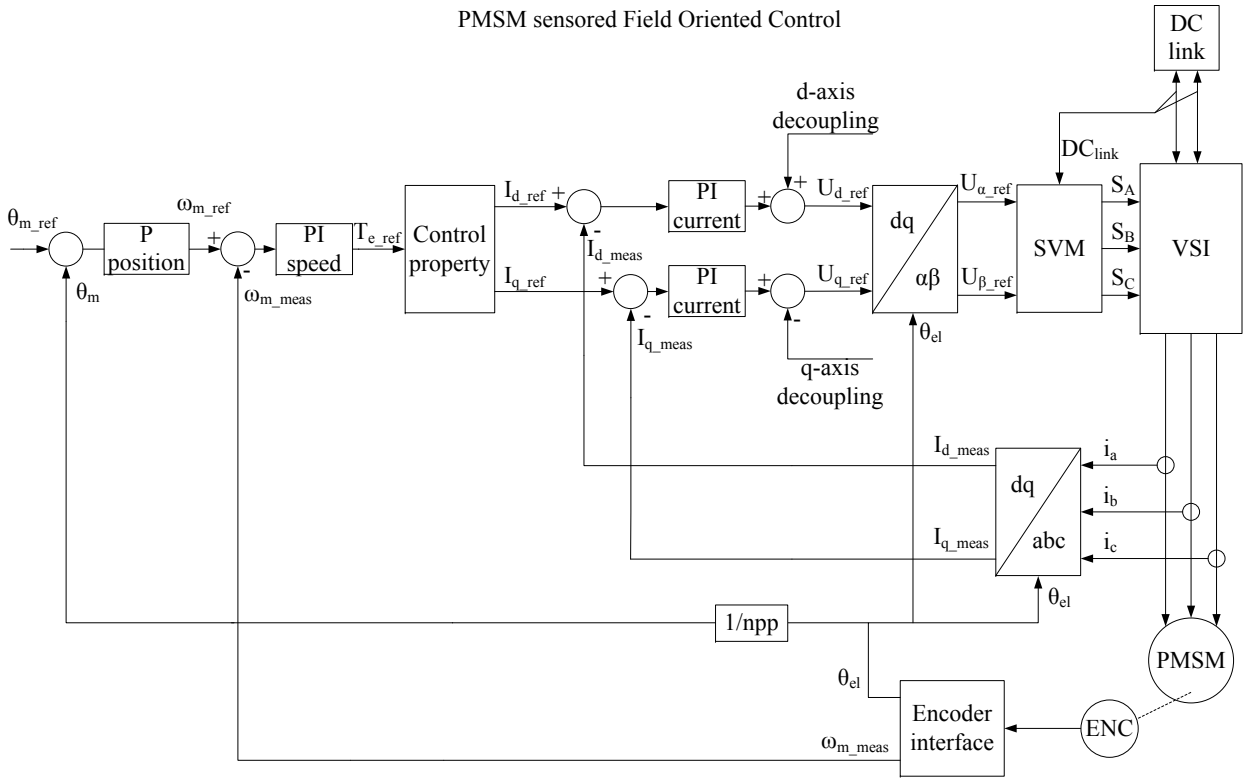

Figure 3.3: *Block diagram of the rotor flux oriented FOC for PMSM (sensored) position control mode*

3.3.2 Design of controllers

When designing the current and speed controllers the following design requirements have been considered:

- The overshoot should be lower than 10% for the current and speed controllers;
- The rise time for the current controller should be lower than 10 sampling periods ($10T_s = 2ms$);
- The rise time for the speed controller should be lower than 100 sampling periods ($100T_s = 20ms$);
- The bandwidth of the speed controller should be at least 10 times lower than the bandwidth of the current controller;

PI controllers have been chosen due to the fact that the control is realized in the rotating dq reference frame and the current and voltages become DC values during steady state thus the PI controller eliminates the steady state error. [11]

Current controllers

The d and q *axis* current controllers are identical because the machine is SMPMSM and $L_d \approx L_q$. The electrical transfer function of the PMSM is derived from the stator voltage equations in the dq reference frame.

The block diagram of the $dq-axis$ current control loops is shown in 3.4.

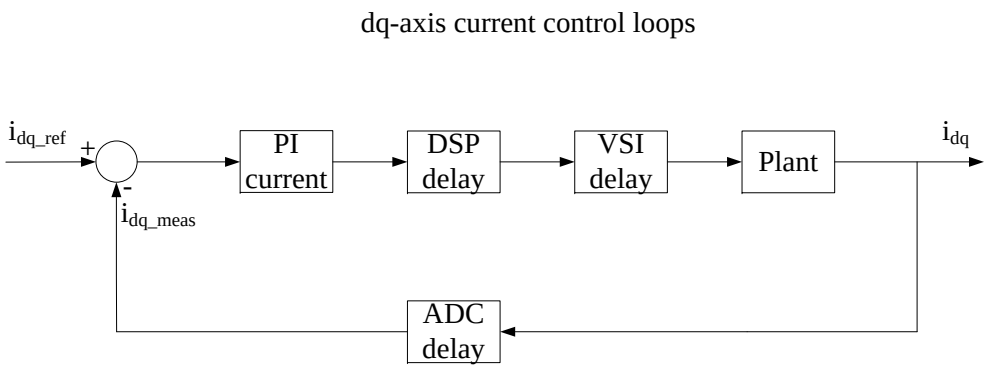

Figure 3.4: *Block diagram of the $dq-axis$ current control loops*

The different delays introduced in the system have been considered in order to make the system more realistic. In the laboratory there are different kind of delays introduced by the ADCs, filters, VSI and DSP. In 3.4 the blocks are as follows:

- **PI current** is the PI controller with the form as shown in 3.10;
- **DSP delay** is the delay introduced by the digital calculation having the form of a first order transfer function with the time constant $T_s = \frac{1}{f_s}$ as shown in 3.11 where f_s is the switching frequency ;
- **VSI delay** is the delay introduced by the voltage source inverter having the form of a first order transfer function as shown in 3.12 with the time constant $0.5T_s$;
- **Plant** is the electrical plant transfer function as shown in 3.13;
- **ADC delay** is the delay introduced by the analog to digital converter having the form of a first order transfer function as shown in 3.22 with the time constant T_s.

The transfer functions of the elements from 3.4 are the following:

$$C(s) = \frac{K_p s + K_i}{s} \tag{3.10}$$

$$D(s) = \frac{1}{T_s s + 1} = \frac{1}{0.0002s + 1} \tag{3.11}$$

$$V(s) = \frac{1}{0.5T_s s + 1} = \frac{1}{0.0001s + 1} \tag{3.12}$$

$$P(s) = \frac{1}{L_{dq} s + R_s} = \frac{1}{0.002s + 0.18} \tag{3.13}$$

$$A(s) = \frac{1}{T_s s + 1} = \frac{1}{0.0002s + 1} \tag{3.14}$$

The transfer functions of the designed continuous and discrete PI controllers are the following:

$$C(s) = \frac{2s + 180}{s} \tag{3.15}$$

$$C(z) = \frac{1.5z - 1.473}{z - 1} \tag{3.16}$$

As it may be seen in 3.5 the rise time for the current controllers is $t_{rise} = 1.15ms$ while the overshoot is $OS = 5.07\%$. The designed current controller complies with the design requirements as both the rise time and overshoot are within acceptable limits. The current settles in $t_{settling} = 3.38ms$ and the final value is 1.

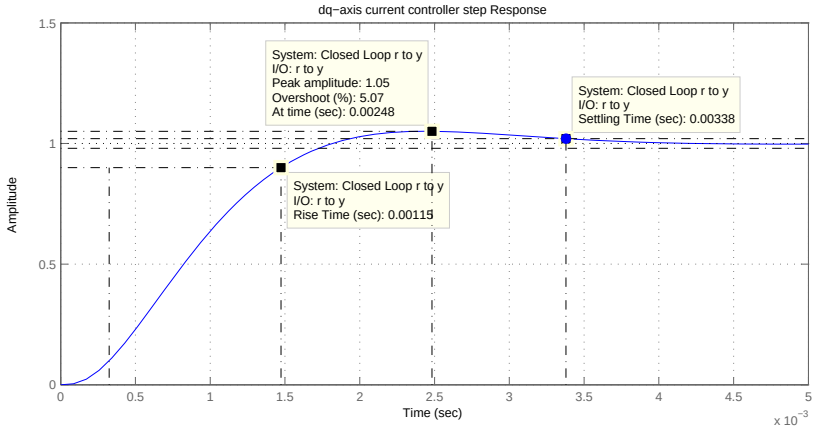

Figure 3.5: *dq − axis current control step response (continuous)*

As it may be seen in 3.6 all the poles and zeros are on the left side of the $s - plane$ indicating that the loop is stable.

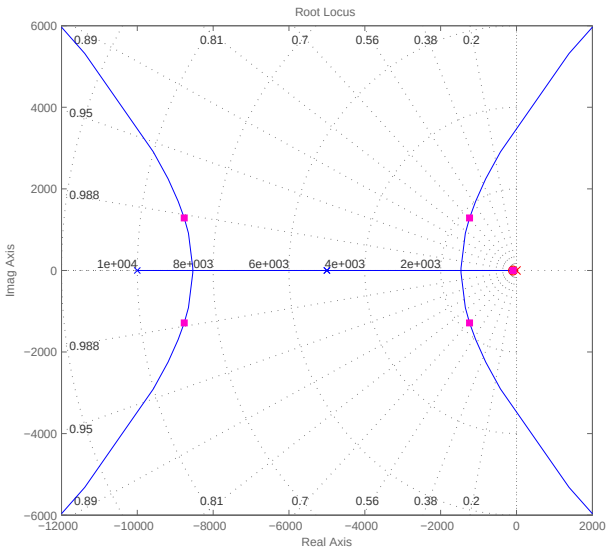

Figure 3.6: *dq − axis current control root locus (continuous)*

Figure 3.7 shows the open loop bode diagram from which the gain margin and phase margin are read to be $GM = 15dB$ and $PM = 62.8deg$. The gain margin is greater than $7dB$ and the phase margin is greater than $45deg$ indicating that the system is stable (as otherwise the root locus shows it).

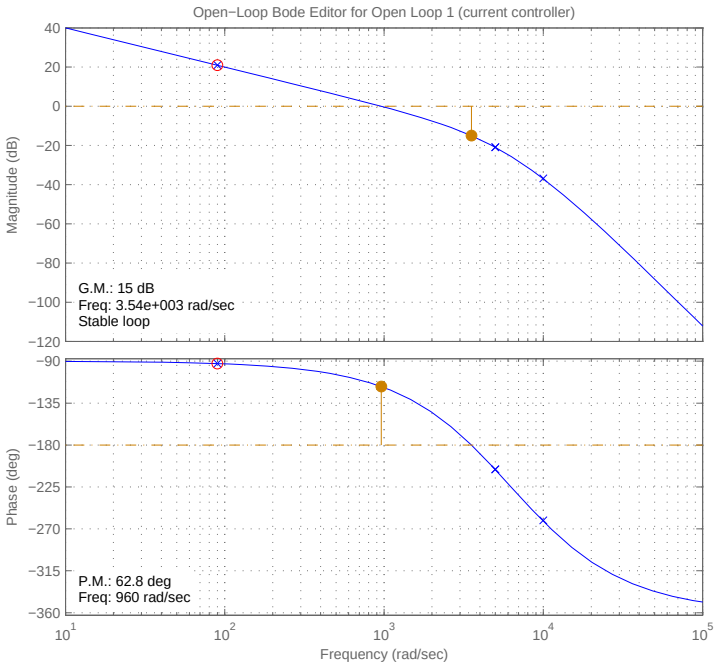

Figure 3.7: *$dq-axis$ current control open loop bode diagram (continuous)*

Figure 3.8 shows the close loop bode diagram for the speed controller from which the bandwidth is read to be $BW_{current-con} = 296Hz$.

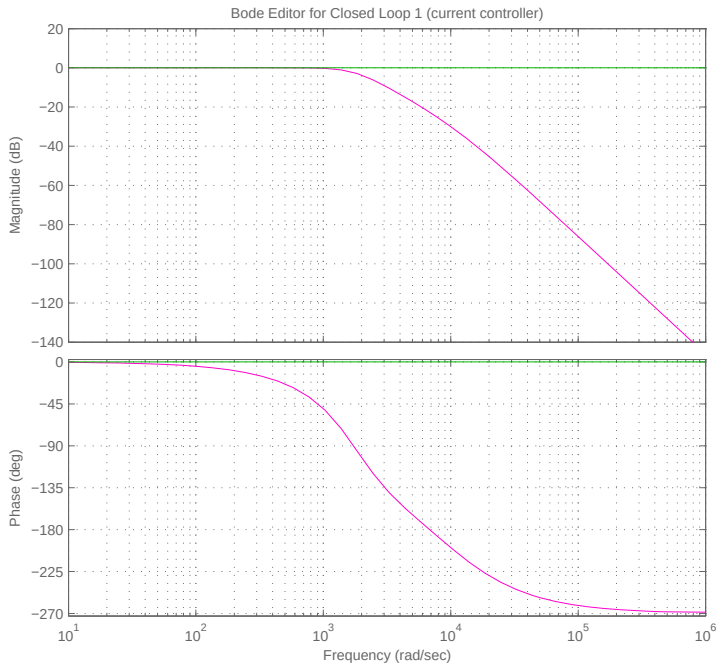

Figure 3.8: *dq − axis current control closed loop bode diagram (continuous)*

The designed continuous domain controller is discretized using *sisotool* and considering a sampling frequency of $5Khz$. Figure 3.9 shows the discrete current controller step response. The rise time is $t_{rise} = 1.39ms$ while the overshoot is $OS = 6.64\%$ both parameters respecting the design requirements. The settling time is a little bit higher than in the case of continuous domain controller being $t_{settling} = 4.3ms$. The final values is equal to 1.

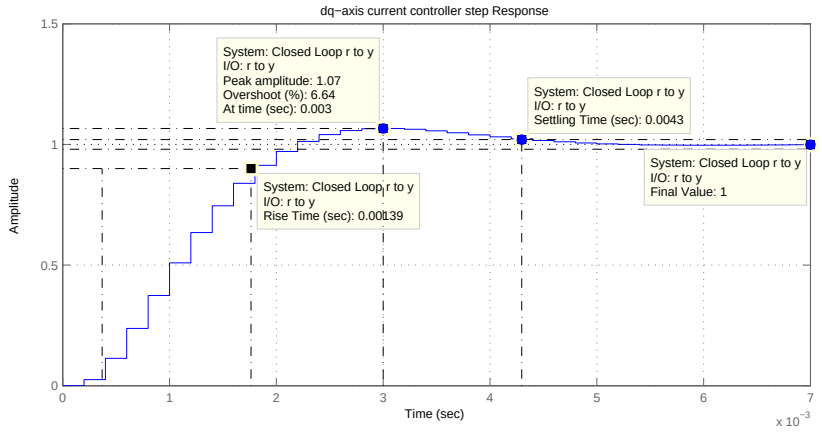

Figure 3.9: *dq − axis current control step response (discrete)*

Figure 3.10 shows the root locus for the discrete current controller. As it may be seen all the poles and zeros are inside the unity circle indicating that the system is stable.

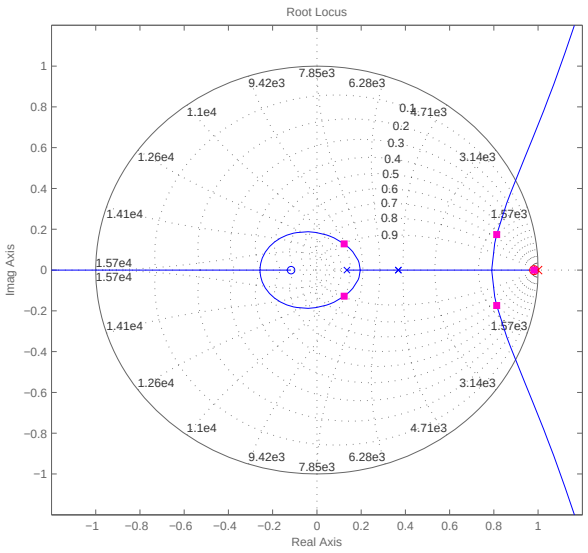

Figure 3.10: *dq − axis current control root locus (discrete)*

Speed controller

The block diagram of the speed control loop is shown in 3.11.

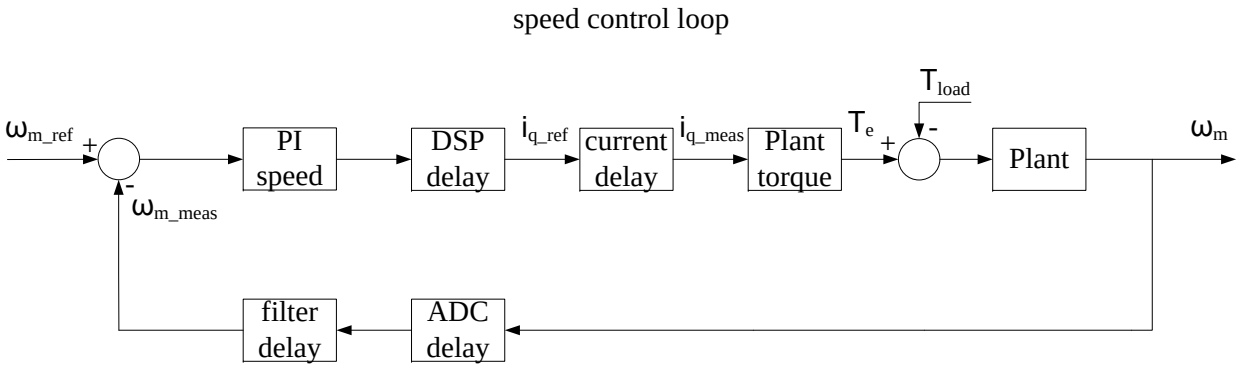

Figure 3.11: *Block diagram of the speed control loop*

During the design process of the speed controller different kind of delays have been considered in order to make the system more realistic. The considered delays are the ADC delay, speed measurement filter delay and the delay introduced by the current control loop. In 3.11 the blocks are as follows:

- **PI speed** is the PI controller with the form as shown in 3.17;
- **DSP delay** is the delay introduced by the digital calculation having the form of a first order transfer function with the time constant $T_s = \frac{1}{f_s}$ as shown in 3.18 where f_s is the switching frequency ;

- **current delay** is the delay introduced by the current control loop having the form of a first order transfer function as shown in 3.19 with the time constant T_{iq};
- **Plant torque** is the simplified torque equation having the form shown in 3.20;
- **Plant** is the mechanical plant transfer function having the form as shown in 3.21;
- **ADC delay** is the delay introduced by the analog to digital converter having the form of a first order transfer function as shown in 3.22 with the time constant T_s.
- **filter delay** is the delay introduced by the speed measurement filter having the form of a first order transfer function as shown in 3.23 with the time constant T_{filter}.

The transfer functions of the blocks shown in 3.11 are:

$$C(s) = \frac{K_p s + K_i}{s} \tag{3.17}$$

$$D(s) = \frac{1}{T_s s + 1} = \frac{1}{0.0002s + 1} \tag{3.18}$$

$$V(s) = \frac{1}{T_{iq} s + 1} = \frac{1}{0.0001s + 1} \tag{3.19}$$

$$T(s) = \frac{3}{2} n_{pp} \psi_{pm} \tag{3.20}$$

$$P(s) = \frac{1}{Js + B} = \frac{1}{0.0117s + 0.0025} \tag{3.21}$$

$$A(s) = \frac{1}{T_s s + 1} = \frac{1}{0.0002s + 1} \tag{3.22}$$

$$F(s) = \frac{1}{T_{filter} s + 1} = \frac{1}{0.796e^{-3}s + 1} \tag{3.23}$$

The transfer functions of the designed continuous and discrete PI controllers are the following:

$$C(s) = \frac{0.3s + 2.001}{s} \tag{3.24}$$

$$C(z) = \frac{0.3z - 0.2997}{z - 1} \tag{3.25}$$

Figure 5.9 shows the step response of the continuous domain speed controller. As it may be seen the rise time is equal to $t_{rise} = 19.7ms$ while the overshoot is $OS = 6.52\%$. Both the rise time and overshoot agree with the design requirements.

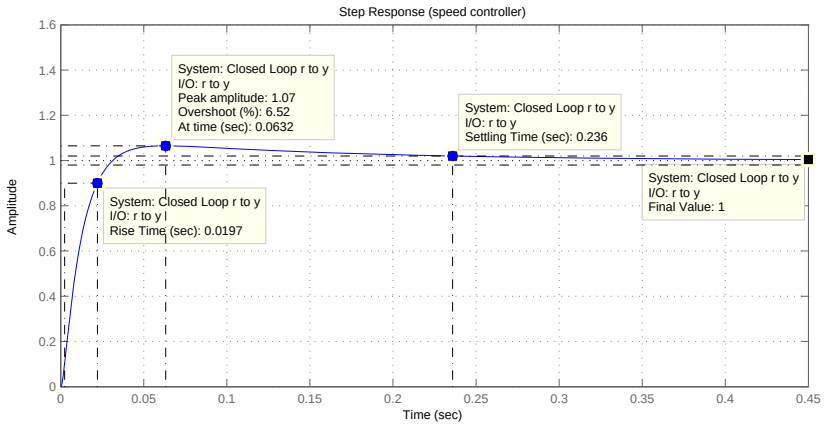

Figure 3.12: *Speed controller step response (continuous)*

Figure 3.13 shows the root locus of the continuous domain speed controller. As it may be seen all the poles and zeros are on the left side of the $s - plane$ indicating that the system is stable.

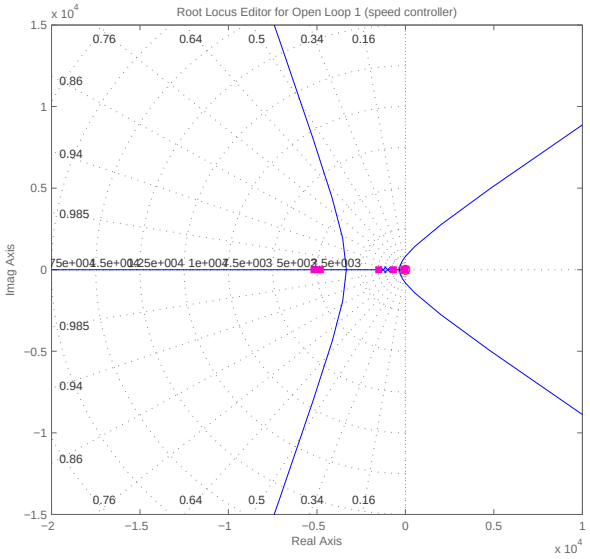

Figure 3.13: *Speed controller root locus (continuous)*

Figure 3.14 shows the open loop bode diagram from which the gain margin and phase margin are read to be $GM = 24.4dB$ and $PM = 75.6deg$. The gain margin is greater than $7deg$ and the phase margin is greater than $45deg$ indicating that the system is stable.

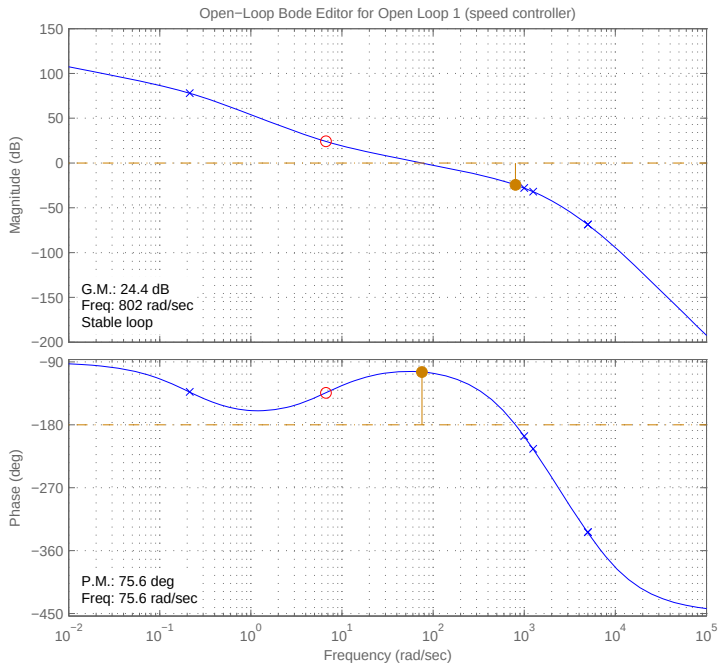

Figure 3.14: *Speed controller open loop bode diagram (continuous)*

Figure 3.15 shows the close loop bode diagram for the continuous domain speed controller from which the bandwidth is read to be $BW_{speed-con} = 15.9Hz$. As the bandwidth of the continuous domain current controller is $BW_{currentcon} = 296Hz$, the ration between the current and speed controller bandwidths is $\frac{296}{15.9} = 18.6$ which respects the design requirements.

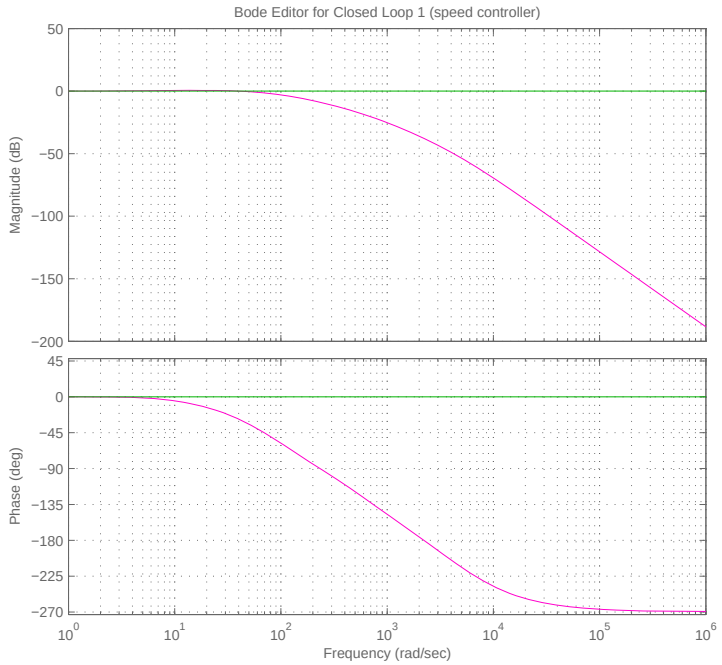

Figure 3.15: *Speed controller closed loop bode diagram (continuous)*

The continuous domain speed controller is discretized using *sisotool* with a frequency of $5Khz$. Figure 3.16 shows the step response of the discretized speed controller. The rise time is $t_{rise} = 19.3ms$ and the overshoot is $OS = 6.57\%$. Both the rise time and overshoot respect the design requirements.

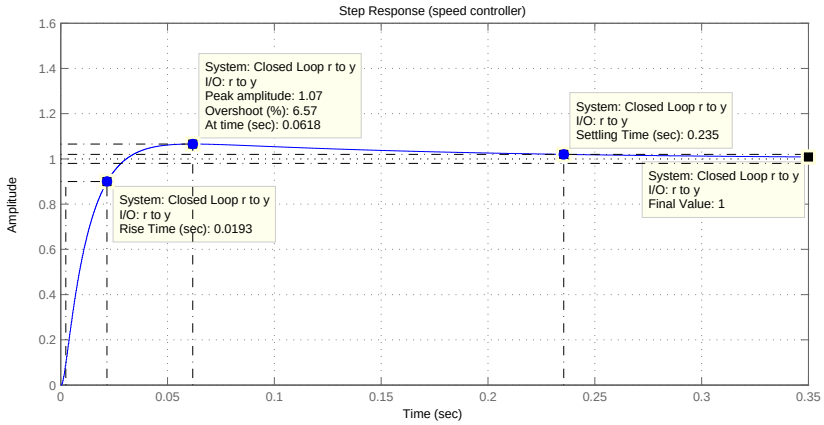

Figure 3.16: *Speed controller step response (discrete)*

Figure 3.17 shows the root locus of the discrete domain speed controller. As it may be seen all the poles are inside the unity circle indicating that the system is stable.

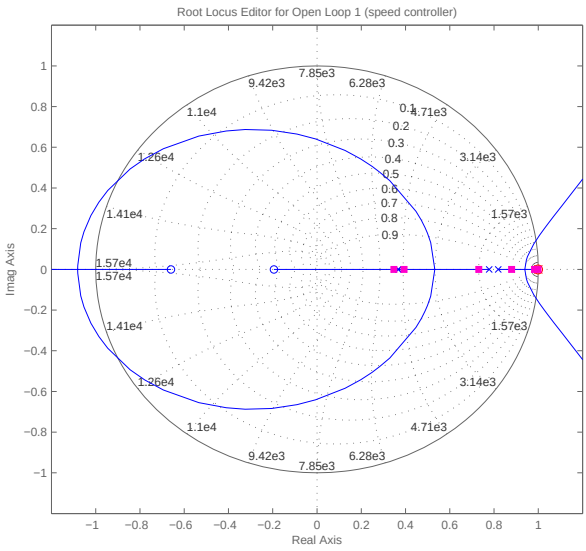

Figure 3.17: *Speed controller root locus (discrete)*

3.4 Sensorless RFOC

3.4.1 Control mode block schemes (torque, speed and position mode)

Figure 3.18 shows the block diagram of the FOC for PMSM without the use of a position encoder estimating the rotor position by means of high frequency signal injection. The use of the control scheme presented in 3.1 allows sensorless torque control of the PMSM. The block diagram presented in 3.18 is similar to the one from 3.1 with the difference that now the rotor position is estimated instead of being measured.

As it may be seen in 3.18 there is high frequency voltage signal injected on the $d-axis$ basically the high frequency voltage is added to the $d-axis$ reference voltage. This injected voltage creates a current on the $d-axis$ which is the flux axis so it has little influence on the produced electromagnetic torque. The measured $dq-axis$ current are low pass filtered in order remove the high frequency signal from the currents which may interfere with the control of the PMSM. A measurement $dmqm-axis$ reference frame is created $-45deg$ electrical in relation to the $dq-axis$. The measured $dmqm-axis$ currents are band pass filtered and then their magnitudes is calculated by a process called heterodyning. By substracting the magnitudes of the $dmqm-axis$ currents an error signal $Ymdiff$ is obtained. The obtained error signal is the input in the PI compensator which outputs the estimated electrical speed. From the estimated electrical speed the electrical rotor position is obtained by means of integration. The PI compensator tries to lock the estimated position to the real position like a PLL. [2]

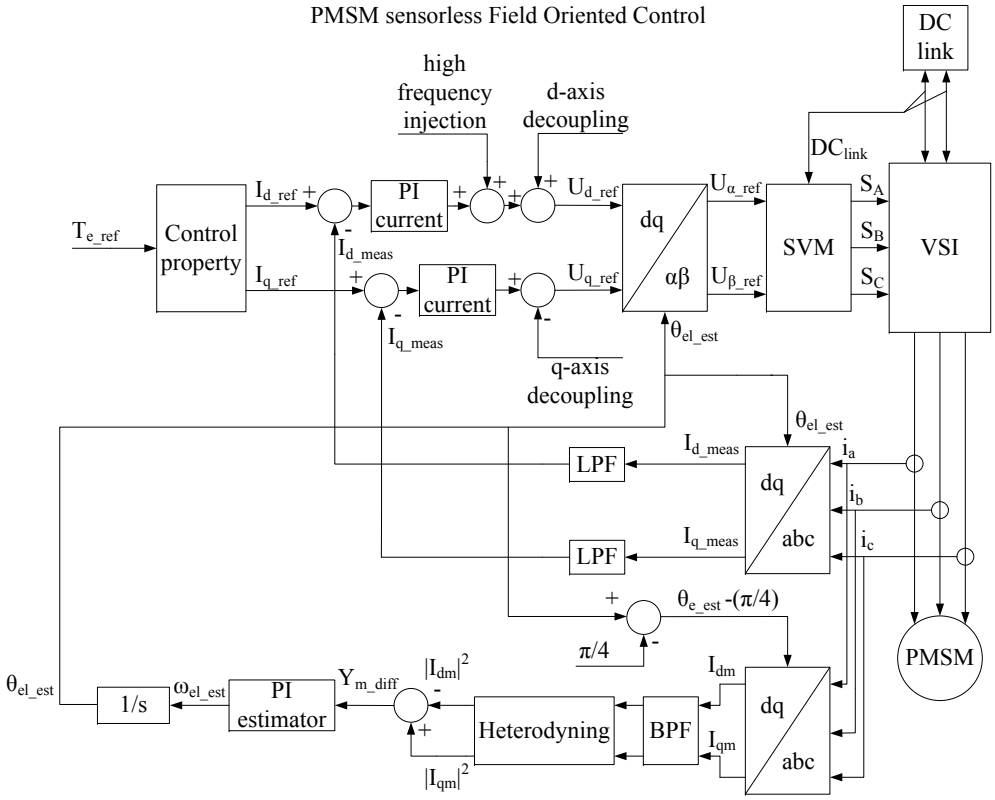

Figure 3.18: *Block diagram of the rotor flux oriented FOC for PMSM (sensorless) torque control mode*

Figure 3.19 shows the block diagram of the sensorles RFOC used for speed control mode. In this case the mechanical speed is obtained from the estimated electrical speed by means of dividing it with the number of pole pairs and low-pass filtering it in order to eliminate the noise. Otherwise this block diagram is similar to the previous one where torque control was possible withe the difference that now a outer speed loop is added. The speed controller generate as much reference torque as it is needed in order to overcome the load torque and maintain the reference speed.

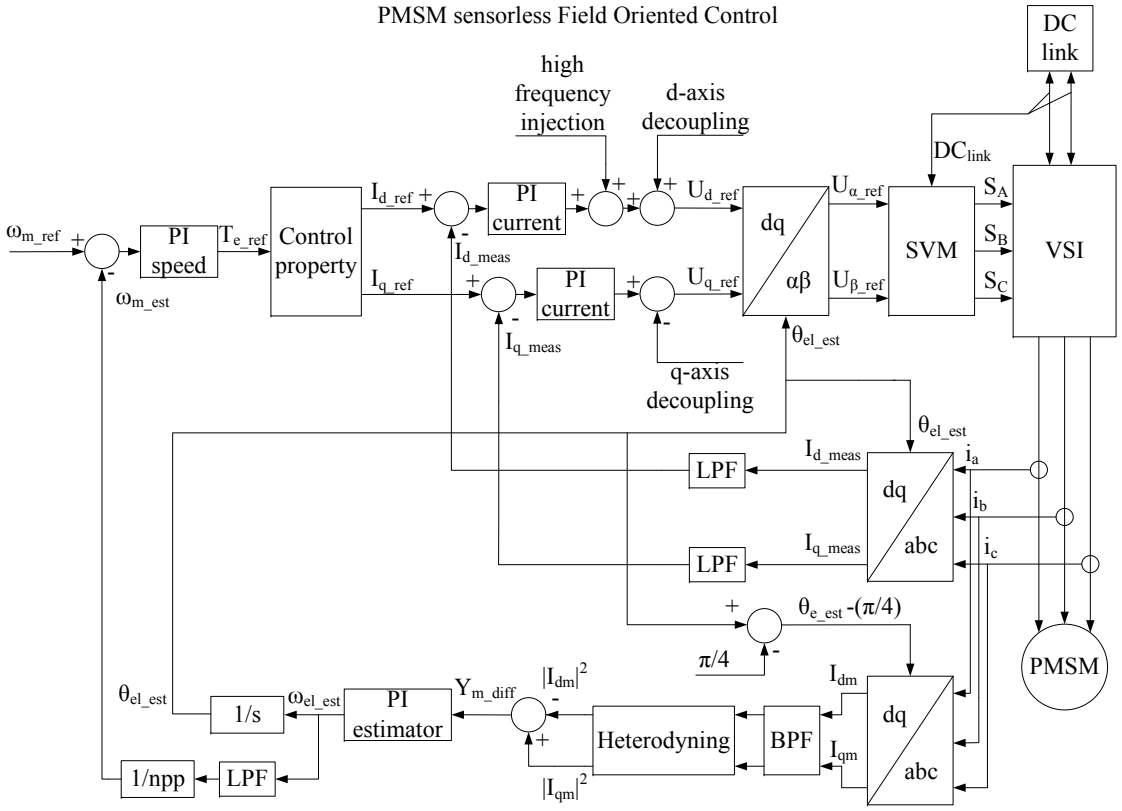

Figure 3.19: *Block diagram of the rotor flux oriented FOC for PMSM (sensorless) speed control mode*

Figure 3.20 shows the block diagram of the sensorles RFOC used for position control. In this case an extra outer position loop is added which is closed with the estimated mechanical rotor position. The mechanical rotor position is calculated from the electrical rotor position with the pole pair relation. The position controller is a simple proportional controller which outputs the reference speed when a position command is given. The gain of the proportional controller determines the response speed.

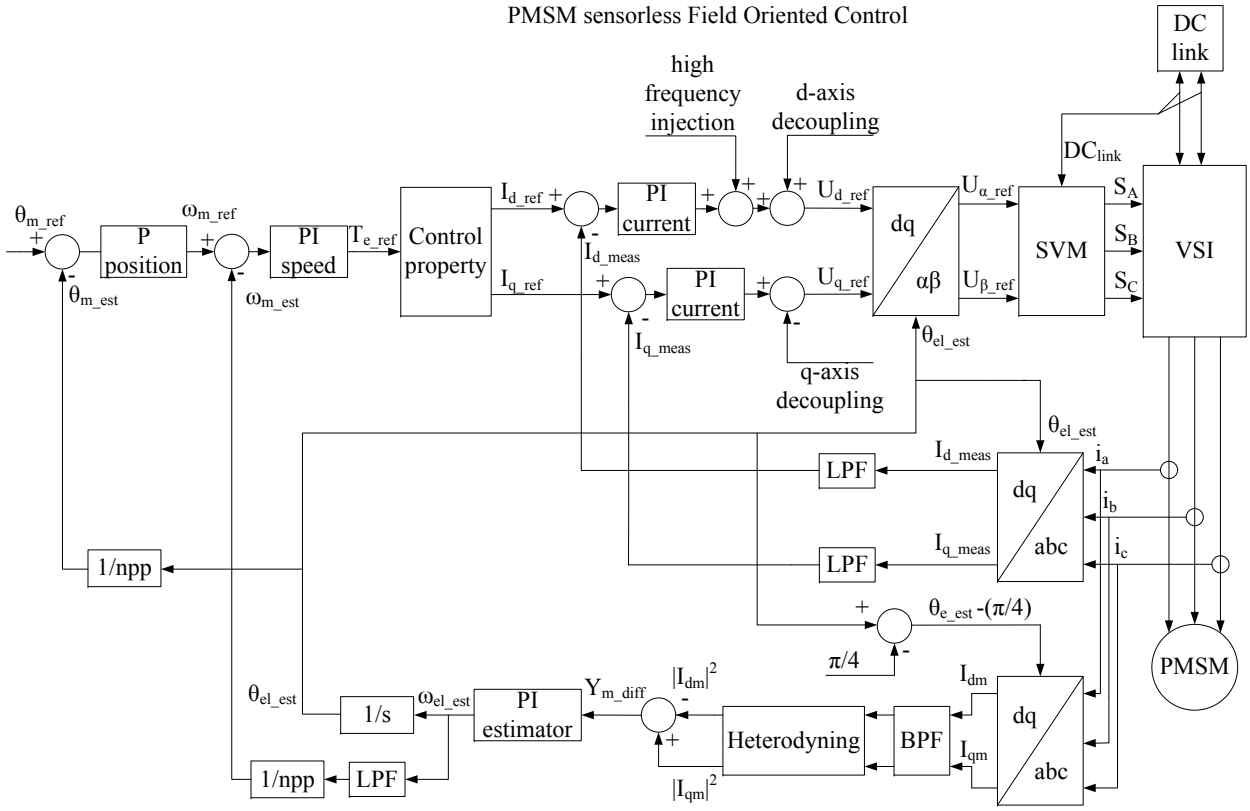

Figure 3.20: *Block diagram of the rotor flux oriented FOC for PMSM (sensorless) position control mode*

3.4.2 Detuning of controllers

In the case of this sensorless control algorithm low-pass filers must be used on the current measurement feedback path in order to eliminate the high frequency component ($500Hz$) of the current which may interfere with the normal operation of the control. As the filters introduce delay, the bandwidth of the current controllers needs to be reduced, being much lower than the bandwidth of the current controllers in the case of the sensored control. If the bandwidth of the current controllers is not reduced than a situation of over-current appears due to the fact that the current controller increases the reference current to a high value because of the delay of the feedback signal. With other words said the current feedback signal needs some time to pass through the low-pass filters on the current feedback path. The low-pass filters on the current feedback path may be seen in 3.18. The bandwidth of the detuned current controller is around $50Hz$. As a consequence of the slower current controllers the bandwidth of the speed controller also needs to be reduced.

3.4.3 Choosing the filters

There are several filters used in this sensorless control algorithm. First there are the low-pass filters on the current feedbask path as shown in 3.18 which have the purpose to eliminate the high frequency signal from the measured $dq - axis$ currents. Second there is the band-pass filters which have the purpose to remove any DC component from the measurement signals

and any high frequency noise and let to pass only the $500Hz$ component. In the heterodyning block there are also low-pass filters which are used in the algorithm to calculate the magnitude of the input signals. In this thesis emphasis on the design of the filters was not placed instead the already designed filters found in the reference list has been used. [2] The low-pass filters used on the current feedback path have the cutout frequency of $100Hz$. The band-pass filters have the cut-out frequencies of $100Hz$ and $2400Hz$.

3.5 Summary

This chapter presents the mathematical model of the PMSM followed by a discussion about control methods for PMSM. Scalar control, DTC and FOC are presented. The most common control properties for FOC are presented and discussed. The block diagram of sensored and sensorless control scheme for PMSM for torque, speed and position control mode are presented. The design of the current and speed controllers are shown for the sensored RFOC. The detuning of the controllers is discussed. This chapter ends with the filter choosing part.

Chapter 4

Modeling and Simulation

This chapter presents the simulation results for the sensored and sensorless RFOC. Several study cases are considered and discussed both for sensored and sensorless control strategies.

The modeling of the sensored and sensorless control is carried out in *Matlab/Simulink* and *Plecs*. A machine model is used from *Plecs* and the parameters of the SMPMSM which are partly given in the data sheet and partly determined from laboratory experiments are used in the model. The VSI model is not used in the simulations partly that is the reason why the simulation results look different from the laboratory results. The parameters of the SMPMSM are given in the apendix at section A.

4.1 Sensored RFOC simulation results

In this section the simulation results for the sensored direct field oriented control of SMPMSM are presented. In this case the SMPMSM is closed loop vector controlled using the position feedback given by an encoder.

Zero speed command with $8Nm$ (40%) load torque steps

In this study case the PMSM's reference speed is kept at $0rpm$ and at $0s$ a step load torque of $8Nm$ is applied. The idea is to see how well the PMSM maintains it's reference speed. Figure 4.1 shows the reference and measured speed. The reference speed is $0rpm$ during the test while the measured speed decreases when the load torque is applied to about $-58rpm$ when the step load torque is applied. The measured speed settles again at $0rpm$ in about $0.8s$. When the load torque is removed the measured speed increases to about $58rpm$ and settles again at $0rpm$ in about $0.8s$. The measured speed deviates from the reference speed during transient periods but it maintains it's reference speed in steady state also during loading.

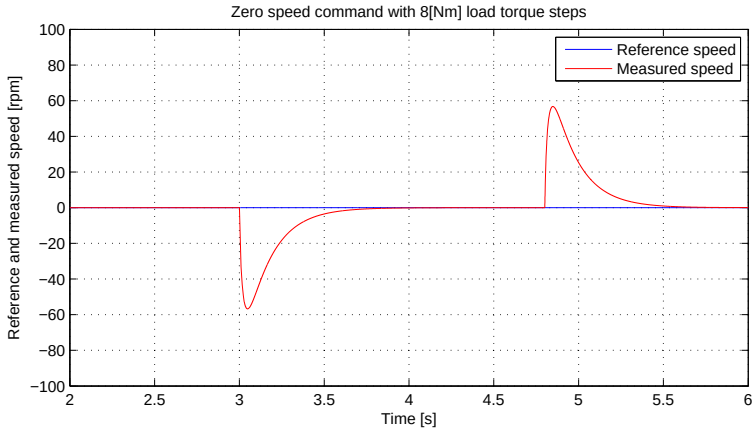

Figure 4.1: *PMSM reference and measured mechanical speed in the case of zero speed command with* $8Nm$ *(*40%*) load torque step applied at* $3s$ *and removed at* $4.8s$ *(simulated sensored control)*

Figure 5.11 shows the load torque produced profile applied to the PMSM. At $3s$ the load torque steps from $0Nm$ to $8Nm$ and at $4.8s$ it steps back to $0Nm$.

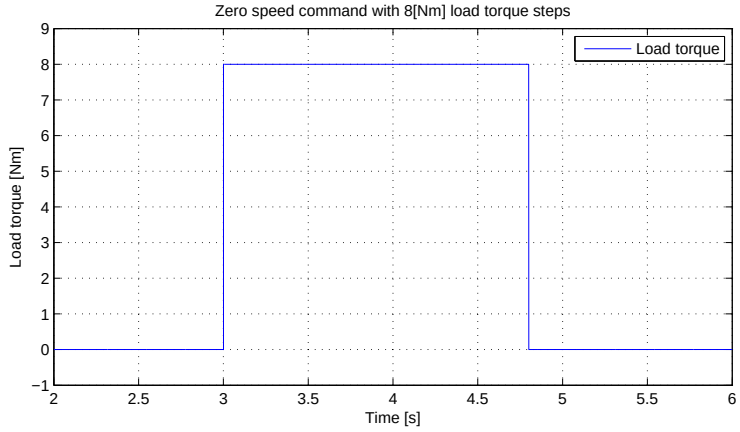

Figure 4.2: *Estimated load torque produced by the IM in the case of zero speed command with* $8Nm$ *(*40%*) load torque step applied at* $3s$ *and removed at* $4.8s$ *(simulated sensored control)*

Figure 4.3 shows the PMSM's $dq-axis$ currents. The $dq-axis$ currents look as expected, both currents have magnitudes of almost $0A$ in the case of no load and only the $q-axis$ current increases during loading of the PMSM. The $d-axis$ current is always $0A$ as expected, only during transient periods when the load torque is applied it deviates from $0A$. The $q-axis$ current settles at about $11.2A$ during loading.

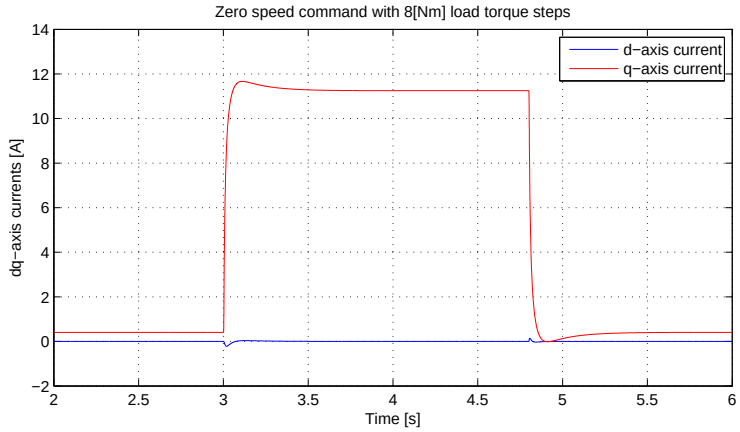

Figure 4.3: *PMSM dq-axis currents in the case of zero speed command with* $8Nm$ *(*40%*) load torque step applied at* $3s$ *and removed at* $4.8s$ *(simulated sensored control)*

Constant $25rpm$ speed command with $8Nm$ (40%) load torque steps

In this study case the PMSM's reference speed is kept at constant $25rpm$ while a load torque of $8Nm$ (40%) is applied in step fashion at $3s$ and removed at $4.8s$. As it may be seen in figure 4.4 the measured speed decreases to about $-30rpm$ during the application of the load torque step and goes back to reference again in about $0.9s$. When the load torque is removed, the measured speed increases to about $82rpm$ and goes back to reference in $0.9s$

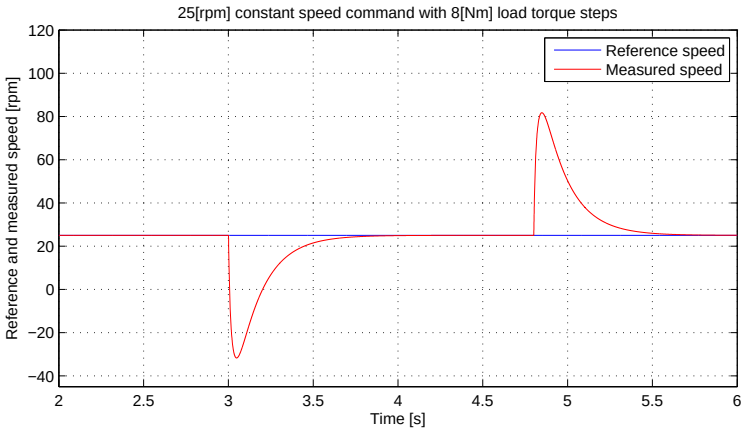

Figure 4.4: *PMSM reference and measured mechanical speed in the case of constant* $25rpm$ *speed command with* $8Nm$ *(*40%*) load torque step applied at* $3s$ *and removed at* $4.8s$ *(simulated sensored control)*

Figure 5.14 the load torque profile. It increases from 0 to $8Nm$ at $3s$ and decreases to 0 again at $4.8s$.

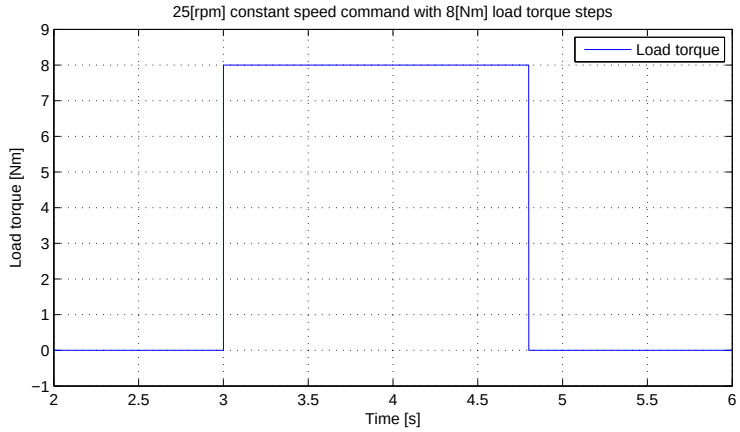

Figure 4.5: *Load torque profile in the case of constant* $25rpm$ *speed command with* $8Nm$ *(40%) load torque step applied at* $3s$ *and removed at* $4.8s$ *(simulated sensored control)*

Figure 4.6 shows the $dq-axis$ currents. The $d-axis$ current is close to zero while the $q-axis$ current increases to about $11.2A$ during the loading period.

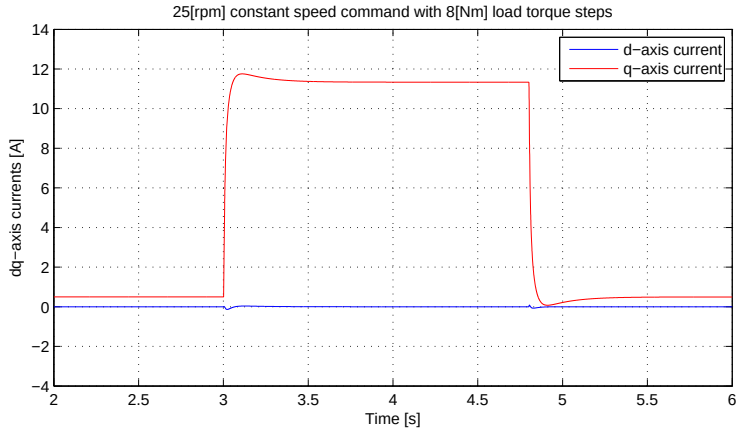

Figure 4.6: *PMSM dq-axis currents in the case of constant* $25rpm$ *speed command with* $8Nm$ *(40%) load torque step applied at* $3s$ *and removed at* $4.8s$ *(simulated sensored control)*

$200rpm$ trapezoidal speed command with no load torque

In this study case the speed reference is changed from 0 to $200rpm$ and then back to 0 in a ramp fashion with the rate of change of $1000rpm/s$. The load torque is $0Nm$ during this study case. Figure 4.7 shows the reference and measured speed. The measured speed follows the reference and there is a speed overshoot of about 5% which is low.

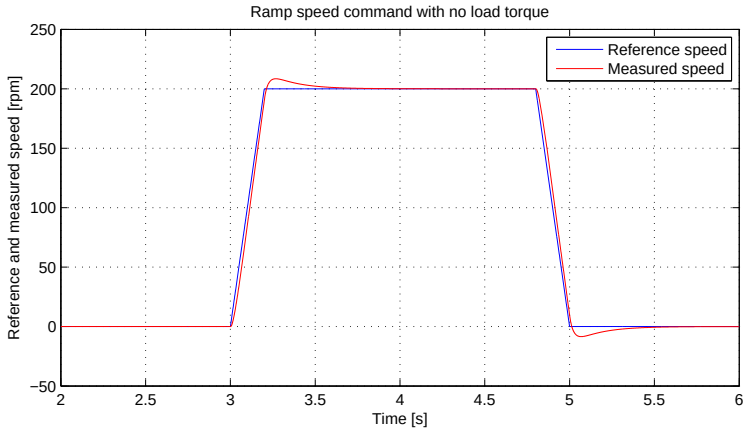

Figure 4.7: *PMSM reference and measured mechanical speed in the case of* $200rpm$ *trapezoidal speed command with no load torque (simulated sensored control)*

Figure 4.8 shows the dq-axis currents. The $d-axis$ current is close to zero as expected while the $q-axis$ current increases during the speed changing period to about $3.4A$ peak.

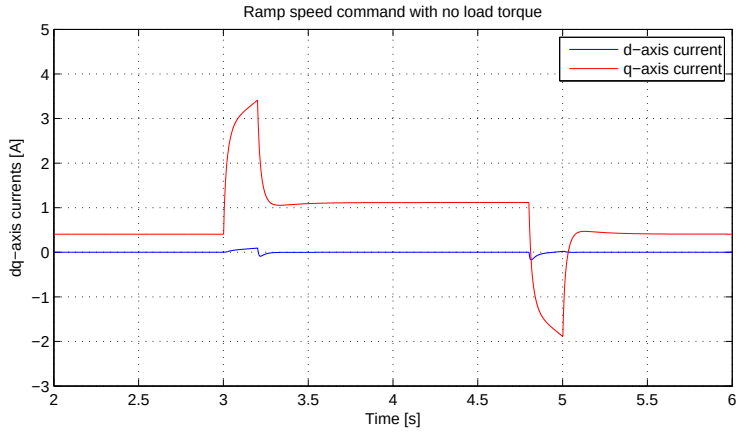

Figure 4.8: *PMSM dq-axis currents in the case of* $200rpm$ *trapezoidal speed command with no load torque (simulated sensored control)*

$200rpm$ trapezoidal speed command with $8Nm$ (40%) constant load torque

In this study case the speed reference is changed from 0 to $200rpm$ and then back to 0 in a ramp fashion with the rate of change of $1000rpm/s$. The load torque is constant $8Nm$ during this study case. Figure 4.9 shows the reference and measured speed. The measured speed follows the reference and there is a speed overshoot of about 5% which is small.

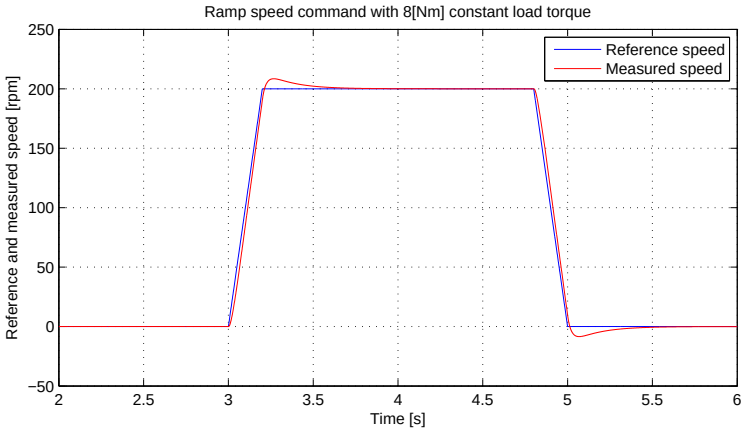

Figure 4.9: *PMSM reference and measured mechanical speed in the case of* $200rpm$ *trapezoidal speed command with* $8Nm$ *(40%) constant load torque (simulated sensored control)*

Figure 4.10 shows the $dq-axis$ currents. The $d-axis$ current has a magnitude of about $11.2A$ during zero speed operation and increases to about $12A$ during the $200rpm$ steady state operation. During the first transient period the $q-axis$ current increases to $14.4A$ because more torque than the actual load torque is needed to increases the speed of the machine and it decreases to $9A$ during the second transient period as less electromagnetic torque than the actual load torque is needed in order to reduce the speed of the machine.

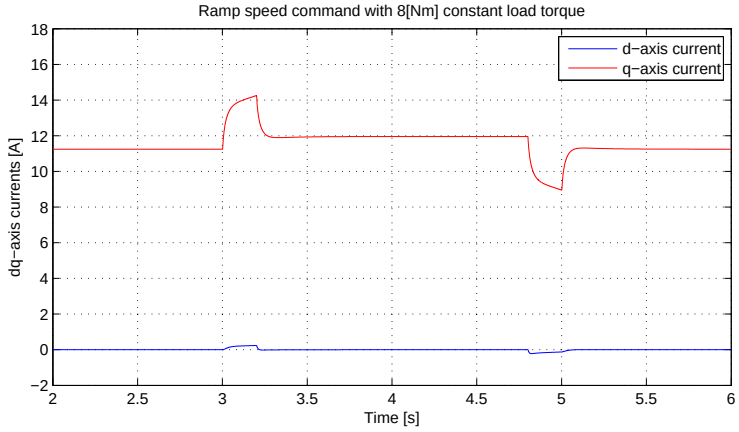

Figure 4.10: *PMSM dq-axis currents in the case of* $200rpm$ *trapezoidal speed command with* $8Nm$ *(40%) constant load torque (simulated sensored control)*

$25rpm$ speed reversal command with $8Nm$ (40%) constant load torque

In this study case the speed reference is changed from $-25rpm$ to $25rpm$ in a ramp fashion with the rate of change of $1000rpm/s$. The load torque is constant $8Nm$ during this study case. Figure 4.11 shows the reference and measured speed. The measured speed follows the reference and there is a small speed overshoot and a small speed error during the reference speed changing.

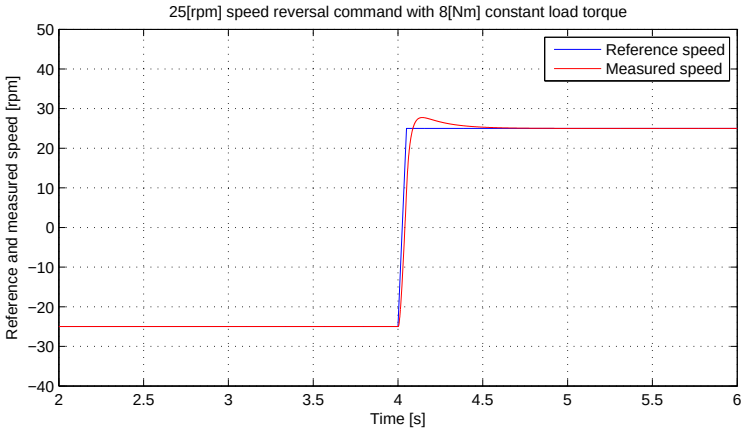

Figure 4.11: *PMSM reference and measured mechanical speed in the case of* $25rpm$ *speed reversal command with* $8Nm$ *(40%) constant load torque (simulated sensored control)*

Figure 4.12 shows the $dq-axis$ currents. The $d-axis$ current is almost $0A$ during the whole period. The $q-axis$ current is about $11.2A$ during the $-25rpm$ speed operation and about 11.4 during the $25rpm$ operation. During the transient period the $q-axis$ current increases to about $13.4A$.

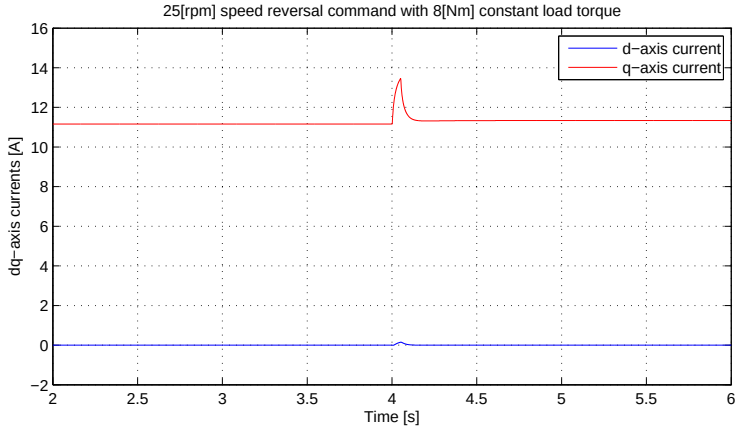

Figure 4.12: *PMSM dq-axis currents in the case of* $25rpm$ *speed reversal command with* $8Nm$ *(40%) constant load torque (simulated sensored control)*

4.2 Sensorless RFOC simulation results

In this section the simulation results from the sensorless RFOC are presented for the same study cases as in the case of sensored control.

Zero speed command with $8Nm$ (40%) load torque steps

In this study case the reference speed is maintained at zero while the load torque is changed in step fashion from 0 to $8Nm$ and then back to $0Nm$. Figure 4.13 shows the reference, measured and estimated speed. The measured and estimated speed decreases to about $-70rpm$ when the load torque is applied. When the load torque is removed the measured an estimated

speed increases to about $70rpm$. During steady state the measured and estimated speed is close to the reference speed.

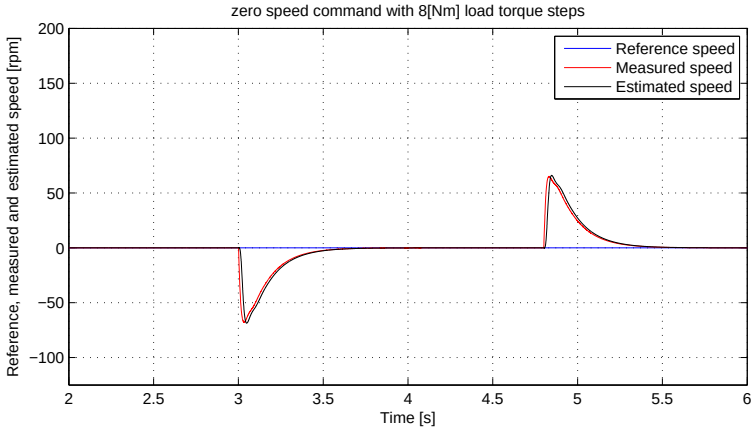

Figure 4.13: *PMSM reference, measured and estimated mechanical speed in the case of zero speed command with* $8Nm$ *(40%) load torque step applied at* $3s$ *and removed at* $4.8s$ *(simulated sensorless control)*

Figure 4.14 shows the estimated load torque profile used to load the PMSM. The load torque is increased from 0 to $8Nm$ at $3s$ and decreased back to $0Nm$ at $4.8s$.

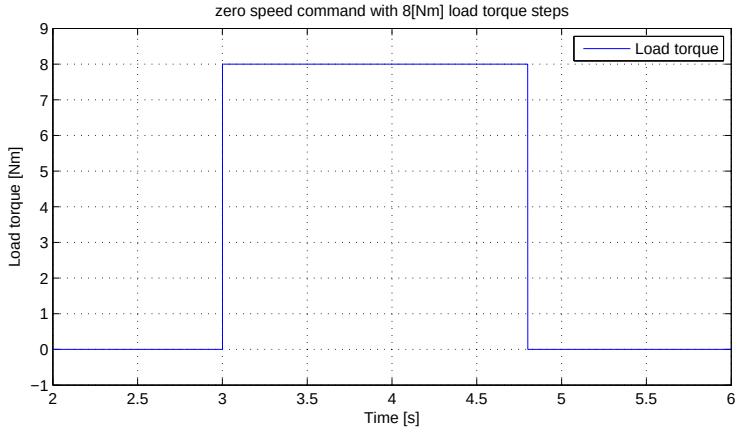

Figure 4.14: *Estimated load torque produced by the IM in the case of zero speed command with* $8Nm$ *(40%) load torque step applied at* $3s$ *and removed at* $4.8s$ *(simulated sensorless control)*

Figure 4.15 shows the $dq-axis$ currents. The $d-axis$ current looks different than the one from the sensored study case because here the $500Hz$ current caused by the $45V$ injection voltage may be seen all the time on the $d-axis$. The $q-axis$ current looks similar to the one in the sensored case with the exception that in the sensorless case there are higher oscillations especially during transient periods. The oscillations are caused by the rotor position estimation error. When there is an error in the rotor position estimation than the $q-axis$ current needs to be higher in order to produce the same electromagnetic torque as in the case of correct position estimation. When there is an error in the rotor position estimation than a current command on the $q-axis$ may produce current on the real $d-axis$ thus reducing the electromagnetic torque.

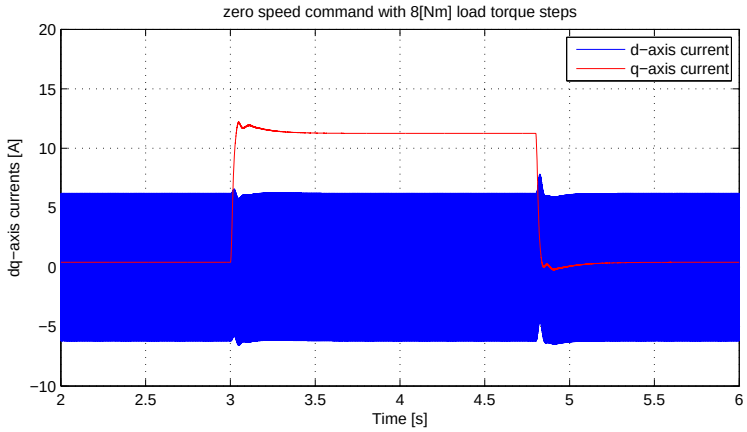

Figure 4.15: *PMSM dq-axis currents in the case of zero speed command with* $8Nm$ *(40%) load torque step applied at* $3s$ *and removed at* $4.8s$ *(simulated sensorless control)*

Figure 4.16 shows the speed estimation error in rpm. During steady state operation the speed estimation error is quite small and it peaks out at about $45rpm$ during the first transient period and $-45rpm$ during the second transient period.

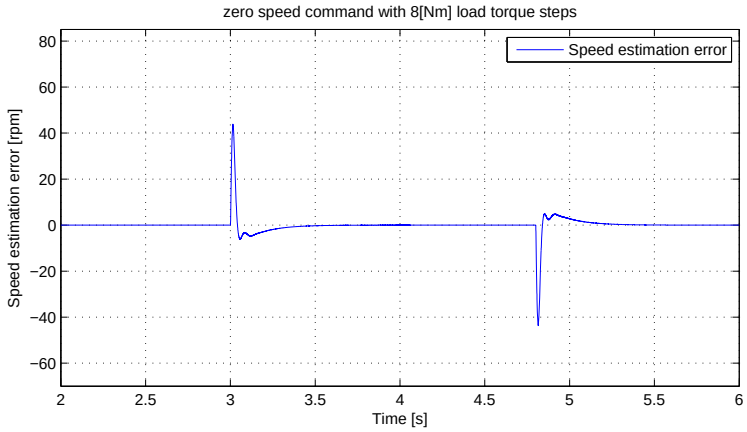

Figure 4.16: *Speed estimation error in the case of zero speed command with* $8Nm$ *(40%) load torque step applied at* $3s$ *and removed at* $4.8s$ *(simulated sensorless control)*

Figure 4.17 shows the electrical rotor position estimation error in deg. During zero speed operation with no load torque the estimation error is close to $0deg$. The electrical rotor position estimation error reaches about $13deg$ during the first transient period (when the load torque is applied) and $-13deg$ during the second transient period (when the load torque is removed).

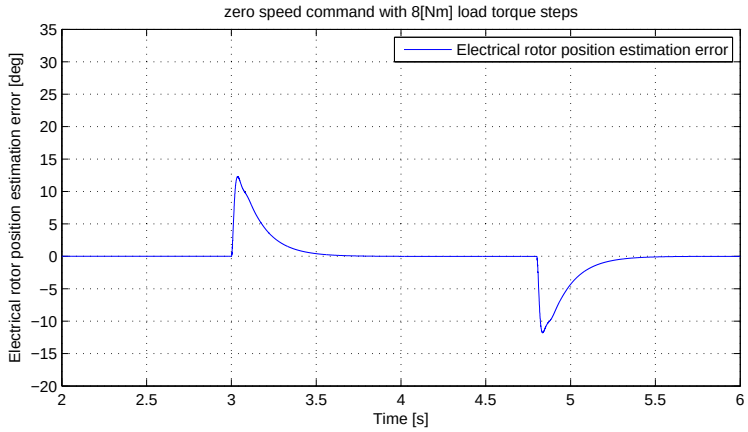

Figure 4.17: *Electrical rotor position estimation error in the case of zero speed command with* $8Nm$ *(*40%*) load torque step applied at* $3s$ *and removed at* $4.8s$ *(simulated sensorless control)*

Constant $25rpm$ speed command with $8Nm$ (40%) load torque steps

In this study case the reference speed is maintained at $25rpm$ while the load torque is changed in step fashion from 0 to $8Nm$ and then back to $0Nm$. Figure 4.18 shows the reference, measured and estimated speed. The measured and estimated speed decreases to about $-48rpm$ when the load torque is applied. When the load torque is removed the measured an estimated speed increases to about $98rpm$. During steady state the measured and estimated speed is close to the reference speed especially during loading when the oscillations are much smaller than during no load.

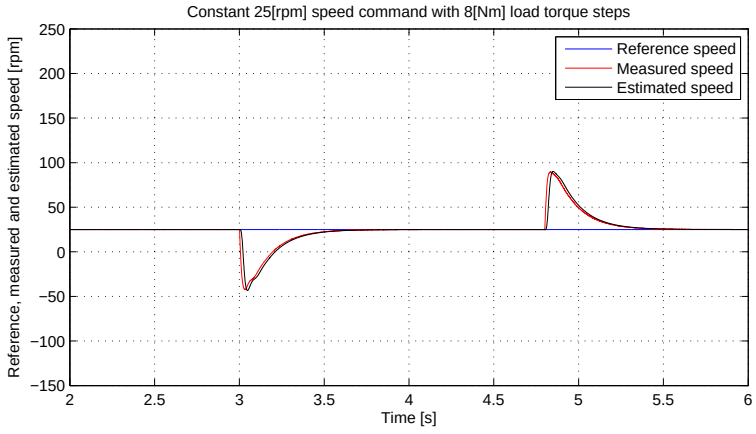

Figure 4.18: *PMSM reference, measured and estimated mechanical speed in the case of constant* $25rpm$ *speed command with* $8Nm$ *(*40%*) load torque step applied at* $3s$ *and removed at* $4.8s$ *(simulated sensorless control)*

Figure 4.19 shows the load torque profile. The load torque has the same profile as in the previous study cases.

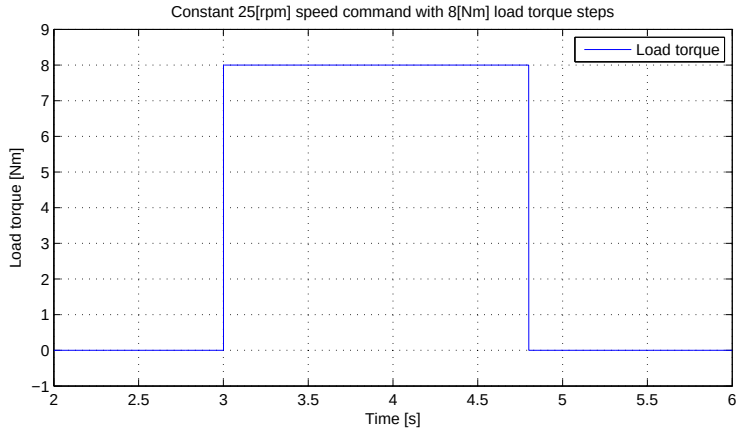

Figure 4.19: *Estimated load torque produced by the IM in the case of constant* $25rpm$ *speed command with* $8Nm$ *(*40%*) load torque step applied at* $3s$ *and removed at* $4.8s$ *(simulated sensorless control)*

Figure 4.20 shows the $dq-axis$ currents. The $d-axis$ current contains only the $500Hz$ injection component while the $q-axis$ current increases to about $12A$ during steady $25rpm$ operation. For the sensorless control the $q-axis$ current peaks at $12.5A$ when the load torque is applied.

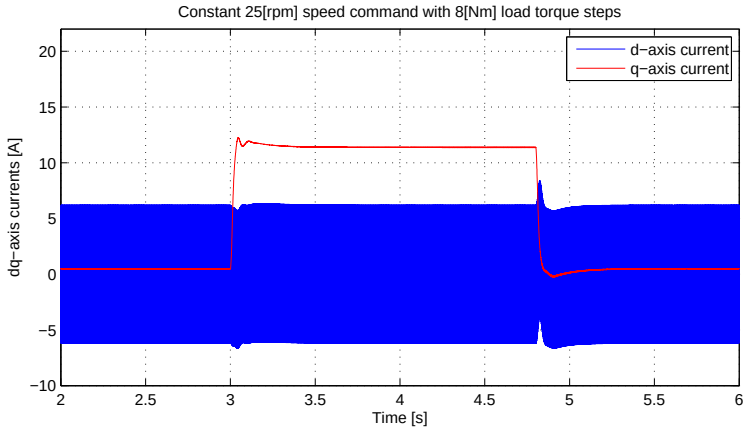

Figure 4.20: *PMSM dq-axis currents in the case of constant* $25rpm$ *speed command with* $8Nm$ *(*40%*) load torque step applied at* $3s$ *and removed at* $4.8s$ *(simulated sensorless control)*

Figure 4.21 shows the speed estimation error during this study case. There is a peak value of $45rpm$ speed error during the first transient period and $45rpm$ during the second transient period. During steady state unloaded operation the speed error is zero.

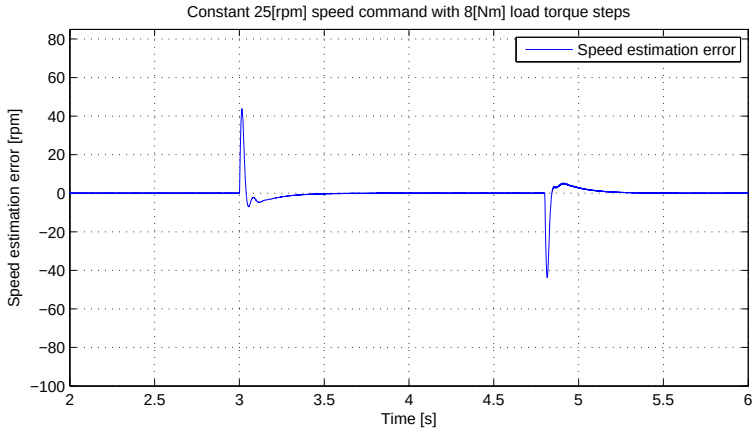

Figure 4.21: *Speed estimation error in the case of constant* $25rpm$ *speed command with* $8Nm$ *(*40%*) load torque step applied at* $3s$ *and removed at* $4.8s$ *(simulated sensorless control)*

Figure 4.22 shows the electrical rotor position estimation error in deg. The estimation error is less than $5deg$ in steady state and it peaks at about $10deg$ during transient periods.

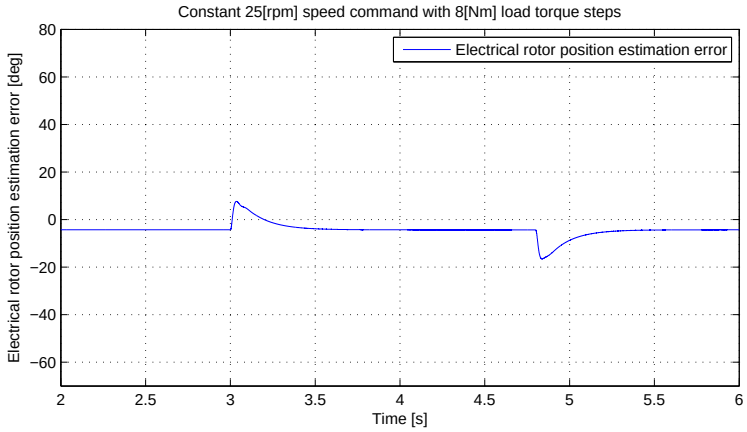

Figure 4.22: *Electrical rotor position estimation error in the case of constant* $25rpm$ *speed command with* $8Nm$ *(*40%*) load torque step applied at* $3s$ *and removed at* $4.8s$ *(simulated sensorless control)*

$200rpm$ trapezoidal speed command with no load torque

In this study case the speed reference is changed from 0 to $200rpm$ and then back to 0 in a ramp fashion with the rate of change of $1000rpm/s$. The load torque is $0Nm$ during this study case. Figure 4.23 shows the reference and measured speed. The measured speed follows the reference and there is a speed overshoot of about 12.5%.

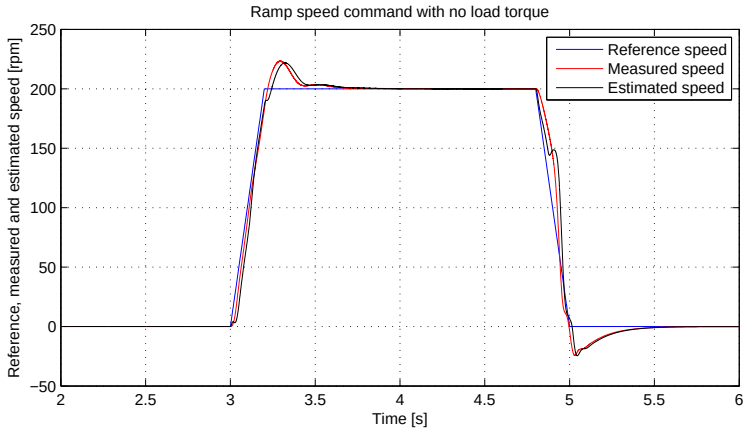

Figure 4.23: *PMSM reference, measured and estimated mechanical speed in the case of* $200rpm$ *trapezoidal speed command with no load torque (simulated sensorless control)*

Figure 4.24 shows the $dq-axis$ currents. The $d-axis$ current contains mainly the $500Hz$ component as in all the other study cases while the $q-axis$ current oscillates around zero during steady state. During the speed increases the $q-axis$ current increases and during the speed decrease the current decreases reaching negative values.

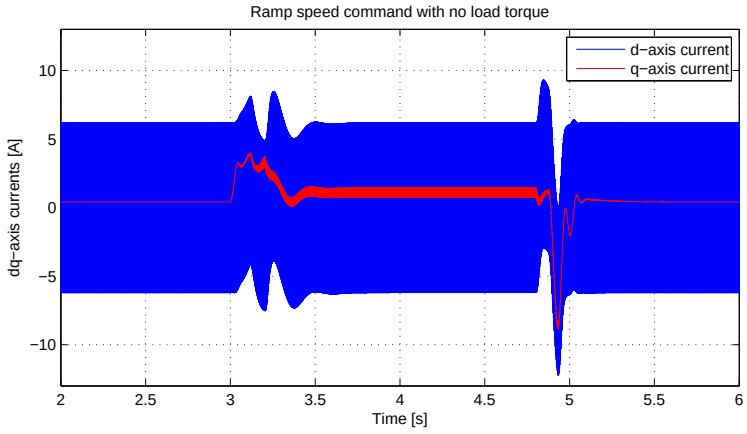

Figure 4.24: *PMSM dq-axis currents in the case of* $200rpm$ *trapezoidal speed command with no load torque (simulated sensorless control)*

Figure 4.25 shows the speed estimation error which in this case peaks at $58rpm$ when the reference speed is decreased from $200rpm$ to zero.

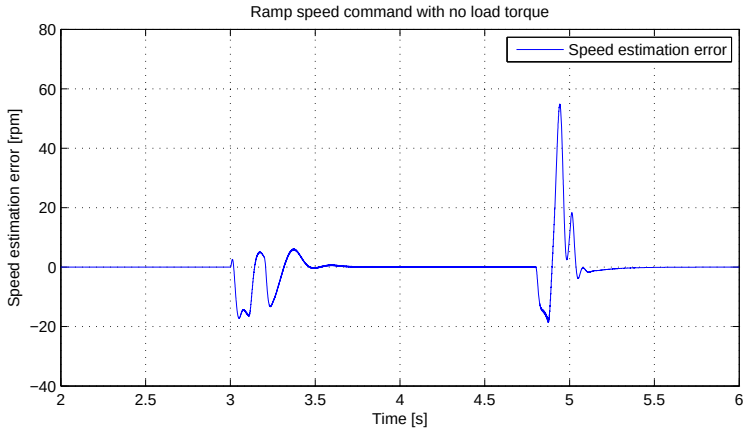

Figure 4.25: *Speed estimation error in the case of* $200rpm$ *trapezoidal speed command with no load torque (simulated sensorless control)*

Figure 4.26 shows the electrical rotor position estimation error which reaches a peak value of $-16deg$ during the first transient and $-41deg$ during the second transient period.

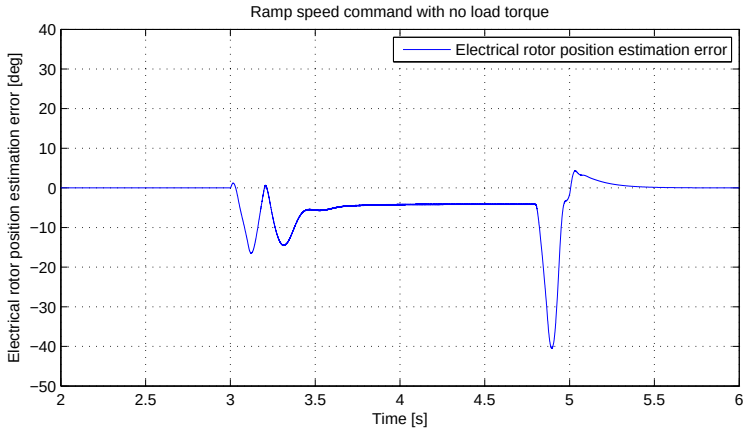

Figure 4.26: *Electrical rotor position estimation error in the case of* $200rpm$ *trapezoidal speed command with no load torque (simulated sensorless control)*

$200rpm$ trapezoidal speed command with $8Nm$ (40%) constant load torque

In this study case the speed reference is changed from 0 to $200rpm$ and then back to 0 in a ramp fashion with the rate of change of $1000rpm/s$. The load torque is constant $8Nm$ during this study case. Figure 4.27 shows the reference and measured speed. The measured speed follows the reference and there is a speed overshoot of about 12%.

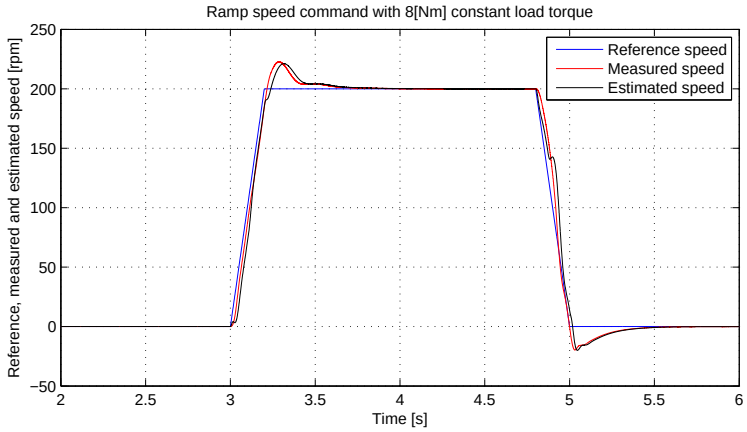

Figure 4.27: *PMSM reference, measured and estimated mechanical speed in the case of* $200rpm$ *trapezoidal speed command with* $8Nm$ *(40%) constant load torque (simulated sensorless control)*

Figure 4.28 shows the $dq-axis$ currents. The $d-axis$ current contains the high frequency injection component while the $q-axis$ current has values of about $12.5A$ and during steady state operation due to the load torque. When the reference speed is increased the $q-axis$ current also increases during the transient and when the speed is decreased so the current decreases during the transient period.

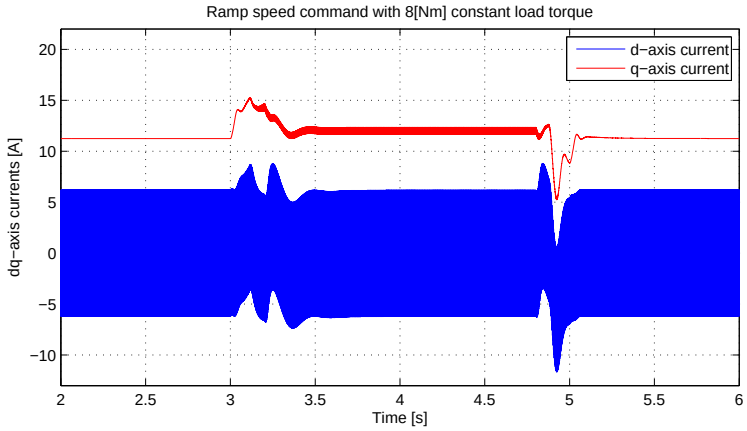

Figure 4.28: *PMSM dq-axis currentsin the case of* $200rpm$ *trapezoidal speed command with* $8Nm$ *(40%) constant load torque (simulated sensorless control)*

Figure 4.29 shows the speed estimation error. The speed error is much lower than in the no load case reaching peak values of about $-18rpm$ while in the case of no load it reached values of $38rpm$.

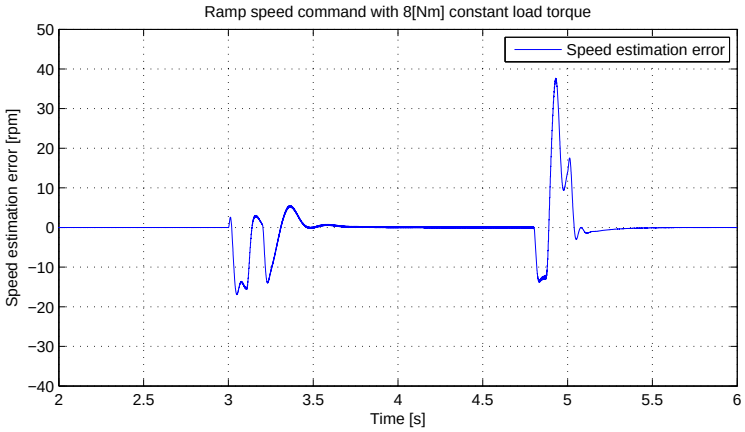

Figure 4.29: *Speed estimation error in the case of* $200rpm$ *trapezoidal speed command with* $8Nm$ *(40%) constant load torque (simulated sensorless control)*

Figure 4.29 shows the electrical rotor position estimation error. The angle error peaks out at around $-37deg$ during the second transient period.

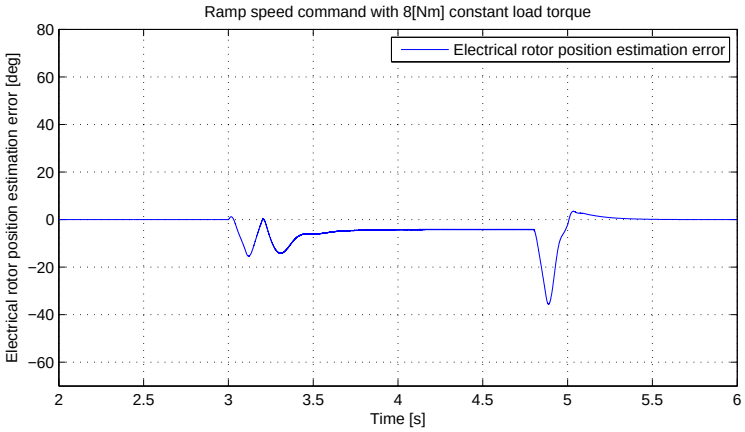

Figure 4.30: *Electrical rotor position estimation error in the case of* $200rpm$ *trapezoidal speed command with* $8Nm$ *(40%) constant load torque (simulated sensorless control)*

$25rpm$ speed reversal command with $8Nm$ (40%) constant load torque

In this study case the speed reference is changed from -25 to $25rpm$ in a ramp fashion with the rate of change of $1000rpm/s$. The load torque is constant $8Nm$ during this study case. Figure 4.31 shows the reference and measured speed. The measured speed follows the reference but not as well as in the case of $200rpm$ operation.

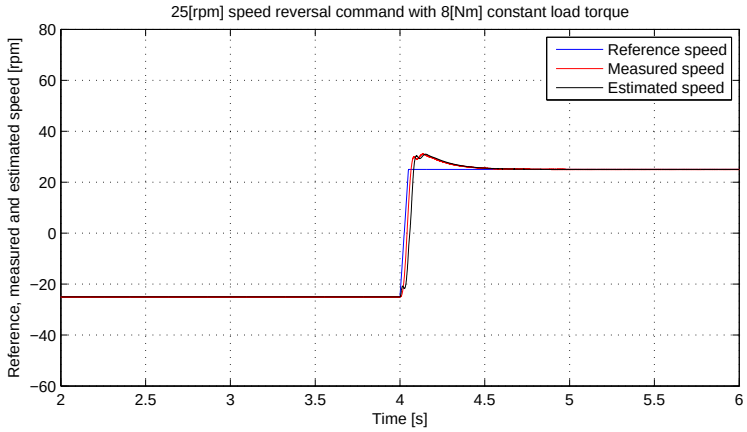

Figure 4.31: *PMSM reference, measured and estimated mechanical speed in the case of* $25rpm$ *speed reversal command with* $8Nm$ *(40%) constant load torque (simulated sensorless control)*

Figure 4.32 shows $dq-axis$ currents. The $d-axis$ current contains the high frequency component while the $q-axis$ current reaches peak values of $14.5A$.

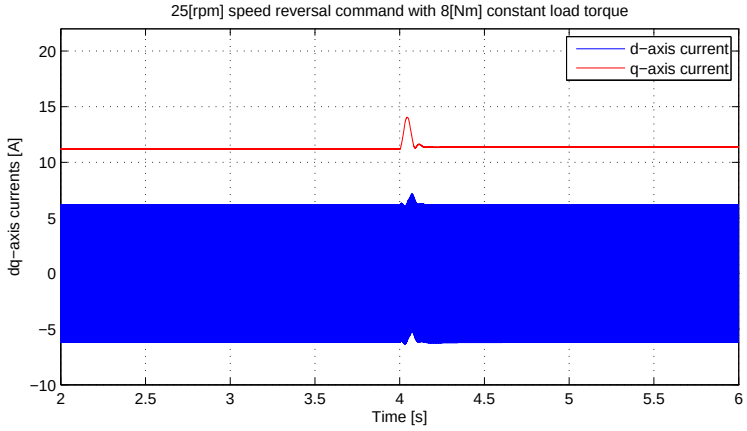

Figure 4.32: *PMSM dq-axis currents in the case of* $25rpm$ *speed reversal command with* $8Nm$ *(40%) constant load torque (simulated sensorless control)*

Figure 4.33 shows the speed estimation error which reaches peak values of about $-19rpm$ during transient periods.

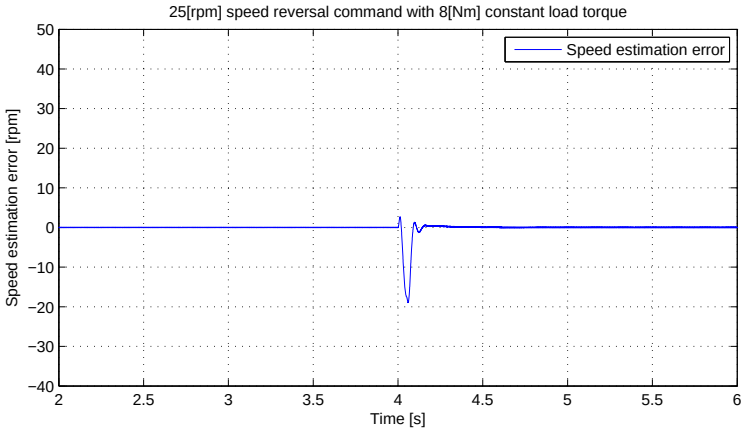

Figure 4.33: *Speed estimation error in the case of* $25rpm$ *speed reversal command with* $8Nm$ *(*40%*) constant load torque (simulated sensorless control)*

Figure 4.34 shows the electrical rotor position estimation error which is lower than $6deg$.

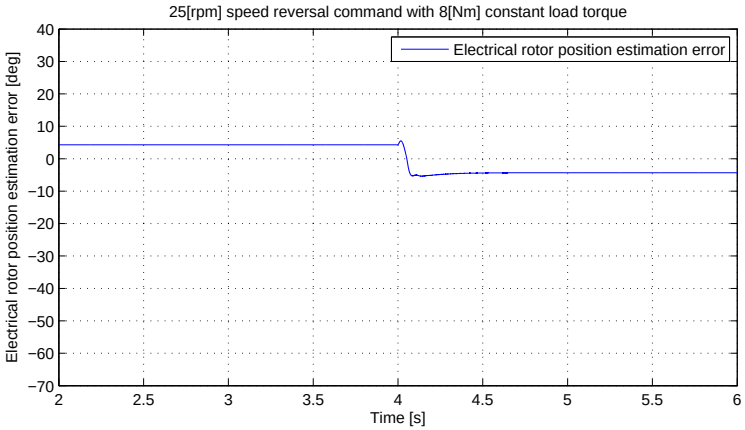

Figure 4.34: *Electrical rotor position estimation error in the case of* $25rpm$ *speed reversal command with* $8Nm$ *(*40%*) constant load torque (simulated sensorless control)*

4.3 Summary

This chapter presents the simulation results for both sensored and sensorless RFOC. Several study casses are considered and discussed.

Chapter 5

Laboratory results

This chapter contains the experimental parts of the project which were carried out in the dSpace laboratory. The chapter begins with the experimental determination of the injection frequency and voltage magnitude for the sensorless control strategy. Also the rotor alignment procedure is presented. The results for the sensored and sensorless control are presented and discussed in detail including current and speed step responses followed by several study cases. The estimation error dependence on load torque is analyzed followed by energy efficiency considerations. The chapter ends with the laboratory results for the control of the loading machine.

5.1 PMSM frequency and current sensitivity analysis

The magnitude and frequency of the injection voltage is determined experimentally by measuring the impedance of the PMSM at different frequencies and voltage magnitudes. The PMSM is a 3 phase machine, phase b and c are connected together and the two terminal system obtained this way is supplied with sinusoidal voltage. A function generator is used to generate the sinusoidal signal which is then amplified by a linear high power amplifier.

The rotor's $d-axis$ (flux axis) is aligned with phase a by means of applying a DC voltage to the PMSM's stator as explained in sub chapter 5.2. The frequency of the signal is adjusted from the signal generator while the amplitude is adjusted from the power amplifier. The frequency and magnitude of the test signal are kept constant during the test procedure and the rotor position is changed with steps of $5deg$ mechanical and the value of the measured currents at each step is saved. As the frequency and magnitude of the test signal are kept constant, the current through the PMSM will change according to the rotors mechanical position. The result obtained this way shows the relationship between mechanical rotor position and high frequency impedance. This relationship between the rotor position and high frequency impedance can be used to estimate the PMSM's rotor position.

After measuring the high frequency impedance for different rotor positions, the high frequency saliency ratio can be calculated. The so called high frequency saliency ratio is defined as shown in 5.1.

$$sr_{hf} = \left(\frac{z_{max} - z_{min}}{z_{max}}\right) 100 \tag{5.1}$$

where,

- sr_{hf} - is the high frequency saliency ratio [%];
- z_{max} - is the high frequency maximum impedance [Ω];
- z_{min} - is the high frequency minimum impedance [Ω];

Figure 5.1 shows the experimental results obtained with a test signal having a frequency of $250Hz$ and current magnitudes of $6...7A$ and $13...14A$ through the PMSM's stator. The mechanical rotor position was changed from 0 to $180deg$ with steps of $5deg$. The PMSM has 4 pole pairs which means that $90deg$ electrical are equivalent to $22.5deg$ mechanical. As a consequence the rotor has to move $22.5deg$ mechanical to produce $90deg$ electrical rotor movement. Since d and q axes are $90deg$ electrical apart it can be also said that the two axes are $22.5deg$ mechanical apart.

As it may be observed in 5.1, in the case of a PMSM there is a minimum high frequency impedance on the $d-axis$ and there is a maximum high frequency impedance on the $q-axis$. In the particular case of a $250Hz$ test signal and currents of $6...7A$ the minimum impedance is around 4.75Ω and the maximum impedance is around 5.21Ω which leads to a high frequency saliency ratio of approximately 8.8%. As figure 5.1 shows it there is a higher high frequency saliency ratio when the current magnitude is around $6...7A$ than for current magnitudes of $13...14A$.

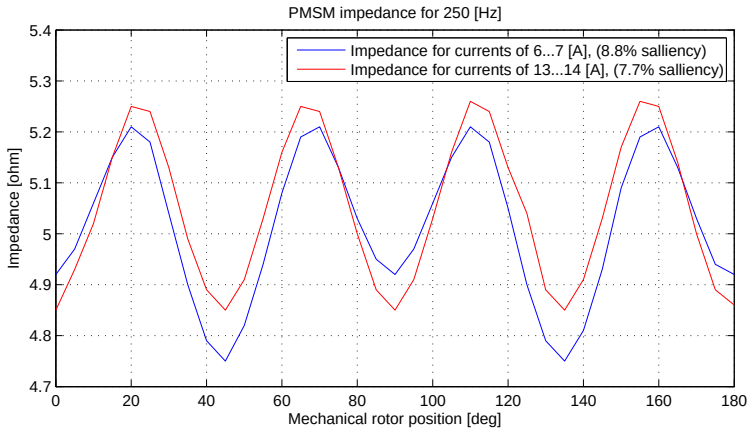

Figure 5.1: *PMSM's impedance as a function of rotor position at* $250Hz$ *for currents of* $6...7A$ *and* $13...14A$

Figure 5.2 shows the results for a test signal of $500Hz$ and current magnitudes of $1A$, $3...4A$ and $9...10A$. The highest saliency ratio obtained in this case is for current magnitudes of $3...4A$ with 10.1% saliency.

Figure 5.3 shows the results for a test signal of $1000Hz$ and current magnitudes of $1A$, $1...2A$ and $5...6A$. For the $1000Hz$ test signal, the highest saliency ratio is obtained for currents with magnitudes of $1...2A$. Must be noted that the highest saliency ratio obtained in the case of the $500Hz$ test signal is for current magnitudes of $3...4A$ while in the case of a $1000Hz$ test signal is for current magnitudes of $1...2A$.

Figure 5.4 shows the results for a test signal of $2000Hz$ and current magnitudes of $1A$ and $2...3A$. The highest saliency ratio is obtained for current magnitudes of $1A$ being 8.9%.

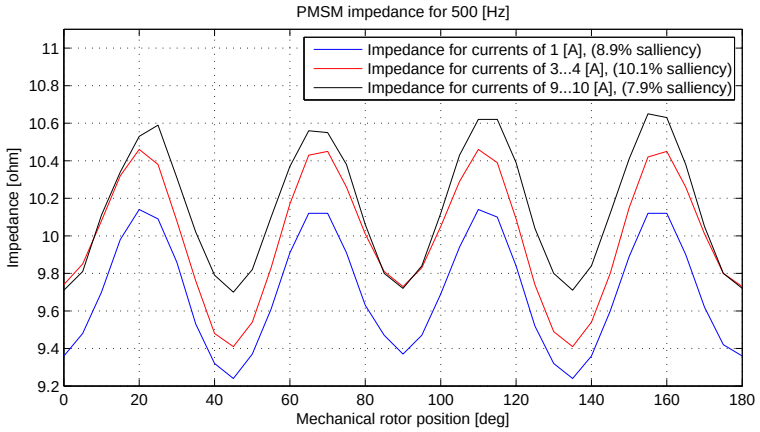

Figure 5.2: *PMSM's impedance as a function of rotor position at 500Hz for currents of* $1A$, $3...4A$ *and* $9...10A$

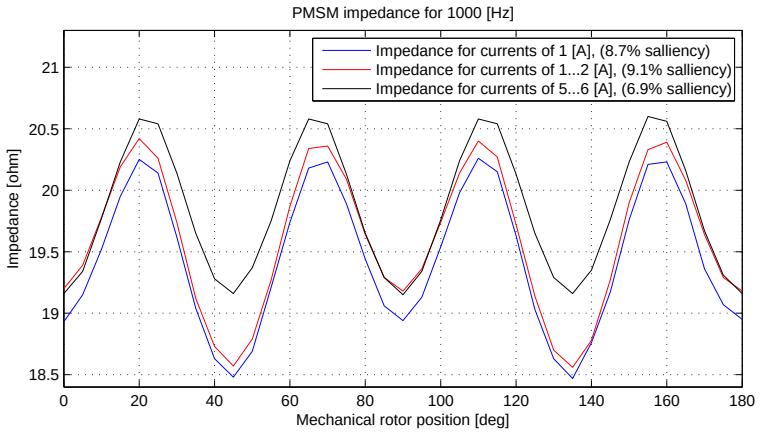

Figure 5.3: *PMSM's impedance as a function of rotor position at* $1000Hz$ *for currents of* $1A$, $1...2A$ *and* $5...6A$

It was not possible to make tests with higher current magnitudes for the $2000Hz$ test signal because of the voltage limitations of the power amplifier.

Figure 5.5 shows a comparison of the results obtained for current magnitudes of $1...2A$ for test signals of 500, 1000 and $2000Hz$. The same amount of high frequency saliency is obtained for the $500Hz$ and $2000Hz$ test signals however is more advantageous to use a $500Hz$ injection signal because it can be done with a lower switching frequency and the same current through the stator windings can be obtained with a lower injection voltage.

The switching frequency used in the dSpace laboratory is $5Khz$ which results in $200us$ switching period, thus one period of the $500Hz$ injection voltage can be reconstructed with 10 points. The $2000Hz$ signal can not be reconstructed accurately enough with a $5Khz$ switching frequency.

Analyzing figure 5.2, the highest saliency ratio of 10.1% is obtained for current magnitudes of $3...4A$ that is why the magnitude of the injection voltage is chosen to be $45V$. The $45V$ injection signal creates currents with the magnitude of $4.25A$ which results in peak currents of $6A$.

As a result of the sensitivity analysis table 5.1 shows the parameters of the chosen injection signal.

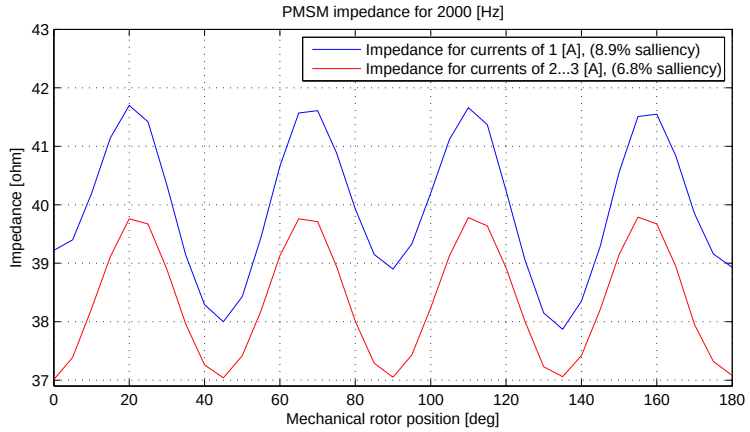

Figure 5.4: *PMSM's impedance as a function of rotor position at* $2000Hz$ *for currents of* $1A$ *and* $2...3A$

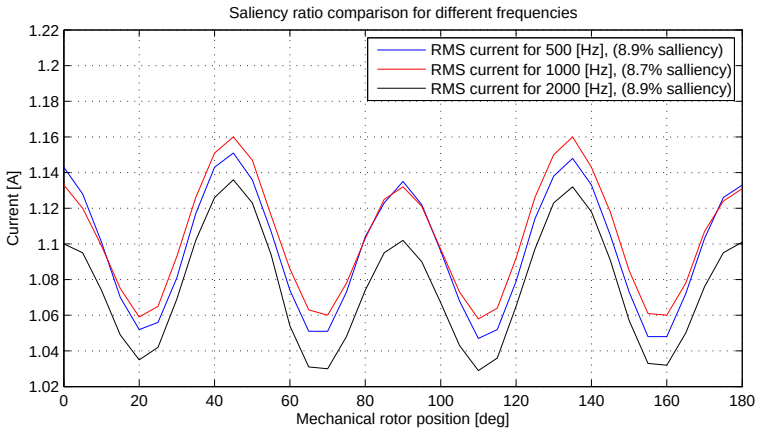

Figure 5.5: *PMSM's impedance comparison*

Parameter	Symbol	Value	Unit
Injection frequency	f_{inj}	500	$[Hz]$
Injection voltage	v_{inj}	45	$[V]$
Resulting stator currents	i_{inj}	4.2	$[A]$

Table 5.1: *Injection signal parameters*

5.2 PMSM rotor alignment to zero position

The initial position of the PMSM's rotor must be known at startup in order to correctly realize the field orientation. One of the possible solutions that may be used to bring the rotor to a known position is to apply a DC voltage on the PMSM's stator thus creating a DC flux which forces the rotor to align to a known position. In this case a positive voltage is applied to phase a while a negative voltage is applied to phases b and c. The current will flow from phase a to phase b and c. The rotor's $d-axis$ will be forced to align with the center of phase a.

In the $Matlab/Simulink$ model the positive DC voltage is applied to phase a by means

of setting a constant duty cycle for phase a of about 0.51. In the model the duty cycle of 0.5 actually means 0V at the inverter's output. The 0.51 duty cycle command outputs a small positive DC voltage which creates a current of about $9A$ through phase a. The duty cycle for phase b and c is commanded to be 0.49 which creates a small negative DC voltage. The currents through phase b and c is about $4.5A$. These constant duty cycles are applied for 1...2 seconds till the rotor aligns. Figure 5.6 shows the PMSM stator currents during the rotor alignment procedure.

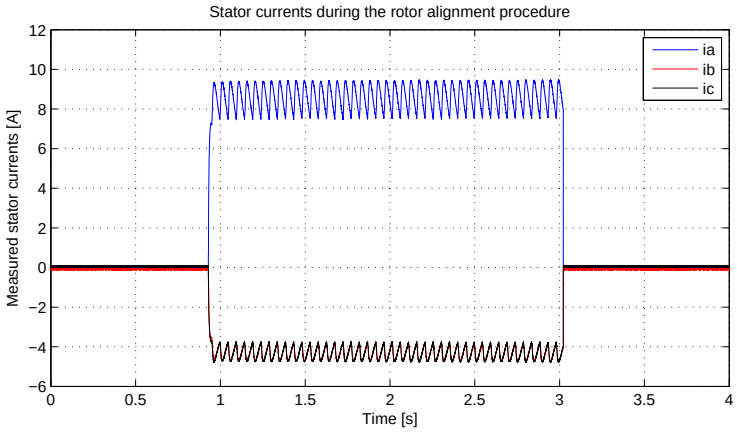

Figure 5.6: *PMSM measured stator currents during the rotor alignment procedure*

In order to be sure that the rotor is correctly aligned to it's zero position, first the application must be loaded to the dSpace board, then the rotor must be aligned by pressing the **align rotor** button in the *ControlDesk* interface. After the rotor has been aligned, the *Matlab/Simulink* model must be built by pressing the **incremental build** button in *Matlab/Simulink*. Failure in aligning the rotor to it's zero position will result in malfunctioning of the PMSM control application. If the initial rotor position is not known correctly then the field orientation is incorrect which means that the d-axis of the rotating reference frame is not fixed on the d-axis of the permanent magnet but on some other random position.

5.3 PMSM sensored RFOC

In this section the laboratory results for the sensored rotor field oriented control of PMSM are presented. In this case the PMSM is closed loop vector controlled using the position feedback given by an encoder. These results are presented because is a good idea to compare them with the results obtained with the sensor-less control algorithm.

5.3.1 $d, q-axis$ current and speed controller step responses

Figure 5.7 shows the $d-axis$ current controller step response when a $10A$ current step command is applied. Both d and $q-axis$ current controllers are designed in such a way that there is no significant current overshoot in order to protect the switches in the inverter. For the $d-axis$ controller the settling time is about $t_{rise} = 3ms$. The measured $d-axis$ current easily oscillates around the commanded $10A$ value.

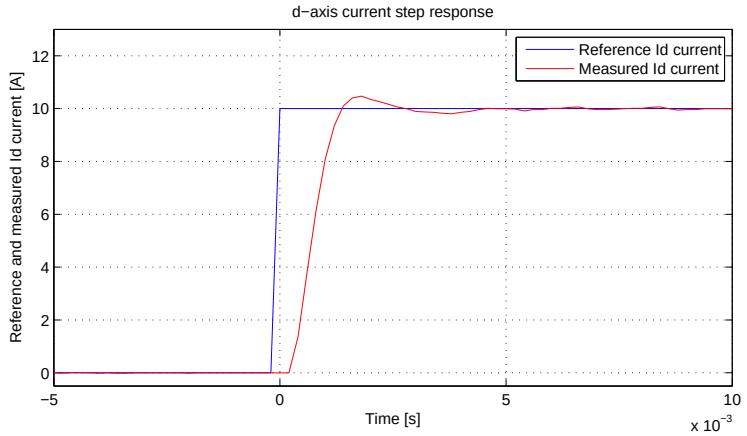

Figure 5.7: *$d-axis$ current controller $10A$ step response for sensored DFOC*

Figure 5.8 shows the $q-axis$ current controller step response when a $10A$ current step command is applied. The settling time is about $t_{settling} = 3ms$. The $q-axis$ measured current also easily oscillates around the commanded $10A$ value.

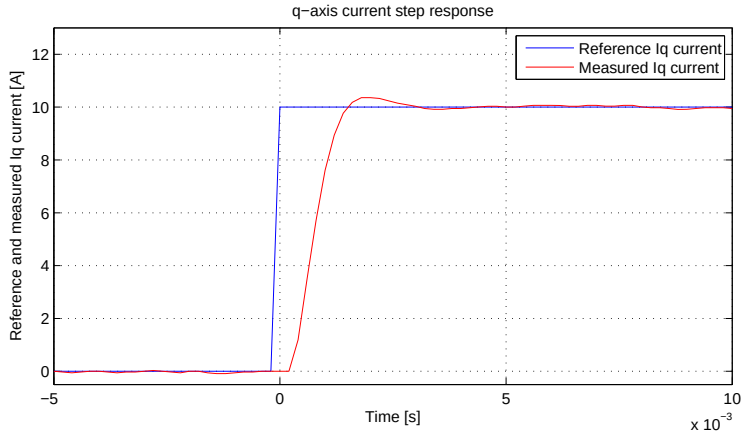

Figure 5.8: *$q-axis$ current controller $10A$ step response for sensored DFOC*

As it may be seen in figures 5.7 and 5.8 both current controllers are working properly.

Figure 5.9 shows the speed response in the case of sensored control for a $100rpm$ step. There is a 6% speed overshoot which is very small. During the test the PMSM is loaded with constant $8Nm$ (40%) load torque.

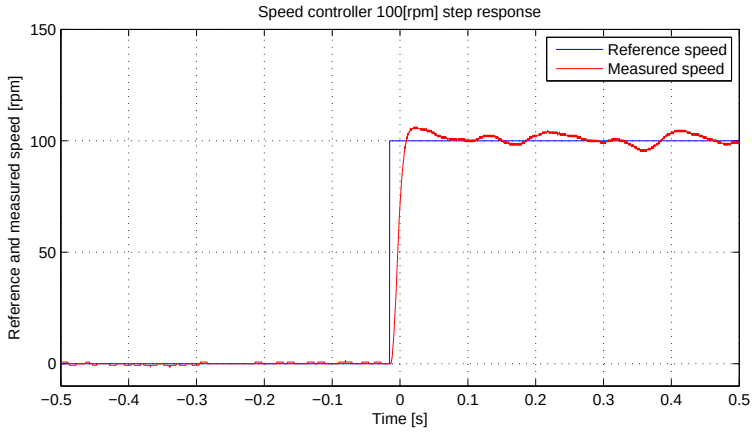

Figure 5.9: *Speed* $100rpm$ *step response for sensored DFOC while loaded with constant* $8Nm$ *(40%) load torque*

5.3.2 Speed control mode

Zero speed command with $8Nm$ (40%) load torque steps

In this study case the PMSM's reference speed is kept at $0rpm$ and at $0s$ a step load torque of $8Nm$ is applied by the IM. The idea is to see how well the PMSM maintains it's reference speed. Figure 5.10 shows the reference and measured speed. The reference speed is $0rpm$ during the test while the measured speed decreases when the load torque is applied to about $-65rpm$ when the step load torque is applied. The measured speed settles again at $0rpm$ in about $0.8s$. When the load torque is removed the measured speed increases to about $65rpm$ and settles again at $0rpm$ in about $0.8s$. The measured speed deviates from the reference speed during transient periods but it maintains it's reference speed in steady state also during loading.

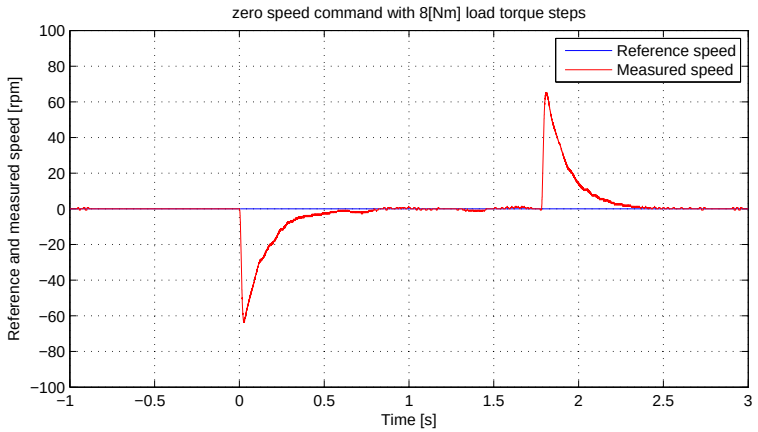

Figure 5.10: *PMSM reference and measured mechanical speed in the case of zero speed command with* $8Nm$ *(40%) load torque step applied at* $0s$ *and removed at* $1.77s$ *(sensored control)*

Figure 5.11 shows the estimated load torque produced by the IM in order to load the PMSM. At $0s$ the load torque steps from $0Nm$ to $8Nm$ and at $1.77s$ it steps back to $0Nm$.

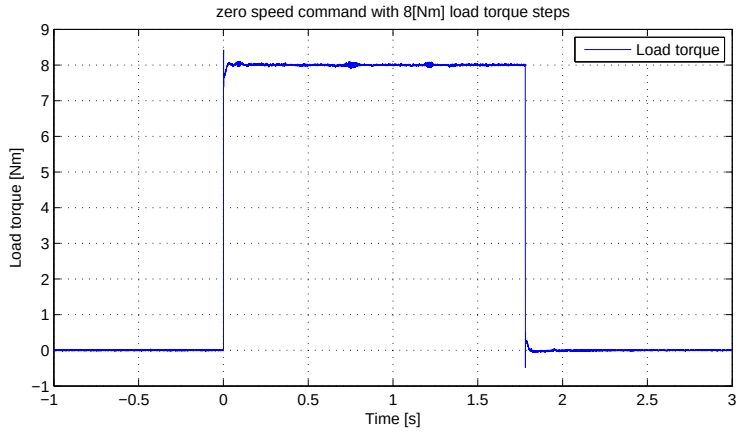

Figure 5.11: *Estimated load torque produced by the IM in the case of zero speed command with* $8Nm$ *(40%) load torque step applied at* $0s$ *and removed at* $1.77s$ *(sensored control)*

Figure 5.12 shows the PMSM's $dq-axis$ currents. The $dq-axis$ currents look as expected, both currents have magnitudes of $0A$ in the case of no load and only the $q-axis$ current increases during loading of the PMSM. The $q-axis$ current is not exactly $0A$ but that might be because of small offsets introduced by the current measurement circuits and ADCs. The $d-axis$ current is always $0A$ as expected, only during transient periods when the load torque is applied it deviates from $0A$. The $q-axis$ current settles at about $11A$ during loading.

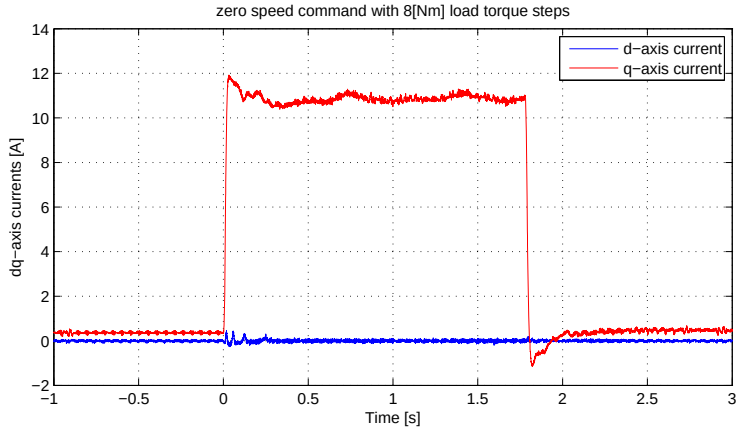

Figure 5.12: *PMSM dq-axis currents in the case of zero speed command with* $8Nm$ *(40%) load torque step applied at* $0s$ *and removed at* $1.77s$ *(sensored control)*

Constant $25rpm$ speed command with $8Nm$ (40%) load torque steps

In this study case the PMSM's reference speed is kept at constant $25rpm$ while a load torque of $8Nm$ (40%) is applied in step fashion at $0s$ and removed at $1.75s$. As it may be seen in figure 5.13 the measured speed decreases to about $-41rpm$ during the application of the load torque step and goes back to reference again in about $0.9s$. When the load torque is removed, the measured speed increases to about $95rpm$ and goes back to reference in $1s$

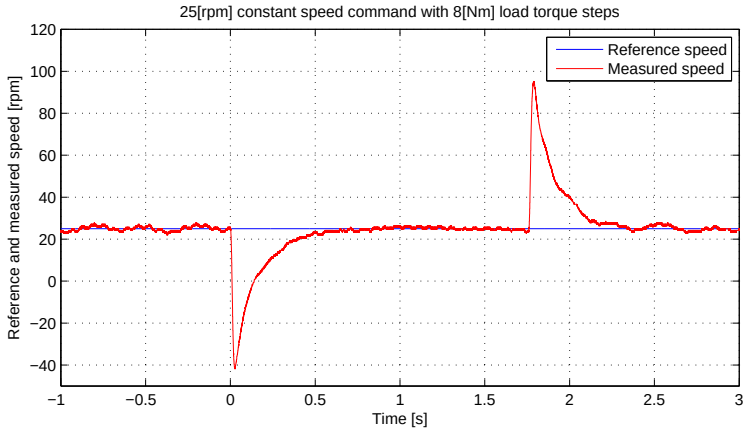

Figure 5.13: *PMSM reference and measured mechanical speed in the case of constant* $25rpm$ *speed command with* $8Nm$ *(*40%*) load torque step applied at* $0s$ *and removed at* $1.75s$ *(sensored control)*

Figure 5.14 the estimated load torque profile produced by the IM. It increases from 0 to $8Nm$ at $0s$ and decreases to 0 again at $1.75s$.

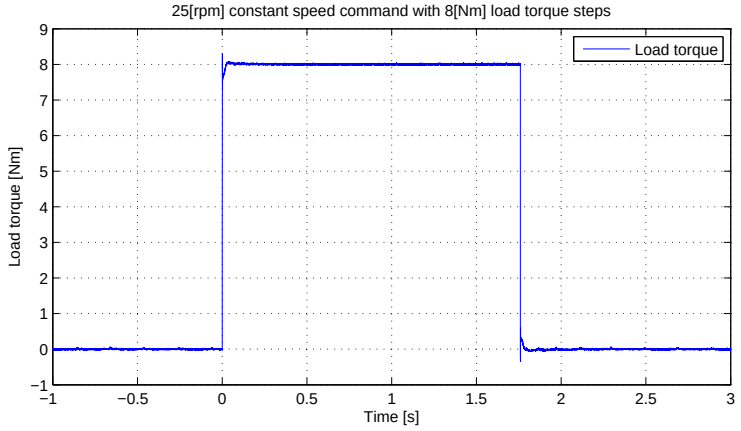

Figure 5.14: *Estimated load torque produced by the IM in the case of constant* $25rpm$ *speed command with* $8Nm$ *(*40%*) load torque step applied at* $0s$ *and removed at* $1.75s$ *(sensored control)*

Figure 5.15 shows the $dq-axis$ currents. The $d-axis$ current is close to zero while the $q-axis$ current increases to about $11A$ during the loading period.

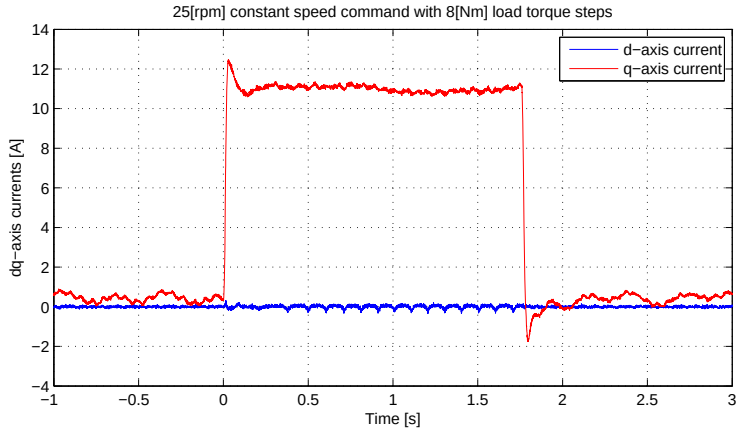

Figure 5.15: *PMSM dq-axis currents in the case of constant* $25rpm$ *speed command with* $8Nm$ *(40%) load torque step applied at* $0s$ *and removed at* $1.75s$ *(sensored control)*

$200rpm$ trapezoidal speed command with no load torque

In this study case the speed reference is changed from 0 to $200rpm$ and then back to 0 in a ramp fashion with the rate of change of $1000rpm/s$. The load torque is $0Nm$ during this study case. Figure 5.16 shows the reference and measured speed. The measured speed follows the reference and there is a speed overshoot of about 7% which is acceptable.

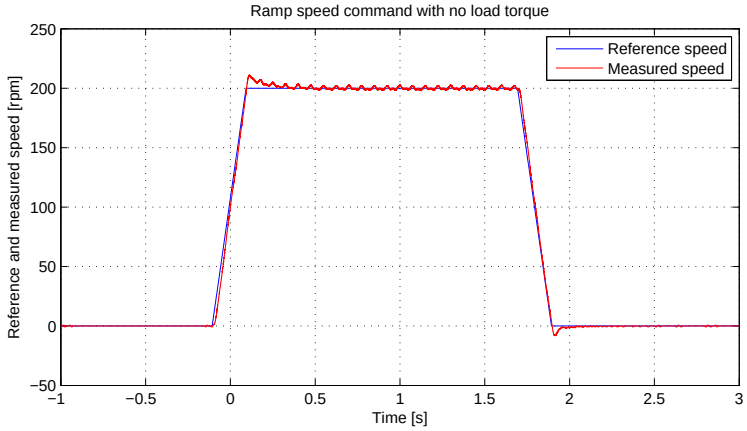

Figure 5.16: *PMSM reference and measured mechanical speed in the case of* $200rpm$ *trapezoidal speed command with no load torque (sensored control)*

Figure 5.17 shows the dq-axis currents. The $d-axis$ current is close to zero as expected while the $q-axis$ current increases during the speed changing period to about $3A$ peak. During the $200rpm$ operation the oscillations in the $q-axis$ current are also higher.

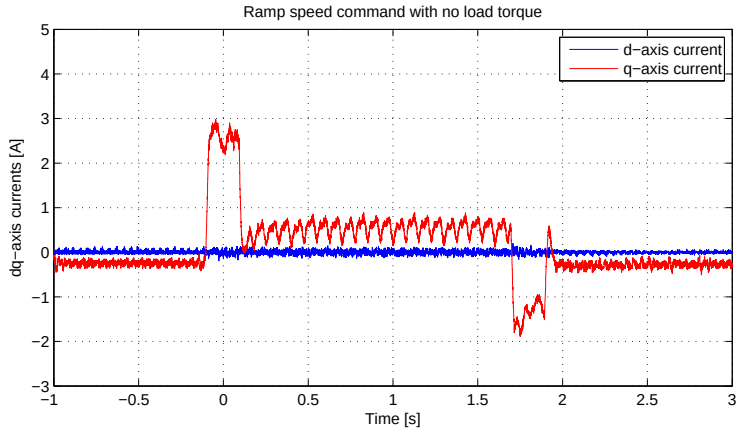

Figure 5.17: *PMSM dq-axis currents in the case of* $200rpm$ *trapezoidal speed command with no load torque (sensored control)*

$200rpm$ trapezoidal speed command with $8Nm$ (40%) constant load torque

In this study case the speed reference is changed from 0 to $200rpm$ and then back to 0 in a ramp fashion with the rate of change of $1000rpm/s$. The load torque is constant $8Nm$ during this study case. Figure 5.18 shows the reference and measured speed. The measured speed follows the reference and there is a speed overshoot of about 7% which is acceptable.

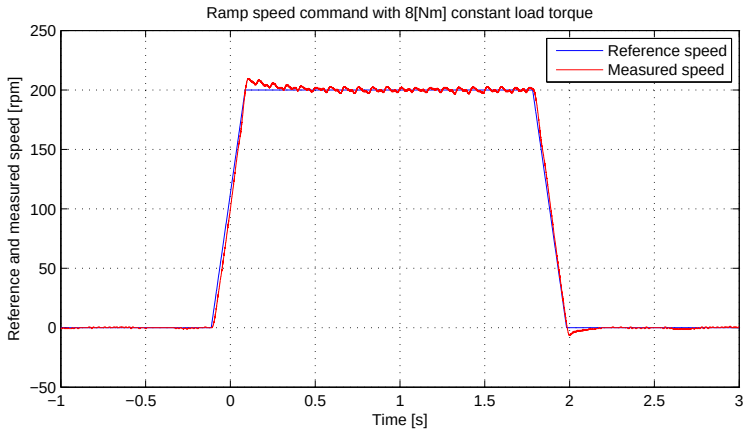

Figure 5.18: *PMSM reference and measured mechanical speed in the case of* $200rpm$ *trapezoidal speed command with* $8Nm$ *(40%) constant load torque (sensored control)*

Figure 5.19 shows the $dq-axis$ currents. The $d-axis$ current has a magnitude of about $11A$ during zero speed operation and increases to about $12A$ during the $200rpm$ steady state operation. During the first transient period the $q-axis$ current increases to $15A$ because more torque than the actual load torque is needed to increases the speed of the machine and it decreases to $9A$ during the second transient period as less electromagnetic torque than the actual load torque is needed in order to reduce the speed of the machine.

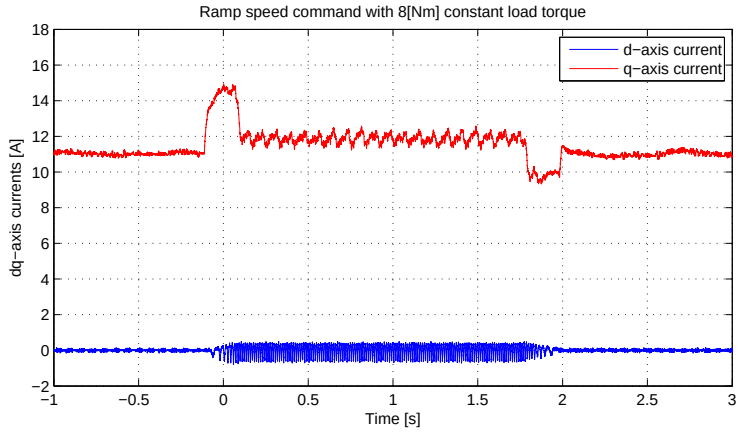

Figure 5.19: *PMSM dq-axis currents in the case of* $200rpm$ *trapezoidal speed command with* $8Nm$ *(40%) constant load torque (sensored control)*

$25rpm$ speed reversal command with $8Nm$ (40%) constant load torque

In this study case the speed reference is changed from $-25rpm$ to $25rpm$ in a ramp fashion with the rate of change of $1000rpm/s$. The load torque is constant $8Nm$ during this study case. Figure 5.20 shows the reference and measured speed. The measured speed follows the reference and there is a small speed overshoot and a small speed error during the reference speed changing.

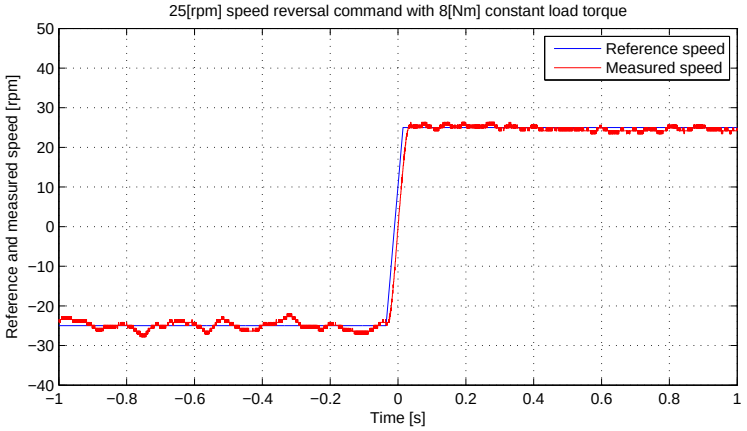

Figure 5.20: *PMSM reference and measured mechanical speed in the case of* $25rpm$ *speed reversal command with* $8Nm$ *(40%) constant load torque (sensored control)*

Figure 5.21 shows the $dq-axis$ currents. The $d-axis$ current is almost $0A$ during the whole period. The $q-axis$ current is about $10.7A$ during the $-25rpm$ speed operation and about 11.5 during the $25rpm$ operation. During the transient period the $q-axis$ current increases to about $13A$.

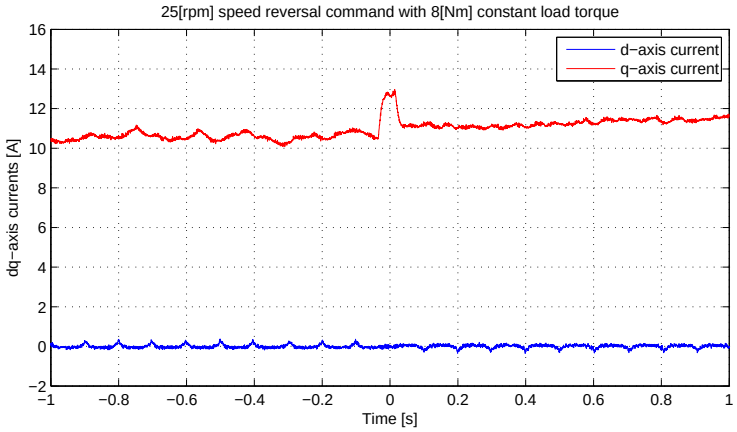

Figure 5.21: *PMSM dq-axis currents in the case of* $25rpm$ *speed reversal command with* $8Nm$ *(40%) constant load torque (sensored control)*

5.4 PMSM Sensorless RFOC

5.4.1 d, $q-axis$ current and speed controller step responses

Figure 5.22 shows the $d-axis$ current controller step response when a $10A$ current step command is applied. Both d and $q-axis$ current controllers are designed in such a way that there is no significant current overshoot in order to protect the switches in the inverter. For the $d-axis$ controller the settling time is about $20ms$. The measured $d-axis$ current easily oscillates around the commanded $10A$ value which is partly due to the $d-axis$ injection voltage. The small oscillations can not be totally eliminated.

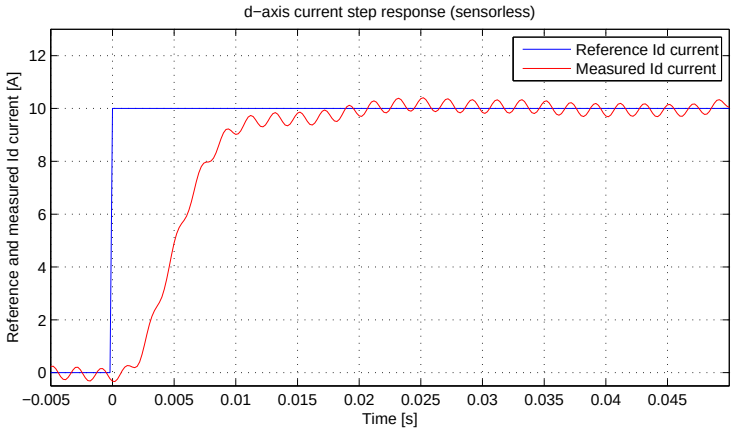

Figure 5.22: $d-axis$ *current controller* $10A$ *step response for sensorless DFOC*

Figure 5.23 shows the $q-axis$ current controller step response when a $10A$ current step command is applied. The settling time is about $20ms$. The $q-axis$ measured current also easily oscillates around the commanded $10A$ value.

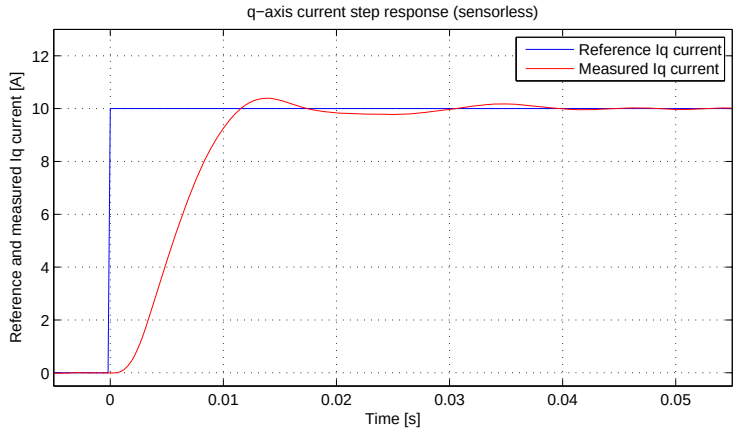

Figure 5.23: *$q-axis$ current controller $10A$ step response for sensorless DFOC*

As it may be seen in figures 5.22 and 5.23 both current controllers are working properly.

Figure 5.24 shows the speed response in the case of sensorless control for a $100rpm$ step. There is a 42% speed overshoot which is much greater than in the case of sensored control. During the test the PMSM is loaded with constant $8Nm$ (40%) load torque.

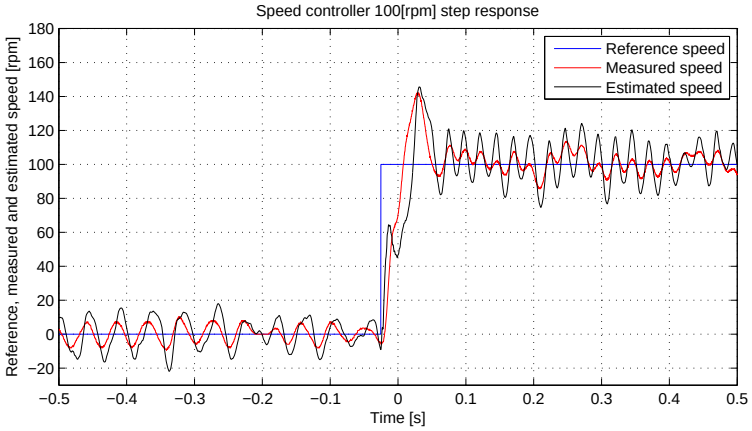

Figure 5.24: *Speed $100rpm$ step response for sensorless DFOC while loaded with constant $8Nm$ (40%) load torque*

5.4.2 Speed control mode

Zero speed command with $8Nm$ (40%) load torque steps

In this study case the reference speed is maintained at zero while the load torque is changed in step fashion from 0 to $8Nm$ and then back to $0Nm$. Figure 5.25 shows the reference, measured and estimated speed. The measured and estimated speed decreases to about $-110rpm$ when the load torque is applied. With the sensored control the speed decreased to about $-65rpm$ only. When the load torque is removed the measured an estimated speed increases to about $115rpm$. During steady state the measured and estimated speed is close to the reference speed.

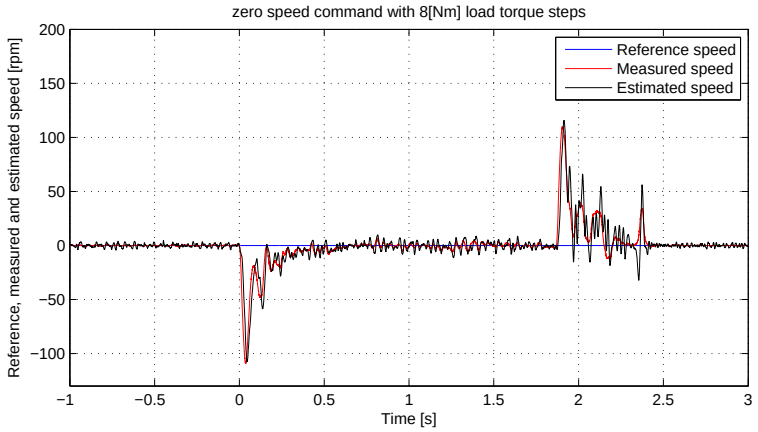

Figure 5.25: *PMSM reference, measured and estimated mechanical speed in the case of zero speed command with* $8Nm$ *(40%) load torque step applied at* $0s$ *and removed at* $1.9s$ *(sensorless control)*

Figure 5.26 shows the estimated load torque produced by the IM in order to load the PMSM. The load torque is increased from 0 to $8Nm$ at $0s$ and decreased back to $0Nm$ at $1.9s$.

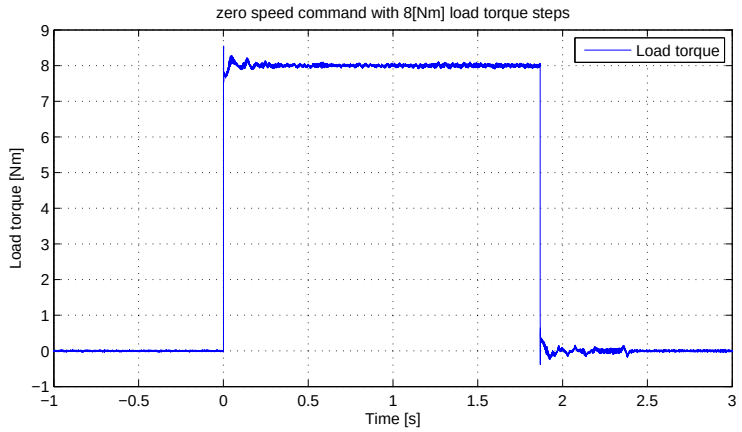

Figure 5.26: *Estimated load torque produced by the IM in the case of zero speed command with* $8Nm$ *(40%) load torque step applied at* $0s$ *and removed at* $1.9s$ *(sensorless control)*

Figure 5.27 shows the $dq-axis$ currents. The $d-axis$ current looks different than the one from the sensored study case because here the $500Hz$ current caused by the $45V$ injection voltage may be seen all the time on the $d-axis$. The $q-axis$ current looks similar to the one in the sensored case with the exception that in the sensorless case there are higher oscillations especially during transient periods. The oscillations are caused by the rotor position estimation error. When there is an error in the rotor position estimation than the $q-axis$ current needs to be higher in order to produce the same electromagnetic torque as in the case of correct position estimation. When there is an error in the rotor position estimation than a current command on the $q-axis$ may produce current on the real $d-axis$ thus reducing the electromagnetic torque.

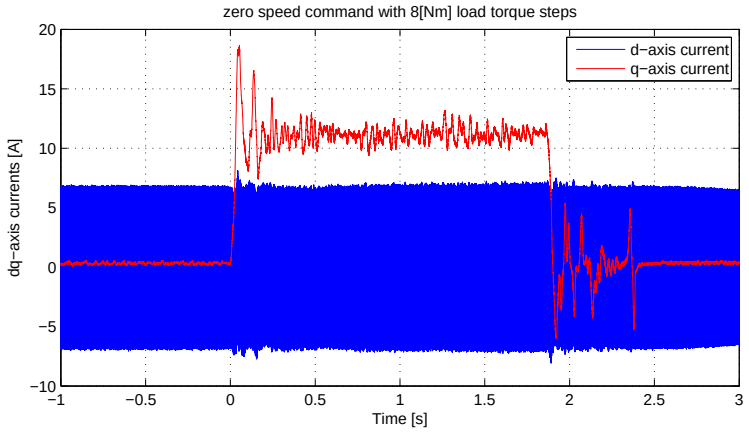

Figure 5.27: *PMSM dq-axis currents in the case of zero speed command with* $8Nm$ *(40%) load torque step applied at* $0s$ *and removed at* $1.9s$ *(sensorless control)*

Figure 5.28 shows the speed estimation error in rpm. During steady state operation the speed estimation error is quite small and it peaks out at about $-48rpm$ during the first transient period and $55rpm$ during the second transient period.

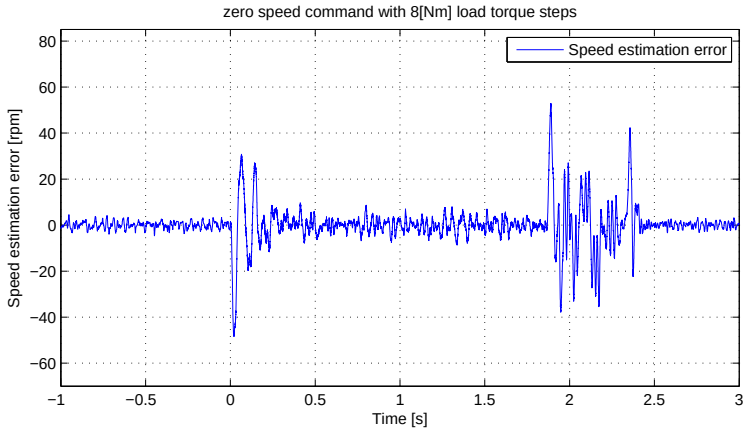

Figure 5.28: *Speed estimation error in the case of zero speed command with* $8Nm$ *(40%) load torque step applied at* $0s$ *and removed at* $1.9s$ *(sensorless control)*

Figure 5.29 shows the electrical rotor position estimation error in deg. During zero speed operation with no load torque the estimation error is close to $0deg$. When the PMSM is loaded the estimation error increases to about $9deg$. The electrical rotor position estimation error reaches about $25deg$ during the first transient period (when the load torque is applied) and $-15deg$ during the second transient period (when the load torque is removed).

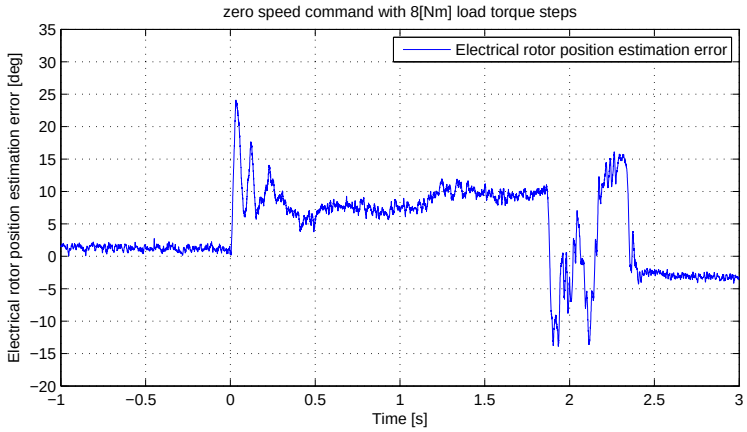

Figure 5.29: *Electrical rotor position estimation error in the case of zero speed command with* $8Nm$ *(*40%*) load torque step applied at* 0*s and removed at* 1.9*s (sensorless control), the high spikes in the estimation error that reach* $60deg$ *are not real*

Constant $25rpm$ speed command with $8Nm$ (40%) load torque steps

In this study case the reference speed is maintained at $25rpm$ while the load torque is changed in step fashion from 0 to $8Nm$ and then back to $0Nm$. Figure 5.30 shows the reference, measured and estimated speed. The measured and estimated speed decreases to about $-120rpm$ when the load torque is applied. With the sensored control the speed decreased to about $-42rpm$ only. When the load torque is removed the measured an estimated speed increases to about $150rpm$. During steady state the measured and estimated speed is close to the reference speed especially during loading when the oscillations are much smaller than during no load. As expected the sensorless control algorithm performs worse than the sensored algorithm but it maintains it's reference speed.

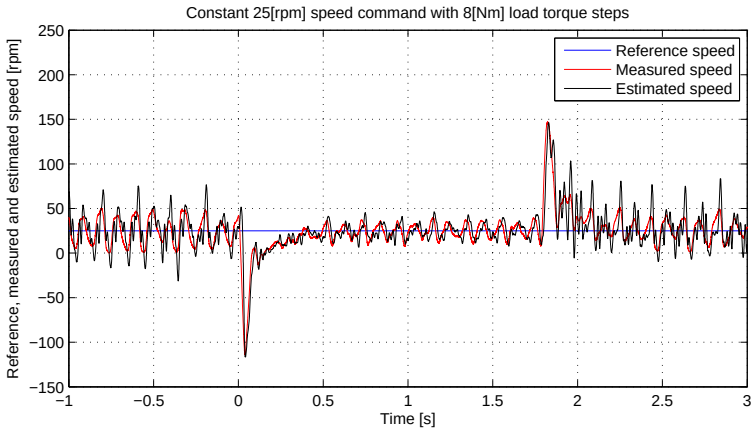

Figure 5.30: *PMSM reference, measured and estimated mechanical speed in the case of constant* $25rpm$ *speed command with* $8Nm$ *(*40%*) load torque step applied at* 0*s and removed at* 1.8*s (sensorless control)*

Figure 5.31 shows the estimated load torque produced by the IM. The load torque has the same profile as in the previous study cases.

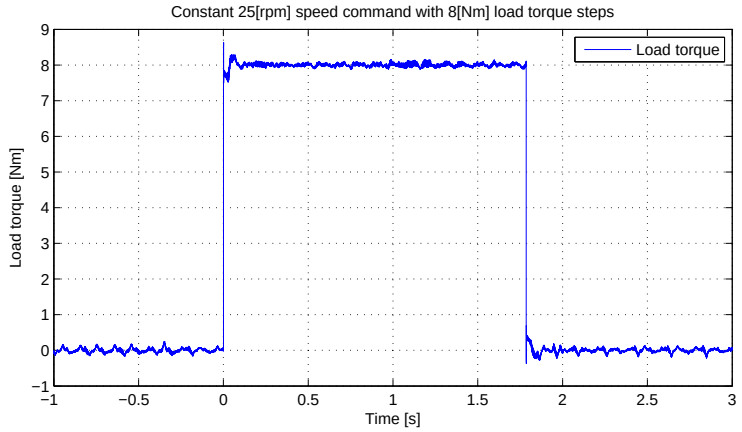

Figure 5.31: *Estimated load torque produced by the IM in the case of constant* $25rpm$ *speed command with* $8Nm$ *(*40%*) load torque step applied at* $0s$ *and removed at* $1.8s$ *(sensorless control)*

Figure 5.32 shows the $dq-axis$ currents. The $d-axis$ current contains only the $500Hz$ injection component while the $q-axis$ current oscillates when unloaded and increases to about $15A$ during steady $25rpm$ operation. The current oscillations are much higher than in the case of sensored control. For the sensorless control the $q-axis$ current peaks at $20A$ when the load torque is applied while for the sensored control it peaks at $12.5A$. The high peak current during the transiend period is present because during transient periods the rotor position estimation error is the highest.

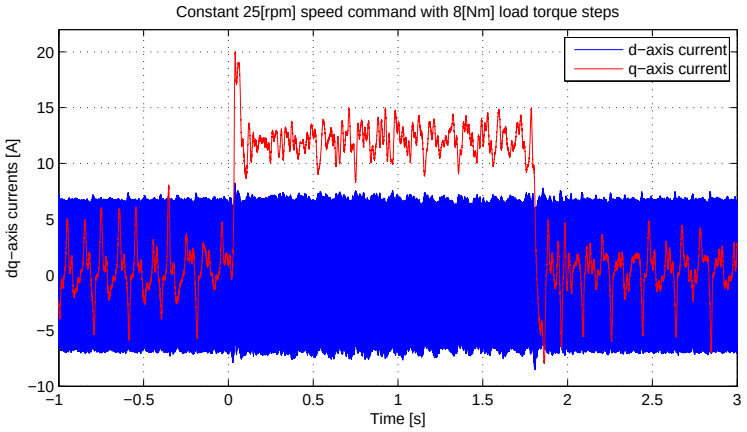

Figure 5.32: *PMSM dq-axis currents in the case of constant* $25rpm$ *speed command with* $8Nm$ *(*40%*) load torque step applied at* $0s$ *and removed at* $1.8s$ *(sensorless control)*

Figure 5.33 shows the speed estimation error during this study case. The speed error is higher when the PMSM is unloaded and it decreases during loading. There is a peak value of $-89rpm$ speed error during the first transient period and $55rpm$ during the second transient period. During loaded operation at $25rpm$ the speed error is less than $20rpm$.

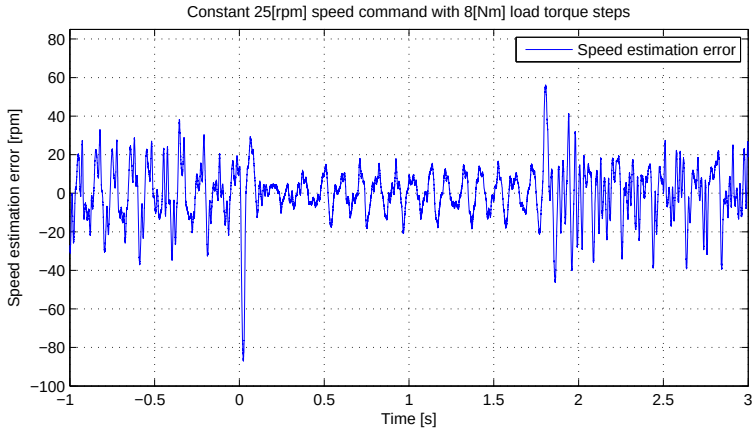

Figure 5.33: *Speed estimation error in the case of constant* $25rpm$ *speed command with* $8Nm$ *(40%) load torque step applied at* $0s$ *and removed at* $1.8s$ *(sensorless control)*

Figure 5.34 shows the electrical rotor position estimation error in deg. The estimation error is less than $12deg$ in steady state and it peaks at about $26deg$ during the first transient period.

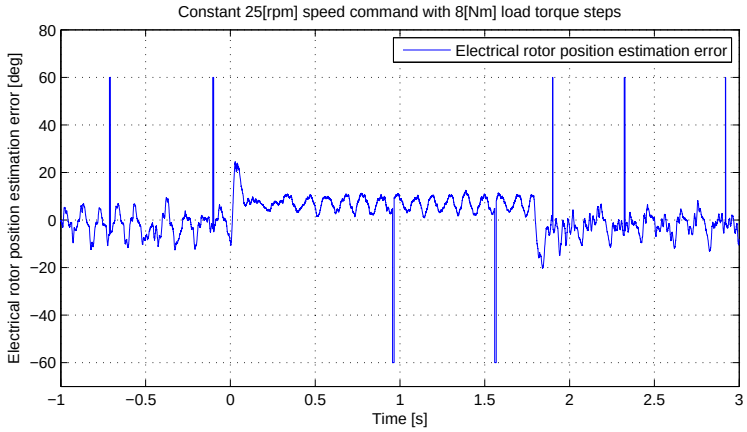

Figure 5.34: *Electrical rotor position estimation error in the case of constant* $25rpm$ *speed command with* $8Nm$ *(40%) load torque step applied at* $0s$ *and removed at* $1.8s$ *(sensorless control), the high spikes in the estimation error that reach* $60deg$ *are not real*

$200rpm$ trapezoidal speed command with no load torque

In this study case the speed reference is changed from 0 to $200rpm$ and then back to 0 in a ramp fashion with the rate of change of $1000rpm/s$. The load torque is $0Nm$ during this study case. Figure 5.35 shows the reference and measured speed. The measured speed follows the reference and there is a speed overshoot of about 15% which is much higher than in the case of sensored control.

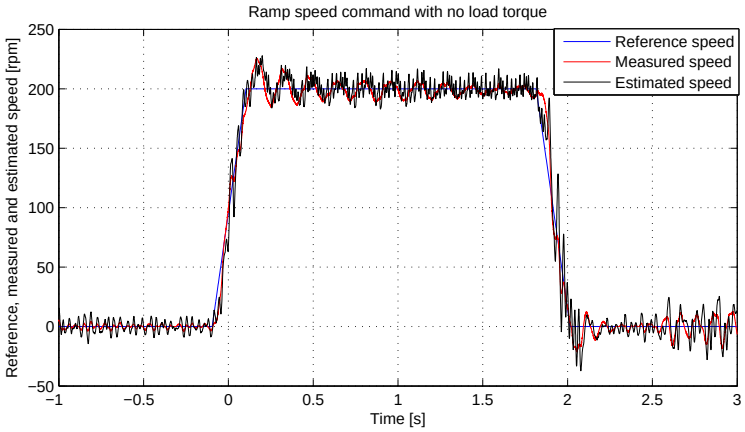

Figure 5.35: *PMSM reference, measured and estimated mechanical speed in the case of* $200rpm$ *trapezoidal speed command with no load torque (sensorless control)*

Figure 5.36 shows the $dq-axis$ currents. The $d-axis$ current contains mainly the $500Hz$ component as in all the other study cases while the $q-axis$ current oscillates around zero during steady state. During the speed increases the $q-axis$ current increases and during the speed decrease the current decreases reaching negative values.

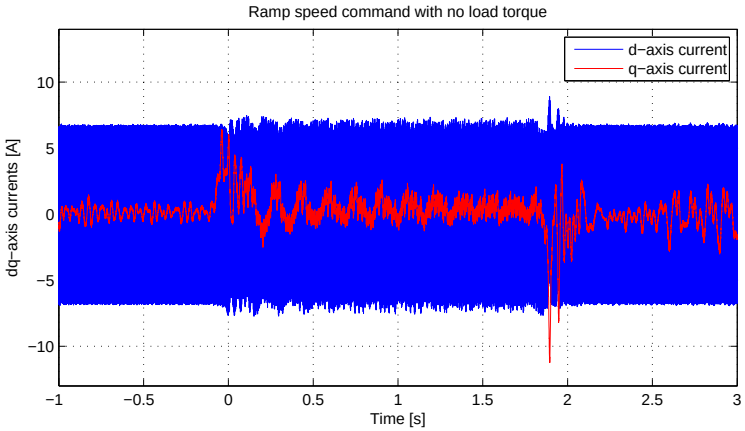

Figure 5.36: *PMSM dq-axis currents in the case of* $200rpm$ *trapezoidal speed command with no load torque (sensorless control)*

Figure 5.37 shows the speed estimation error which in this case peaks at $-55rpm$ when the reference speed is decreased from $200rpm$ to zero.

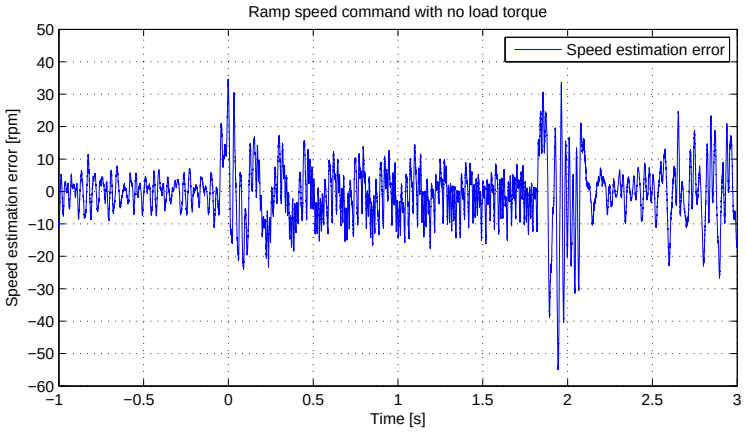

Figure 5.37: *Speed estimation error in the case of* $200rpm$ *trapezoidal speed command with no load torque (sensorless control)*

Figure 5.38 shows the electrical rotor position estimation error which reaches a peak value of $-20deg$ during the first transient and $-30deg$ during the second transient period.

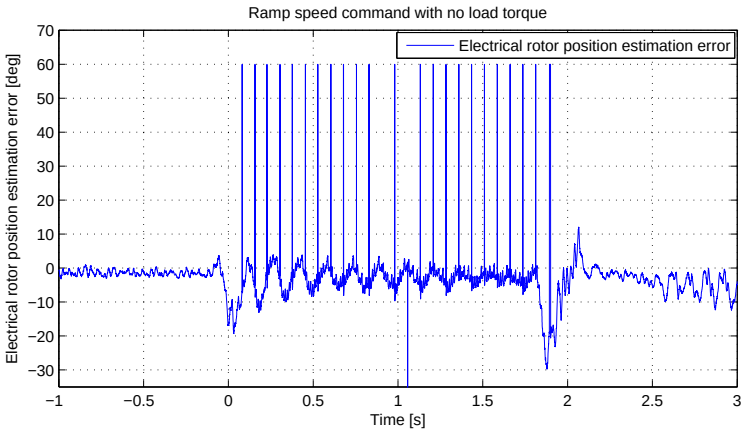

Figure 5.38: *Electrical rotor position estimation error in the case of* $200rpm$ *trapezoidal speed command with no load torque (sensorless control), the high spikes in the estimation error that reach* $60deg$ *are not real*

$200rpm$ trapezoidal speed command with $8Nm$ (40%) constant load torque

In this study case the speed reference is changed from 0 to $200rpm$ and then back to 0 in a ramp fashion with the rate of change of $1000rpm/s$. The load torque is constant $8Nm$ during this study case. Figure 5.39 shows the reference and measured speed. The measured speed follows the reference and there is a speed overshoot of about 12% which is much larger than the 7% overshoot in the case of sensored control.

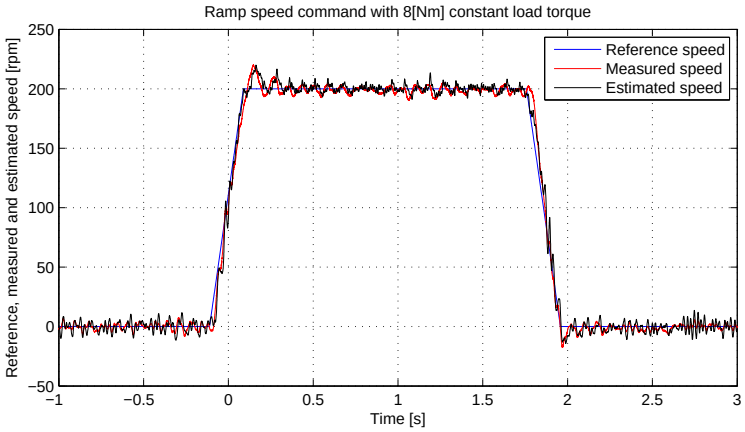

Figure 5.39: *PMSM reference, measured and estimated mechanical speed in the case of* $200rpm$ *trapezoidal speed command with* $8Nm$ *(40%) constant load torque (sensorless control)*

Figure 5.40 shows the $dq-axis$ currents. The $d-axis$ current contains the high frequency injection component while the $q-axis$ current has peak values of about $13A$ and during steady state operation due to the load torque. When the reference speed is increased the $q-axis$ current also increases during the transient and when the speed is decreased so the current decreases during the transient period.

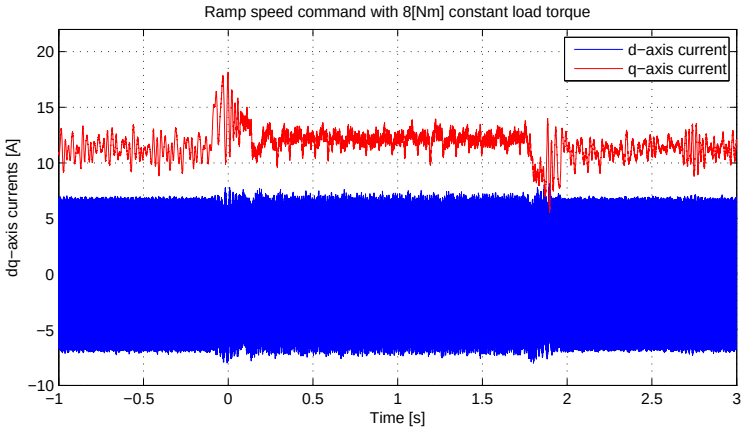

Figure 5.40: *PMSM dq-axis currents in the case of* $200rpm$ *trapezoidal speed command with* $8Nm$ *(40%) constant load torque (sensorless control)*

Figure 5.41 shows the speed estimation error. The speed error is much lower than in the no load case reaching peak values of about $22rpm$ while in the case of no load it reached values of $55rpm$.

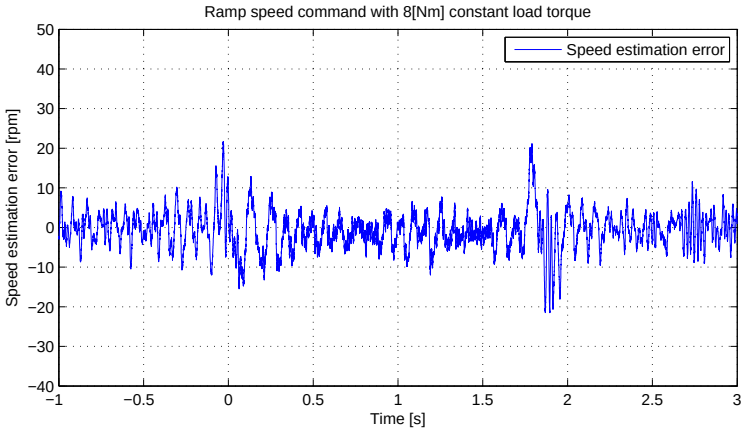

Figure 5.41: *Speed estimation error in the case of* $200rpm$ *trapezoidal speed command with* $8Nm$ *(40%) constant load torque (sensorless control)*

Figure 5.41 shows the electrical rotor position estimation error. The angle error shows less oscillations than in the no load case and the peak error is around $-17deg$ during the second transient period. The angle estimation is much better when the PMSM is loaded. During the no load test the estimation error had a peak value of $-30deg$ which is almost twice than the peak value for this case.

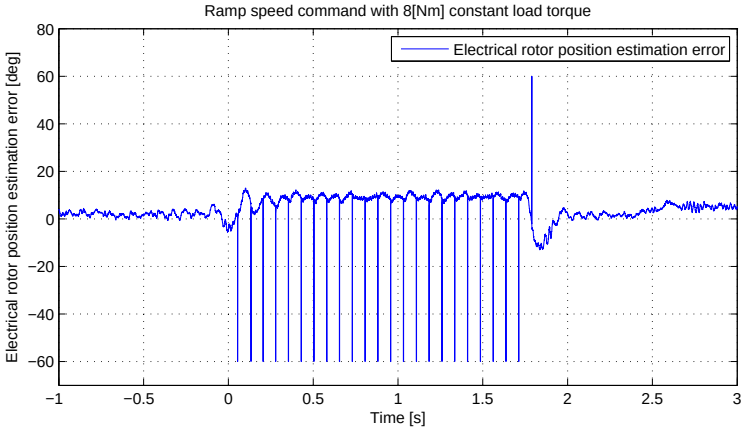

Figure 5.42: *Electrical rotor position estimation error in the case of* $200rpm$ *trapezoidal speed command with* $8Nm$ *(40%) constant load torque (sensorless control), the high spikes in the estimation error that reach* $60deg$ *are not real*

$25rpm$ speed reversal command with $8Nm$ (40%) constant load torque

In this study case the speed reference is changed from -25 to $25rpm$ in a ramp fashion with the rate of change of $1000rpm/s$. The load torque is constant $8Nm$ during this study case. Figure 5.43 shows the reference and measured speed. The measured speed follows the reference but not as well as in the case of $200rpm$ operation.

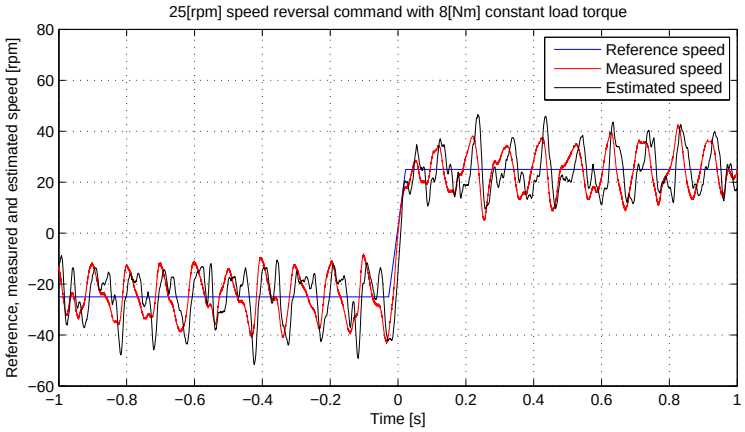

Figure 5.43: *PMSM reference, measured and estimated mechanical speed in the case of* $25rpm$ *speed reversal command with* $8Nm$ *(40%) constant load torque (sensorless control)*

Figure 5.44 shows $dq-axis$ currents. The $d-axis$ current contains the high frequency component while the $q-axis$ current reaches peak values of $15A$. The $q-axis$ current oscillates more in this study case than in others because now the angle estimation error is higher and thus the needed $q-axis$ current also becomes higher in order to overcome the load torque.

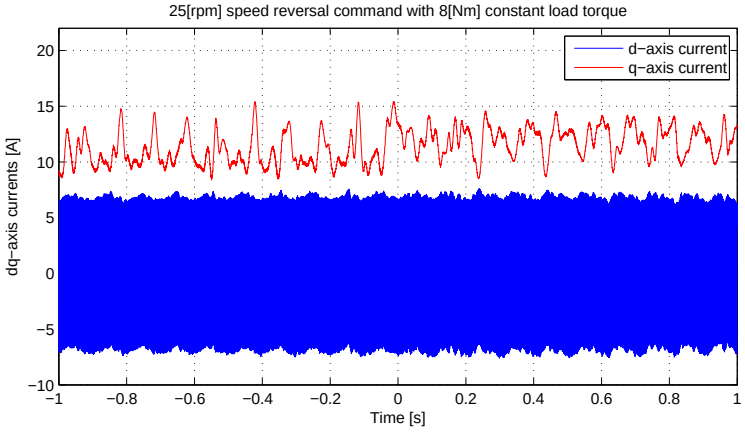

Figure 5.44: *PMSM dq-axis currents in the case of* $25rpm$ *speed reversal command with* $8Nm$ *(40%) constant load torque (sensorless control)*

Figure 5.45 shows the speed estimation error which is relatively high compared to the other study cases and it reaches peak values of about $23rpm$.

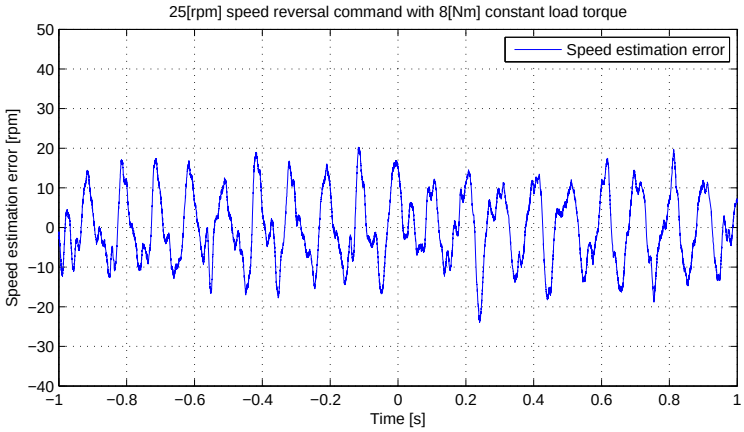

Figure 5.45: *Speed estimation error in the case of* $25rpm$ *speed reversal command with* $8Nm$ *(40%) constant load torque (sensorless control)*

Figure 5.46 shows the electrical rotor position estimation error which oscillates around $10deg$ during the $-25rpm$ operation and then decreases a little to about $6deg$ during the $25rpm$ operation.

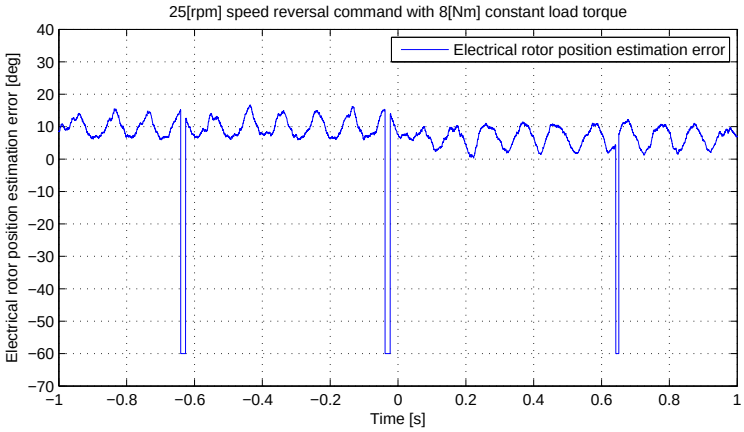

Figure 5.46: *Electrical rotor position estimation error in the case of* $25rpm$ *speed reversal command with* $8Nm$ *(40%) constant load torque (sensorless control), the high spikes in the estimation error that reach* $60deg$ *are not real*

Zero and very low speed operation with and without load torque

This study case presents the results obtained at zero and very low speeds. In the first case the reference speed is set to $0rpm$. The behavior of the PMSM is observed under no load and load conditions. Figure 5.47 shows the reference, measured and estimated speed in the no load case. The estimated speed reaches peak values of about $14rpm$ while the measured speed reaches peak values of $4rpm$.

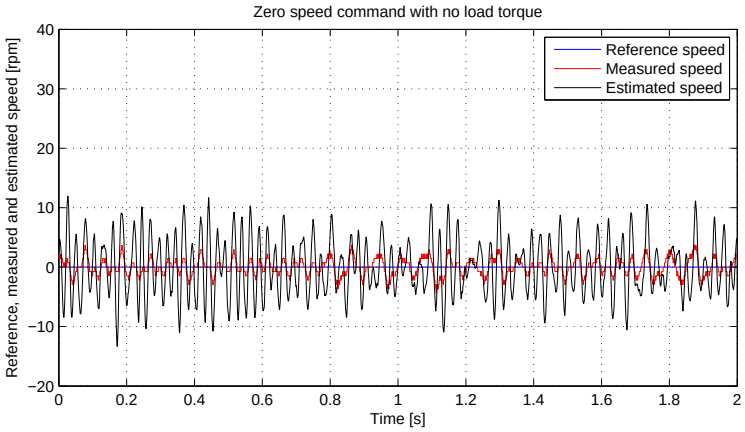

Figure 5.47: *PMSM reference, measured and estimated mechanical speed in the case of* $0rpm$ *constant speed command with no load torque (sensorless control)*

Figure 5.48 shows the reference, measured and estimated speed in the loaded case. The reference speed is the same as in the previous test but now the machine is loaded with $8Nm$ (40%) constant load torque. As it may be observed in 5.47 and 5.48 there is a very little difference between the no load and loaded case the results the oscillations in the measured speed increasing a little. The estimated speed reaches peak values of $12rpm$ while the measured speed reaches peak values of $8rpm$.

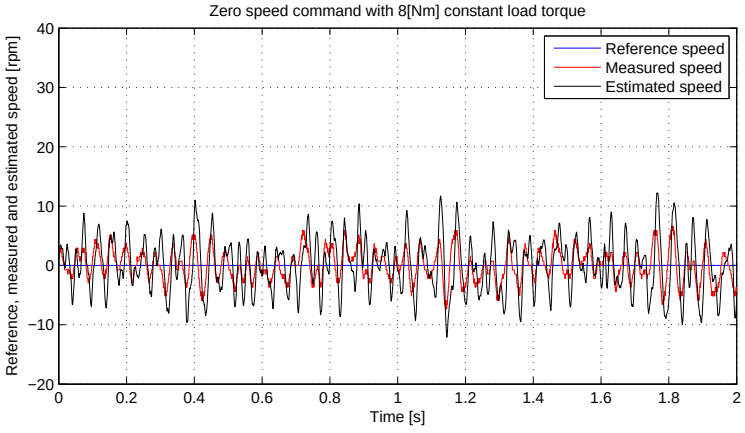

Figure 5.48: *PMSM reference, measured and estimated mechanical speed in the case of* $0rpm$ *constant speed command with* $8Nm$ *(40%) constant load torque (sensorless control)*

Figure 5.49 and 5.50 show the results for the case when the reference speed is kept at $1rpm$. Figure 5.49 show the reference, measured and estimated speed for the no load case. The estimated speed reaches peak values of $36rpm$ while the measured speed reaches peak values of $19rpm$.

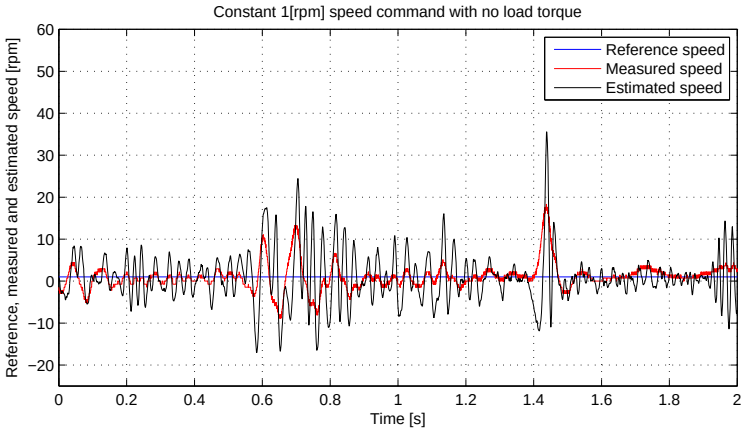

Figure 5.49: *PMSM reference, measured and estimated mechanical speed in the case of* $1rpm$ *constant speed command with no load torque (sensorless control)*

Figure 5.50 show the reference, measured and estimated speed for the loaded case. While the machine is loaded the estimated speed reaches peak values of $15rpm$ and the measured speed reaches peak values of $8rpm$. The added load torque seems to stabilize the machine reducing the oscillations in the measured and estimated speed.

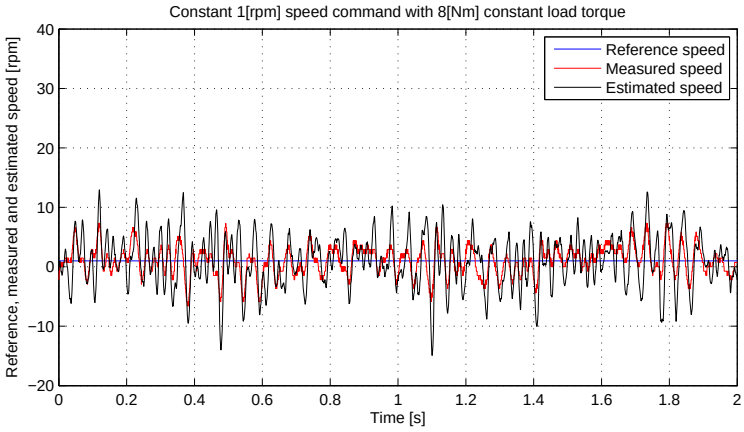

Figure 5.50: *PMSM reference, measured and estimated mechanical speed in the case of* $1rpm$ *constant speed command with* $8Nm$ *(40%) constant load torque (sensorless control)*

Figure 5.51 and 5.52 show the results for the case when the reference speed is kept at $5rpm$. As it may be seen in 5.51 the estimated speed reaches peak values of $75rpm$ and the measured speed reaches peak values of $44rpm$.

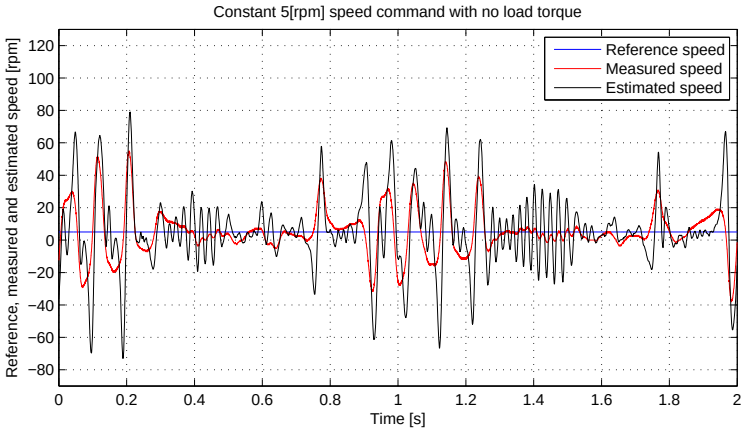

Figure 5.51: *PMSM reference, measured and estimated mechanical speed in the case of* $5rpm$ *constant speed command with no load torque (sensorless control)*

As 5.52 shows it in the no load case the estimated speed reaches peak values of $15rpm$ and the measured speed reaches peak values of $9rpm$. Also in this case the load torque has a stabilizing effect thus reducing speed oscillations.

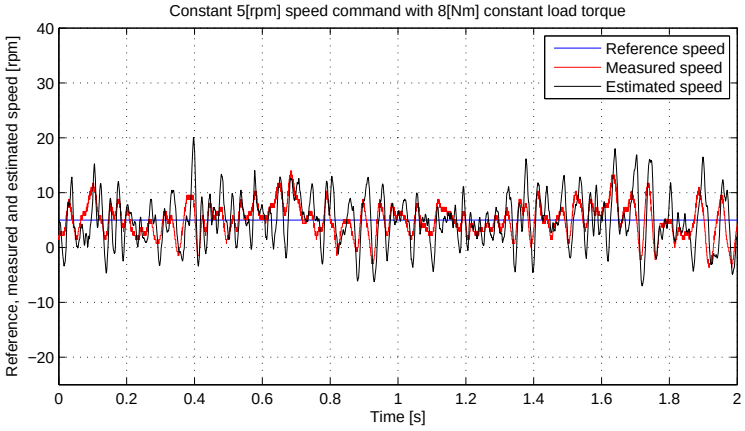

Figure 5.52: *PMSM reference, measured and estimated mechanical speed in the case of* $5rpm$ *constant speed command with* $8Nm$ *(40%) constant load torque (sensorless control)*

Figure 5.53 and 5.54 show the results for the case when the reference speed is kept at $10rpm$. As it may be seen in 5.53 the estimated speed reaches peak values of $69rpm$ and the measured speed reaches peak values of $49rpm$.

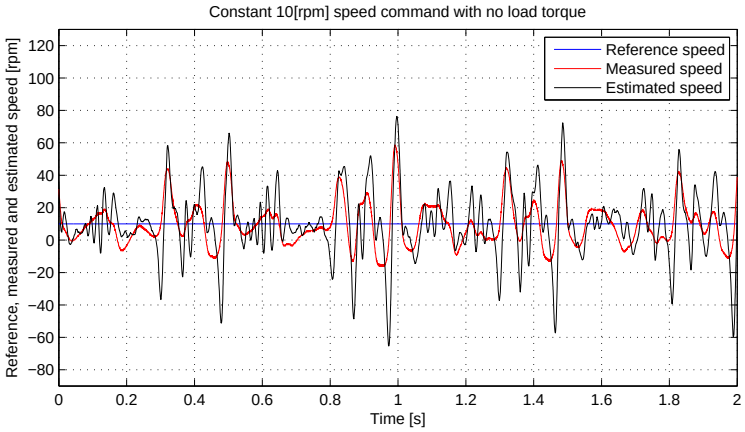

Figure 5.53: *PMSM reference, measured and estimated mechanical speed in the case of* $10rpm$ *constant speed command with no load torque (sensorless control)*

As 5.54 shows it the estimated speed reaches peak values of $12rpm$ and the measured speed reaches peak values of $10rpm$. The added low torque has the greatest impact in the case when the machine is operated at $10rpm$. The oscillations in measured and estimated speed are greatly reduced when the load torque is added.

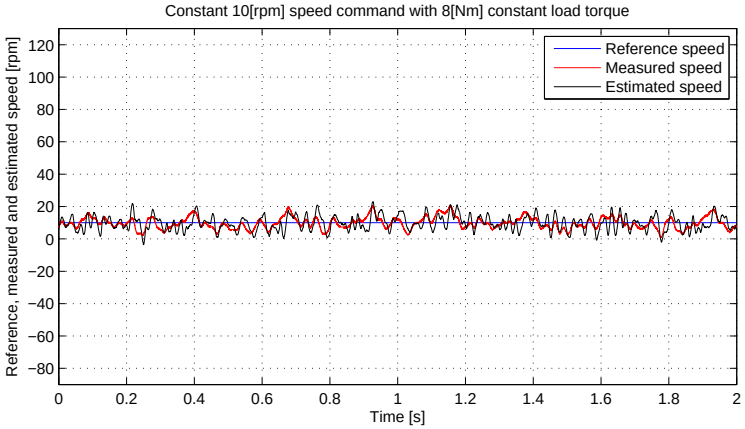

Figure 5.54: *PMSM reference, measured and estimated mechanical speed in the case of* $10rpm$ *constant speed command with* $8Nm$ *(40%) constant load torque (sensorless control)*

5.4.3 Position control mode

Zero position command with $8Nm$ (40%) load torque steps

In this study case the reference position is maintained at zero while the load torque is changed in step fashion from 0 to $8Nm$ and then back to $0Nm$. Figure 5.55 shows the reference, measured and estimated position. The measured and estimated position increases to about $0.5rad$ mechanical when the load torque is applied. When the load torque is removed the measured an estimated position decreases to about $-0.5rad$ mechanical. During steady state the measured and estimated position is close to the reference position.

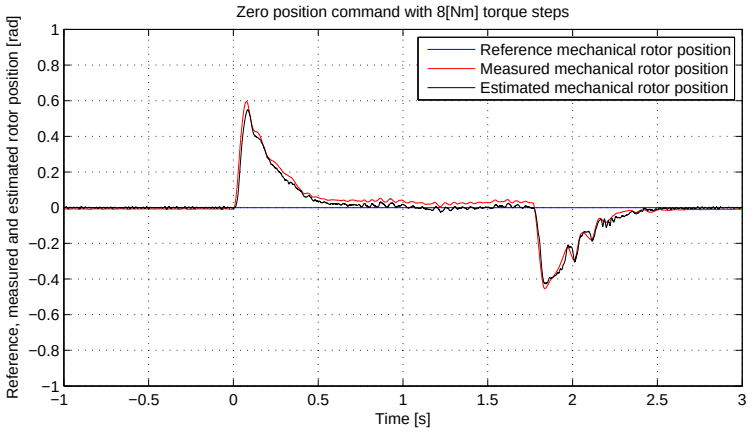

Figure 5.55: *Reference, measured and estimated mechanical rotor position in the case of* $0rad$ *position command with* $8Nm$ *(*40%*) load torque steps (sensorless control)*

Figure 5.56 shows the load torque profile. As it may be seen it is applied at $0s$ increasing from 0 to $8Nm$ and then removed at $1.75s$ reaching again values of $0Nm$.

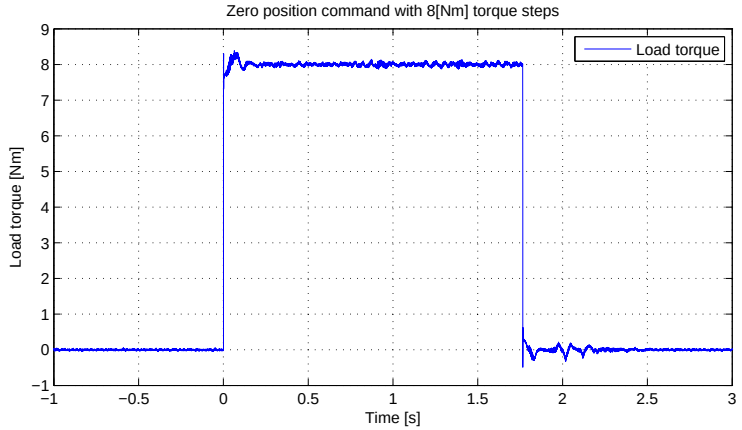

Figure 5.56: *Estimated load torque produced by the IM in the case of* $0rad$ *position command with* $8Nm$ *(*40%*) load torque steps (sensorless control)*

Figure 5.57 shows the reference, measured and estimated speed. During steady state operation all three speeds have similar values. During the first transient period when the load torque is applied the measured and estimated speed reach values of $-125rpm$ because the load torque is applied and the shaft begins to rotate backwards while the reference speed slowly increases to about $55rpm$. The shaft starts to rotate backward because the position controller needs some time to act. During the second transient period when the load torque is removed the measured and estimated speed reach values of $118rpm$ while the reference speed decreases to $43rpm$ in order to keep the rotor at it's reference position.

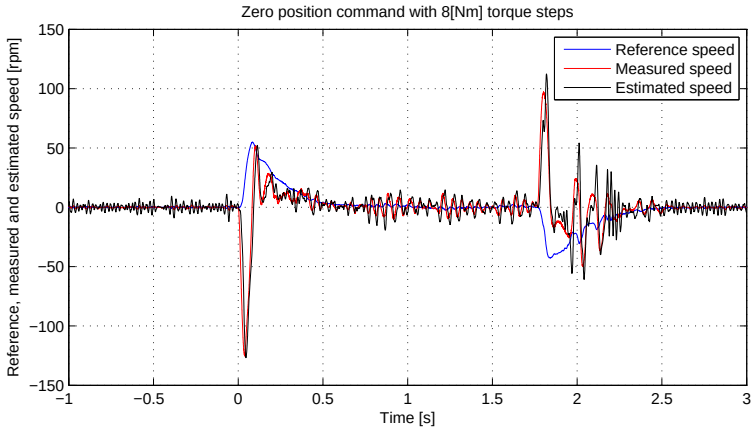

Figure 5.57: *PMSM reference, measured and estimated mechanical speed in the case of* $0rad$ *position command with* $8Nm$ *(*40%*) load torque steps (sensorless control)*

Figure 5.58 shows the $dq-axis$ currents during this study case. The $d-axis$ current contains the high frequency component while the $q-axis$ current is almost $0A$ during the no load steady state operation and reaches peak values of about $15A$ during the loaded steady state operation. During the first transient period the current reaches peak values of $21A$.

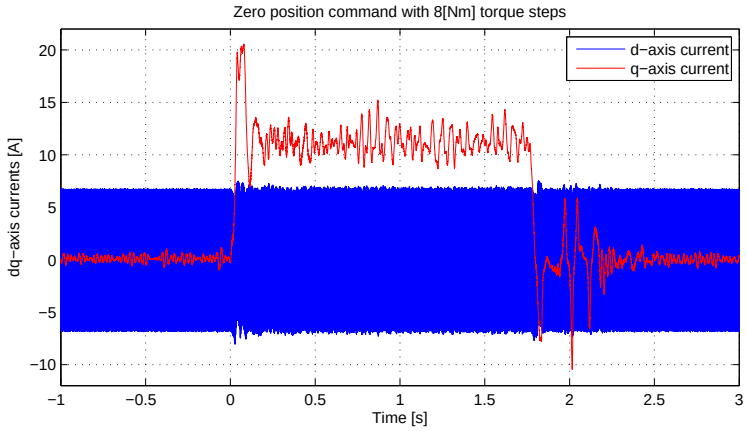

Figure 5.58: *PMSM dq-axis currents in the case of* $0rad$ *position command with* $8Nm$ *(*40%*) load torque steps (sensorless control)*

Figure 5.59 shows the speed estimations error which reaches peak values of $61rpm$ during the first transient period.

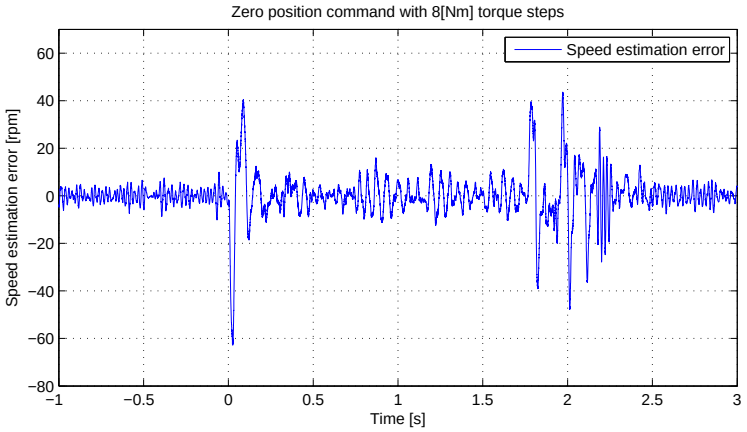

Figure 5.59: *Speed estimation error in the case of* $0rad$ *position command with* $8Nm$ *(*40%*) load torque steps (sensorless control)*

Figure 5.60 shows the electrical rotor position estimation error. When the machine is unloaded the error is close to $0deg$ and during transient periods it reaches peak values of $29deg$.

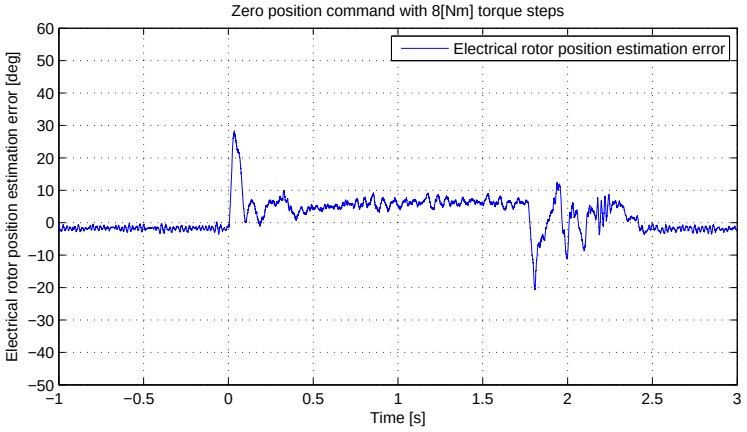

Figure 5.60: *Electrical rotor position estimation error in the case of* $0rad$ *position command with* $8Nm$ *(*40%*) load torque steps (sensorless control), the high spikes in the estimation error that reach* $60deg$ *are not real*

$1800deg$ mechanical ramp position command with $8Nm$ (40%) constant load torque

In this study case the reference position is changed from $0rad$ to $1800rad$ in a ramp fashion while the load torque is maintained at constant $8Nm$ (40%). The rate of the change in position is $1080rad/s$.

Figure 5.61 shows the reference, measured and estimated position. During steady state the measured and estimated position are close to the reference position.

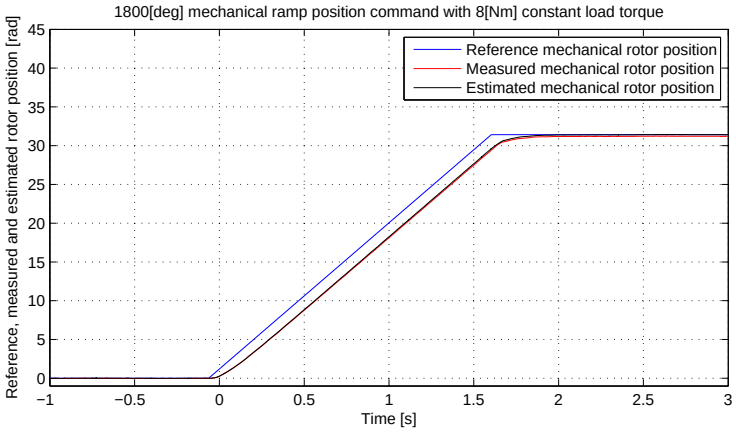

Figure 5.61: *Reference, measured and estimated mechanical rotor position in the case of* $1800deg$ *mechanical ramp position command with* $8Nm$ *(40%) constant load torque (sensorless control)*

Figure 5.62 shows the reference, measured and estimated speed. When the position change command is applied at $-0.05s$ the reference speed slowly increases to about $175rpm$. The limit of $175rpm$ is set because of the high speed limitations of the sensorless control algorithm.

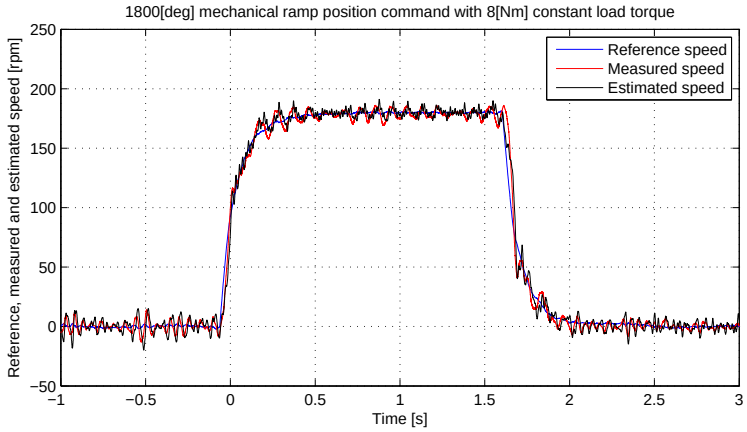

Figure 5.62: *PMSM reference, measured and estimated mechanical speed in the case of* $1800deg$ *mechanical ramp position command with* $8Nm$ *(40%) constant load torque (sensorless control)*

Figure 5.63 shows the $dq-axis$ currents. The $q-axis$ current oscillates around a fixed value in order to produce enough electromagnetic torque to overcome the load torque.

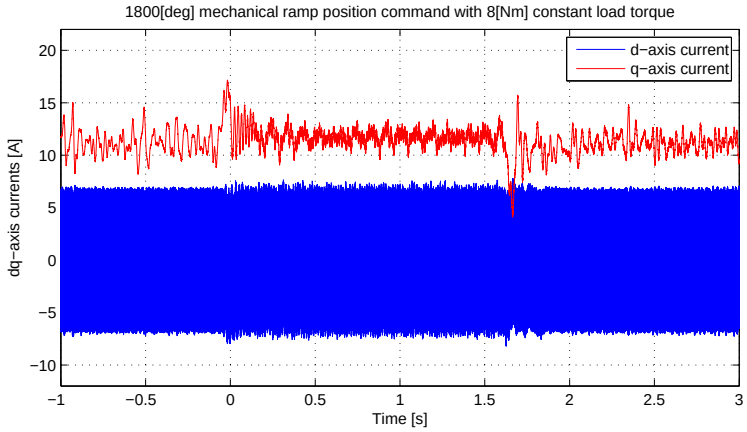

Figure 5.63: *PMSM dq-axis currents in the case of* $1800deg$ *mechanical ramp position command with* $8Nm$ *(*40%*) constant load torque (sensorless control)*

Figure 5.64 shows the speed estimation error which increases during transient periods.

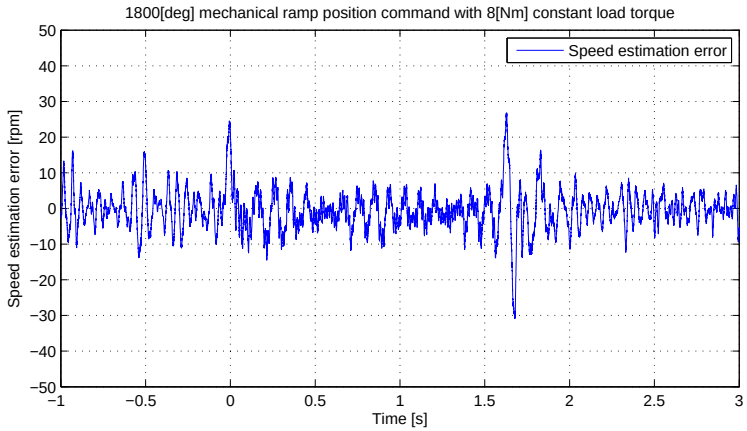

Figure 5.64: *Speed estimation error in the case of* $1800deg$ *mechanical ramp position command with* $8Nm$ *(*40%*) constant load torque (sensorless control)*

Figure 5.65 shows the electrical rotor position estimation error. During steady state the estimation error is close to $9deg$ and it increases to about $-18deg$ during the second transient period.

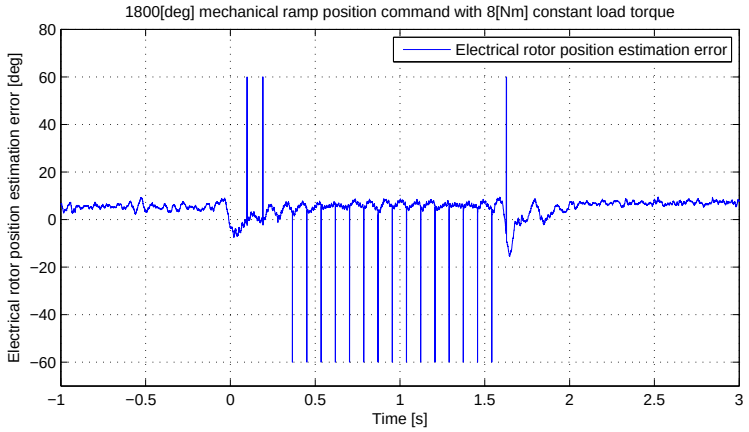

Figure 5.65: *Electrical rotor position estimation error in the case of* $1800deg$ *mechanical ramp position command with* $8Nm$ *(40%) constant load torque (sensorless control), the high spikes in the estimation error that reach* $60deg$ *are not real*

5.5 Estimation error dependence on load torque

Figure 5.66 shows the electrical rotor position estimation error dependence on load torque. As the PMSM is loaded the $q-axis$ current increases in order to produce electromagnetic torque to overcome the load. The high $q-axis$ current produces a magnetic flux on the $q-axis$ which leads to a deviation of the minimum impedance point.

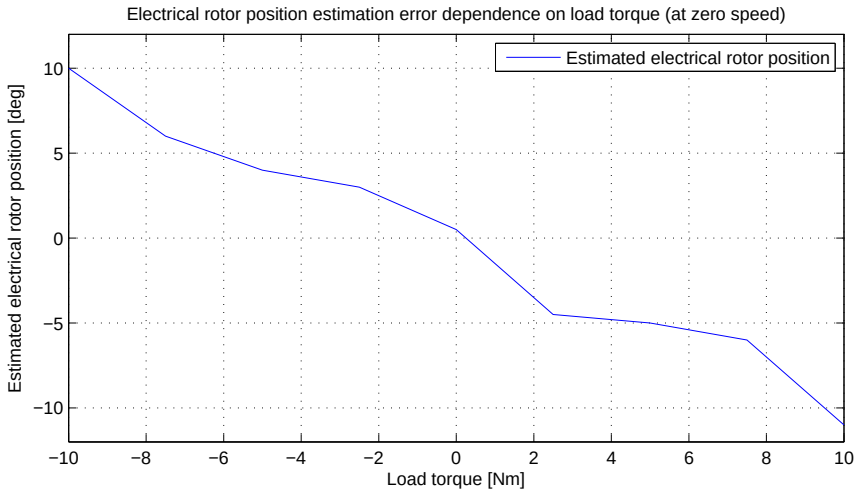

Figure 5.66: *Electrical rotor position estimation error dependence on load torque (zero speed operation)*

As it may be observed at no load the estimation error is close to zero. There might be a small estimation error of a few degrees due to incorrect rotor alignment (which is inevitable) before the building procedure of the simulation model. As the PMSM is loaded, the estimation error increases almost proportionally withe the load torque. For a $10Nm$ load torque there is a $-11deg$ estimation error while for a $-10Nm$ load torque there is a $10deg$ estimation error. This estimation error introduced by the loading of the machine might be

compensated by using a look-up table which contains the estimation error and load torque data. The development of such a compensation method is beyond the scope of this project.

5.6 Energy efficiency considerations

The energy use optimization in the case of the chosen sensorless control algorithm is done by choosing the constant torque angle (maximum torque per ampere) control property which is the same as the maximum efficiency control property if the core losses are neglected.

The sensorless RFOC is less energy efficient than the sensored RFOC due to more reasons. One of the reasons is that there is always voltage injected on the estimated $d-axis$ regardless of load or speed (low speed operating region). In this case the injection voltage is $45V$ which leads to a $d-axis$ current with the peak value of about $6A$. As the frequency of the injection voltage is $500Hz$ the big part of the high frequency current is reactive. This reactive current limits the maximum usable power of the inverter and SMPMSM.

Another source of energy loss in this sensorless control algorithm is the rotor position estimations error. Whenever there is a rotor position estimation error, the $q-axis$ current becomes higher in order to overcome the load torque. If there is an estimation error in the rotor position then the $q-axis$ current is projected both on the real d and $q-axes$ producing further energy losses.

A good way to experimentally determine the energy losses associated with this sensorless control algorithm would be to measure the $DC-link$ power and to calculate the mechanical power for both sensored and sensorless control algorithms and compare them. The $DC-link$ power can be estimated by using the command duty cycles, measured stator currents and measured $DC-link$ voltage. The mechanical power can be calculated by multiplying the estimated torque with the measured angular speed.

Nevertheless sensorless control reduces the cost of the motor drive and increases the reliability of the whole system.

5.7 IM IFOC (loading machine)

In this section the laboratory results of IM control are presented. The IM was used to load the PMSM in order to test it's control under different loading conditions. The shaft of the IM and PMSM is mechanically connected. The indirect field oriented control (IFOC) for the IM is implemented in the laboratory. [12]

5.7.1 d and $q-axis$ current controller step response

Figure 5.67 shows the $d-axis$ current controller step response when a $3A$ current step command is applied. The settling time is about $4ms$. The current controllers were designed in such a way that there is no significant current overshoot in order to protect the switches in the inverter as it may be also observed in figures 5.67 and 5.68.

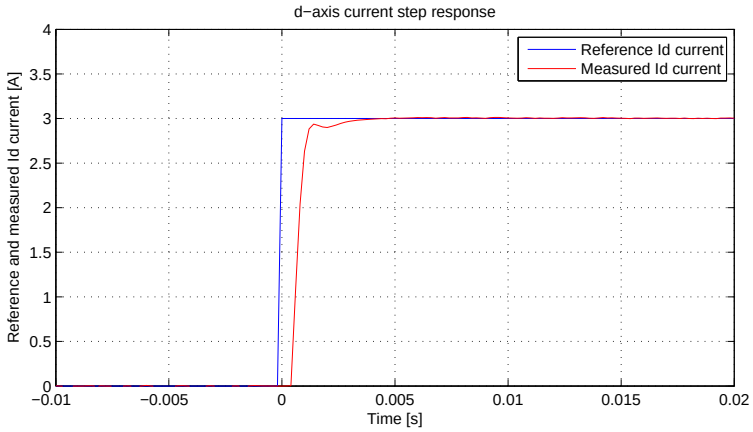

Figure 5.67: *$d-axis$ current controller $3A$ step response for the IM IFOC*

Figure 5.68 shows the $q-axis$ current controller step response when a $3A$ current step command is applied. The settling time in this case is also about $4ms$ and there is no current overshoot.

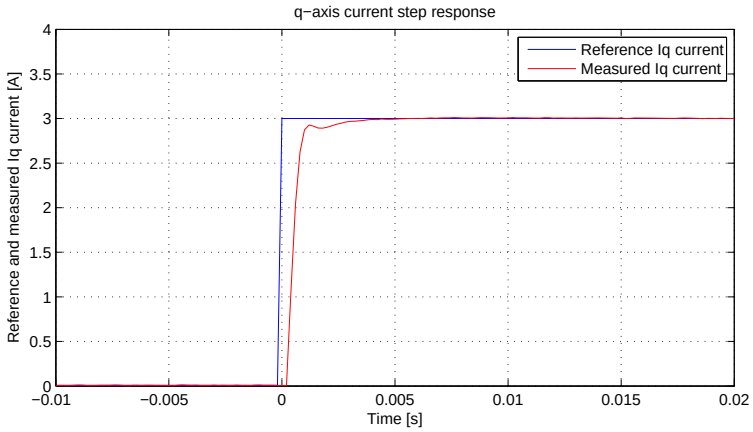

Figure 5.68: *$q-axis$ current controller $3A$ step response for the IM IFOC*

5.7.2 Speed control mode

Zero speed command with $8Nm$ (54%) load torque steps

In this study case the reference speed is maintained at $0rpm$ while a step load torque of $8Nm$ is applied at $0s$ and removed at $1.65s$. The $8Nm$ load torque corresponds to (54%) of the IM nominal load torque. Figure 5.69 shows the reference speed given to the IM and the measured mechanical speed. As it may be seen in 5.69 the measured speed deviates from it's reference during the application and removel of the load torque. The measured speed reaches peak values of $60rpm$ during transient periods and it goes back to it's reference value of $0rpm$ in about $0.48s$.

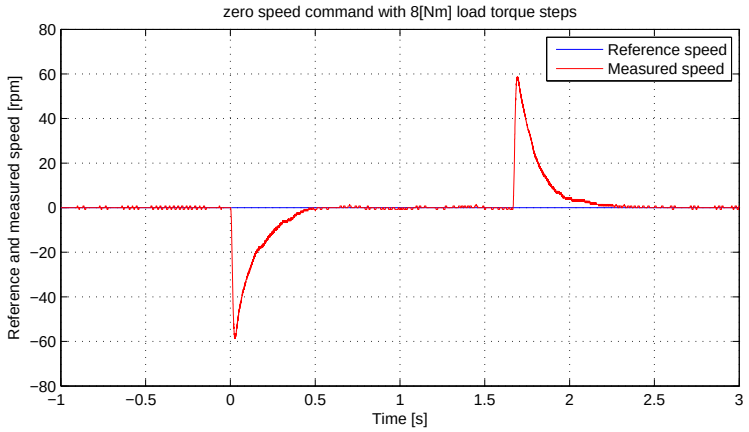

Figure 5.69: *IM reference and measured mechanical speed in the case of zero speed command with* $8Nm$ *(*54%*) load torque step applied at* $0s$ *and removed at* $1.65s$

Figure 5.70 shows the estimated load torque produced by the PMSM in order to load the IM. At $0s$ the torque steps from 0 to $8Nm$ and at $1.65s$ it steps back to $0Nm$

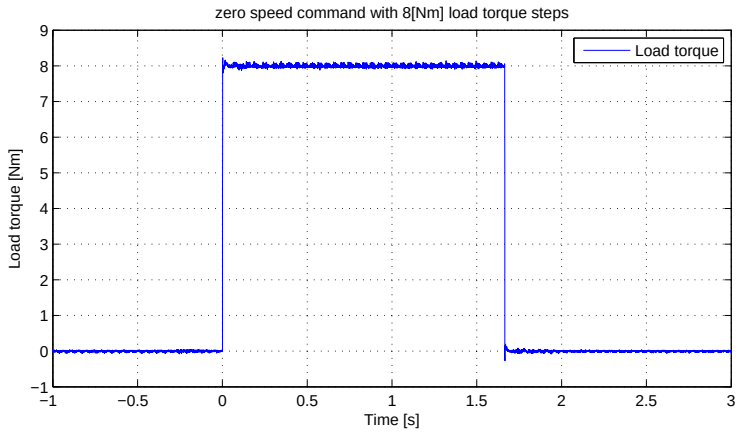

Figure 5.70: *Estimated load torque produced by the PMSM in the case of zero speed command with* $8Nm$ *(*54%*) load torque step applied at* $0s$ *and removed at* $1.65s$

Figure 5.71 shows the $dq-axis$ currents of the IM. The $d-axis$ current is maintained at $4.1A$ during the whole time, even in the case of zero speed and no load torque because it is responsible for flux production. The $q-axis$ current is $0A$ when there is no load torque and it increases to about $3.1A$ when the load torque is applied.

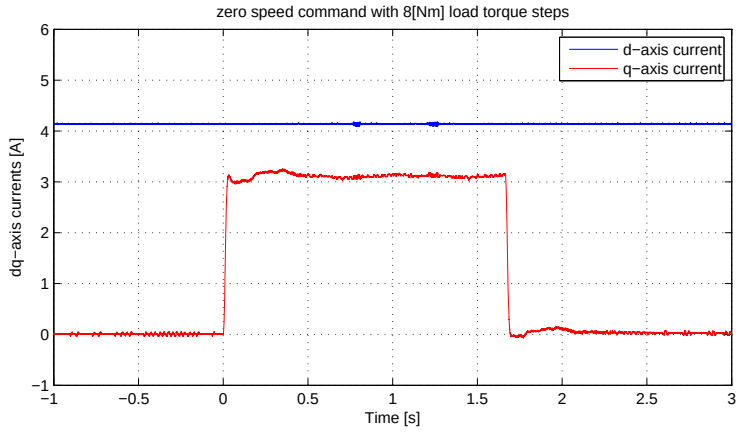

Figure 5.71: *IM dq-axis currents in the case of zero speed command with* $8Nm$ *(*54%*) load torque step applied at* $0s$ *and removed at* $1.65s$

$250rpm$ trapezoidal speed command with $8Nm$ (54%) constant load torque

In this study case the load torque is maintained at $8Nm$ while the IM is given a trapezoidal speed reference of $250rpm$. The speed reference is changed from 0 to $250rpm$ in $0.2s$. The rate of change of reference speed is $1000rpm/s$. Figure 5.72 shows the reference and measured speed, as it may be observed, the reference speed first starts changing at $-0.15s$ and then again at $1.8s$. The measured speed follows the reference speed quite well. There is a 4% overshoot in the speed response both after acceleration and deceleration which is acceptable.

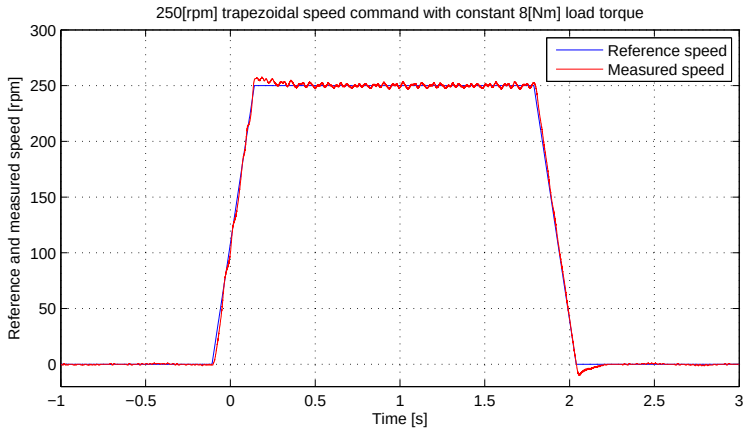

Figure 5.72: *IM reference and measured mechanical speed in the case of* $250rpm$ *trapezoidal speed command with* $8Nm$ *(*54%*) constant load torque*

Figure 5.73 shows the $dq-axis$ currents for this study case. The $d-axis$ current maintains it's reference values of $4.14A$ during the whole time however there are some small spikes during the $250rpm$ operation. The $q-axis$ current have a magnitude of about $3.1A$ during constant speed operation, with some bigger spikes during the $250rpm$ operation. During trasient periods there is a change in the $q-axis$ current, it increases to about $3.8A$ during acceleration and it decreases to about $2.7A$ during deceleration as expected.

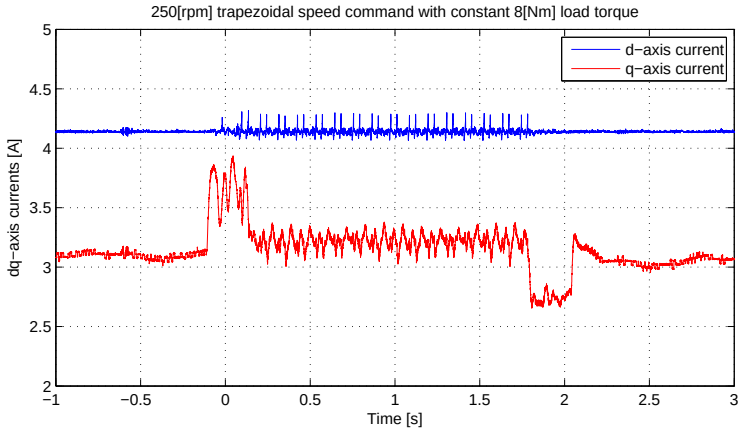

Figure 5.73: *IM dq-axis currents in the case of* $250rpm$ *trapezoidal speed command with* $8Nm$ *(54%) constant load torque*

Figure 5.74 shows the estimated electrical rotor position during this study case. During zero speed operation, the electrical rotor position actually changes slowly due to the fact that the load torque is applied and slip is needed to produce electromagnetic torque to counteract the load torque.

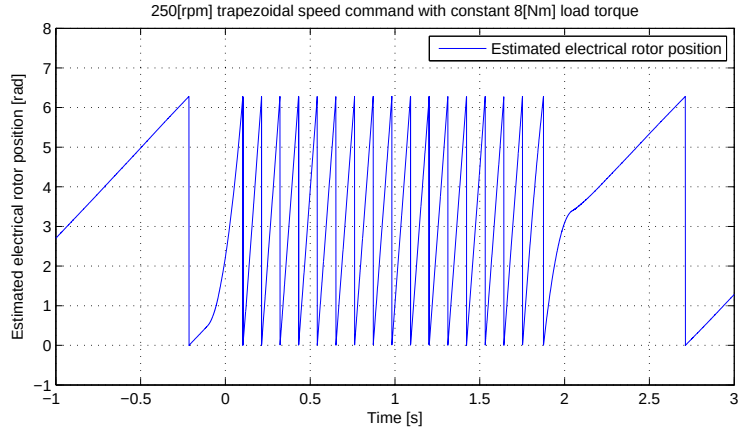

Figure 5.74: *IM estimated electrical rotor position in the case of* $250rpm$ *trapezoidal speed command with* $8Nm$ *(54%) constant load torque*

5.7.3 Load torque validation

As it may be seen in 5.11 the estimated load torque produced by the IM in this study case is $8Nm$. In order to make sure that the real load torque is the same as the estimated one the electromagnetic torque produced by the PMSM may be calculated. As in the above study case the rotor speed is $0rpm$ the dry and viscous friction torque are equal to $0Nm$ thus more accurate results are obtained. The electromagnetic torque produced by the SMPMSM (neglecting reluctance torque) may be calculated using 5.2. As it may be seen in 5.12 the $q-axis$ current has the magnitude of approximately $11A$ while the machine is loaded. The calculated electromagnetic torque produced by the PMSM is $8.11Nm$ which is quite close to the estimated load torque of $8Nm$.

$$T_e = \frac{3}{2} npp \lambda_m i_{qs}^r = \frac{3}{2} \times 4 \times 0.123 \times 11 = 8.11 Nm \tag{5.2}$$

When the PMSM's rotor is rotating with $200rpm$ and the machine is loaded with $8Nm$ load torque the $q-axis$ current is about $12A$ as it may be seen in 5.19 which leads to an electromagnetic torque of $8.85Nm$ as the calculations show it in 5.3. The slightly higher calculated electromagnetic torque for the $200rpm$ operation could be caused by the dry and viscous friction torques which are non zero in this case. Even the $8.85Nm$ calculated electromagnetic torque is close to the $8Nm$ estimated load torque.

$$T_e = \frac{3}{2} npp \lambda_m i_{qs}^r = \frac{3}{2} \times 4 \times 0.123 \times 12 = 8.85 Nm \tag{5.3}$$

The calculations from 5.2 and 5.3 indicate that the estimated load torque is close to the real load torque which can not be directly measured.

5.8 Summary

This chapter begins with the experimental determination of the injection frequency and voltage magnitude. After that the rotor alignment to it's initial position is demonstrated by means of applying a DC voltage using the VSI. The laboratory results for the sensored control are presented in detail followed by the results for the sensorless control. The sensored and sensorless laboraotry results include current and speed step responses followed by several study cases. Next the estimation error dependence on load torque is analyzed followed by energy efficiency considerations. The chapter ends with the laboratory results for the loading machine control and load torque validation calculations.

Chapter 6

Conclusions and Future Work

6.1 Conclusions

Due to it's high efficiency PMSMs are a good alternative in industrial applications instead of IMs. A main problem with the control of a PMSM is the need of a position sensor which increases the cost of the whole drive. This cost issue can be solved by using a sensorless control strategy. That is why this thesis focuses on sensorless control of SMPMSMs.

Sensorless control of a SMPMSM in low speed high dynamic applications is problematic and classical approaches like the back-EMF or flux linkage based methods can not be used at very low speeds. A promising control method is the high frequency signal injection method which allows sensorless control of SMPMSM at very low speeds down to standstill.

As the results show it the high frequency signal injection method implemented in this thesis allows sensorless control of a SMPMSM even at zero speeds

Since the controlled machine is a SMPMSM and the saliency of such a machine is almost inexistent the most suitable control property is the constant torque angle strategy which is equivalent to the maximum torque per ampere strategy in the case of a SMPMSM and also maximum efficiency strategy if the core losses are neglected.

Some disadvantages of the high frequency signal injection algorithm are:

- audible noise is produced due to the $500Hz$ injected signal which can be a problem in some special applications;
- there are oscillations in the mechanical speed especially when the machine is not loaded due to the position and speed estimation errors;
- the rotor's initial position can not be detected but this problem can be solved as presented in the project by mens of applying a DC voltage using the VSI to bring the rotor to a known position.

Advantages of the high frequency signal injection algorithm are as follows:

- it eliminates the need of using a position sensor thus reducing the cost of the drive;
- it increases the reliability of the drive since there are less components that can brake down;
- even if there is audible noise produced this might be no problem in many industrial applications;

- as the experimental results show it sensorless control up to speeds of $200rpm$ was obtained by using this strategy. At speeds above $200rpm$ the back-EMF method could be used to obtain a whole speed range sensorless operation since the voltage is high enough;

6.1.1 Contributions

- Simulation of the sensored and sensorless RFOC for the PMSM has been carried out using $Matlab/Simulink$ and $Plecs$;
- The simulations have been validated in the laboratory using a $dSpace$ setup;
- The initial rotor position detection issue for the PMSM has been solved by means of applying a DC voltage using the VSI in order to bring the rotor to a known position;
- SMPMSM frequency and current sensitivity analysis have been carried out in order to determine the frequency and the magnitude of the injection voltage used in the sensorless control algorithm;
- The control for the IM (IFOC) has been implemented in the laboratory which allows the testing of the PMSM control under loading conditions;
- A $ControlDesk$ interface (dSpace) has been developed which offers the opportunity of controlling the PMSM by using a position sensor or sensorlessly in torque, speed or position mode. The IM can be controlled either in torque mode or speed mode. For example the PMSM can be controlled with the use of a position sensor or sensorlessly in speed and position mode while the IM in torque mode. If the IM is controlled in speed mode then the PMSM must work in torque mode.

6.2 Future work

The studied high frequency signal injection based algorithm could be tested only up to 40% load torque due to some problems with the setup. Test could be carried out under full load torque if the problem with the setup is solved. A more detailed analysis and comparison of energy efficiency of sensored and the proposed sensorless control algorithm could be done.

Appendix A

SMPMSM parameters

Parameter	Simbol	Value	Unit
Rated phase voltage	U_n	164	$[V]$
Rated speed	n_n	4500	$[rpm]$
Rated current	I_n	20	$[A]$
Rated power	P_n	9.42	$[KW]$
Rated torque	T_n	20	$[Nm]$
Stator phase resistance	R_s	0.19	$[\Omega]$
Synchronous inductance	L_d	2	$[mH]$
Synchronous inductance	L_q	2	$[mH]$
No. of pole pairs	n_{pp}	4	$-$
Permanent magnet flux linkage	ψ_m	0.123	$[Wb]$
Rotor moment of inertia	J	0.0048	$[kg \cdot m^2]$

Table A.1: *Parameters of the PMSM from the laboratory*

Appendix B

Contents of CD-ROM

- **Articles:**
  - This folder contains all articles used as references in the project.
- **Report files:**
  - This folder contains all source files in the LATEX project file structure.
- **MATLAB/Simulink files:**
  - This folder contains the *Matlab/Simulink* files.

Bibliography

[1] I. Boldea and S. A. Nasar, *The Induction Machine Handbook*. CRC Press, Boca Raton London New York Washington, D.C., 2002.

[2] O. Goksu, "Shaft transducerless vector control of the interior permanent magnet motor with speed and position estimation using high frequency signal injection and flux observer methods," Master's thesis, The Graduate School of Natural and Applied Sciences of Middle East Technical University, May 2008.

[3] ABB, *Energy efficiency makes a difference*, 2008.

[4] C.-M. Ong, *Dynamic simulation of electric machinery (using Matlab/Simulink)*. Prentice Hall PTR, 1997.

[5] J.-H. Jang and S.-K. Sul, "Sensorless drive of smpm motor by high frequency signal injection," p. 7, 2002.

[6] P. D. C. Perera, *Sensorless Control of Permanent-Magnet Synchronous Motor Drives*. PhD thesis, Institute of Energy Technology Aalborg University, December 2002.

[7] A. Consoli, G. Scarcella, G. Scelba, S. Royak, and M. M. Harbaugh, "Implementation issues in voltage zero-sequence-based encoderless techniques," *IEEE transactions on industry applications*, vol. 44 no. 1, p. 9, 2008.

[8] A. Consoli, G. Scarcella, and G. Tutino, "Zero frequency rotor position detection for synchronous pm motors," p. 6, 2000.

[9] M. Stulrajter, V. Hrabovcova, and M. Franko, "Permanent magnets synchronous motor control theory," *Journal of electrical engineering*, vol. 58, p. 6, 2007.

[10] S. V. Paturca, M. Covrig, and L. Melcescu, "Direct torque control of permanent magnet synchronous motor (pmsm) - an aproach by using space vector modulation (svm)," *Int. conf. on Electric power systems, Tenerife, Spain*, p. 6, 2006.

[11] F. Haugen, *PID Control*. Tapir Academic Press, 2004.

[12] M. P. Kazmierkowski, R. Krishnan, and F. Blaabjerg, *Control in power electronics (selected problems)*. Academic press, 2002.